EPA-600/4-81-067
August 1981

FLOW AND DISPERSION OF POLLUTANTS OVER TWO-DIMENSIONAL HILLS

Summary Report on Joint Soviet-American Study

ENVIRONMENTAL SCIENCES RESEARCH LABORATORY
OFFICE OF RESEARCH AND DEVELOPMENT
U.S. ENVIRONMENTAL PROTECTION AGENCY
RESEARCH TRIANGLE PARK, NC 27711

EPA-600/4-81-067
August 1981

FLOW AND DISPERSION OF POLLUTANTS OVER TWO-DIMENSIONAL HILLS

Summary Report on Joint Soviet-American Study

by

Leon H. Khurshudyan
Main Geophysical Observatory
Leningrad, U.S.S.R.

William H. Snyder
Meteorology and Assessment Division
Environmental Sciences Research Laboratory
U.S. Environmental Protection Agency
Research Triangle Park, NC 27711

Igor V. Nekrasov
Institute of Mechanics
State University of Moscow
Moscow, U.S.S.R.

ENVIRONMENTAL SCIENCES RESEARCH LABORATORY
OFFICE OF RESEARCH AND DEVELOPMENT
U.S. ENVIRONMENTAL PROTECTION AGENCY
RESEARCH TRIANGLE PARK, NC 27711

DISCLAIMER

This report has been reviewed by the Environmental Sciences Research Laboratory, U.S. Environmental Protection Agency and the Main Geophysical Observatory, Leningrad, U.S.S.R., and approved for publication. Mention of trade names or commercial products does not constitute endorsement or recommendation for use.

William H. Snyder is a physical scientist in the Meteorology and Assessment Division, Environmental Sciences Research Laboratory, U.S. Environmental Protection Agency, Research Triangle Park, NC. He is on assignment from the National Oceanic and Atmospheric Administration, U.S. Department of Commerce.

PREFACE

This report presents a portion of the results of a US-USSR cooperative program in the study of environmental protection. It culminates the joint activities of three scientists working together over a period of five months. A wind-tunnel study of flow and dispersion of pollutants over two-dimensional hills was conducted. Simultaneously, computer programs were run to make comparisons with various theories and prediction techniques.

In this cooperative venture, a very large amount of data was collected in a short time period. It was possible, in the time at hand, to assimilate only a small fraction of the observations and to make only limited comparisons between the data collected and the multitude of theories. This report is intended, then, as an overview of the methods and techniques of data collection and a presentation of the most important conclusions. It is also intended to give the reader some flavor of the quantity and quality of the data collected and to exemplify the kinds of information contained in the data volumes as well as the kinds of comparisons that can be made with theory; in short, this report is intended to whet the appetite of the reader and to encourage him to exercise the data for useful purposes.

ABSTRACT

Wind tunnel experiments and theoretical models concerning the flow structure and pollutant diffusion over two-dimensional hills of varying aspect ratio are described and compared. Three hills were used, having small, medium and steep slopes. Measurements were made of mean and turbulent velocity fields upwind, over and downwind each of the hills. Concentration distributions were measured downwind of tracer sources placed at the upwind base, at the crest, and at the downwind base of each hill. These data were compared with the results of two mathematical models developed in the U.S.S.R. for treating flow and dispersion over two-dimensional hills. Measured concentration fields were reasonably well predicted by the models for a hill of small slope. The models were less successful for hills of steeper slope, because of flow separation from the lee side of the steepest hill and high turbulence and much-reduced mean velocity downwind of the hill of medium slope.

CONTENTS

FIGURES

TABLES

ACKNOWLEDGEMENTS

The cooperation of the staff at the Fluid Modeling Facility is gratefully acknowledged. The authors are particularly indebted to Messrs. L. A. Knight, R. E. Lawson, Jr., and W. R. Pendergrass, III for their help with the myriad details involved in the collection of data, Mr. M. S. Shipman for his difficult and innovative programming of the minicomputer, and Mr. M. Manning for the construction of the models.

Dr. I. P. Castro, University of Surrey (England) provided assistance with the pulsed-wire anemometer measurements during the spring and summer of 1980. Mr. M. Capuano, North Carolina State University, helped with the remeasurement of suspect data and supplementary measurements as well as data processing. Drs. I. M. Zrazhevsky, E. L. Genikhovich, V. B. Kisselev and Mrs. I G. Gracheva participated in useful discussions of the results of this study during the US-USSR experts' meeting in Leningrad, U.S.S.R., in April, 1980.

Finally, thanks are extended to Messrs. A. D. Busse and C. Gale for their assistance with the Univac computer and Mrs. B. Hinton for her toil in typing the manuscript.

1. INTRODUCTION

This report presents preliminary results of the Joint Soviet-American Work Program for studying air flows and dispersion of pollutants in hilly terrain. The work was conducted in the Fluid Modeling Facility of the U.S. Environmental Protection Agency, Research Triangle Park, NC.

Investigations of pollutant transport and dispersion in the atmosphere over complex relief are critical for the protection of air quality, since industrial enterprises and other sources of air pollution frequently locate within complex terrain. Although much effort has already be expended in elucidating this problem and establishing guidelines for industry and control organizations to use in predicting of air pollution, the problem is far from solved. At present, three main approaches are used to study the problem:

THEORETICAL MODELING

To calculate pollutant dispersion, it is necessary to know how irregularities of the ground surface distort the mean and turbulent structure of the incident flow. Some investigations of peculiarities of turbulent dispersion in distorted flows (even separated flows) have been made (Hunt and Mulhearn, 1973; Puttock and Hunt, 1979). Practically speaking, however, those results can be used only if the distorted mean flow field (mean streamline pattern) is known. Since mathematical modeling of flow structure is quite difficult, these diffusion theories have been applied only with highly simplified assumptions about the mean flow, e.g., potential flow. The most realistic models of flows (some including diffusion calculations) over irregular terrain constructed thus far have been obtained through solution of simplified equations of viscous flow with additional simplifying assumptions about the turbulence structure (Berlyand and Genikhovich, 1971; Taylor and Gent,

1974; Jackson and Hunt, 1975). In spite of differences between these models, their underlying assumptions limit their applicability to gentle relief (hills of small slope). As a further restriction, most of these theories are too complicated to be used in the daily practice of air pollution prediction. Hence, simpler models have become wide-spread. These simpler models usually assume potential (or "quasi-potential") flow over irregular terrain (Berlyand et al, 1968; Egan, 1975; Isaacs et al, 1979; the latter incorporates the Hunt-Mulhearn theory). In the U.S., models are used that neglect, even for neutral flow, the convergence of streamlines over obstacles as in the EPA Valley Model (Burt and Slater, 1977). More recently, attempts have been made to describe the flow structure over steeper obstacles where flow separation may occur (Mason and Sykes, 1979). But these attempts deal only with laminar flows (numerical solutions of Navier-Stokes equations at small to moderate Reynolds number).

FIELD EXPERIMENTS

Full-scale experiments are very important, but expensive and time-consuming, especially in complex terrain (Barr et al, 1977; Hovind et al, 1979). Extensive measurements and analyses are required of wind, temperature and concentration distributions in order to gain sufficient insight and understanding of the fundamental physics so that mathematical models may be constructed that are at least correct in principle. The generalization from field data is difficult because of the peculiarities of specific sites and meteorological conditions. Controlled variation of independent variables is generally not possible. Complicating factors are generally abundant. However, to obtain credibility, all models must ultimately be tested by comparison with real-world data. Significant field experiments in complex terrain are now being conducted by the Department of Energy (Dickerson and Gudiksen, 1980), the Electric Power Research Institute (Hilst, 1978), and the Environmental Protection Agency (Holzworth, 1980).

WIND TUNNEL MODELING

The difficulties of mathematical and field investigations of atmospheric flows and pollutant dispersion in complex cases such as hilly terrain have stimulated the development of wind tunnel modeling, where the atmospheric boundary layer and diffusion processes are simulated. This method has such advantages as the simplicity of fixing and controlling the governing parameters as well as the reproducibility of conditions, which is impossible in the real atmosphere. There remains, however, the technical impossibility of simultaneously satisfying all similarity criteria. Most investigators now have a consensus opinion of how to approximate atmospheric processes of different scales in wind tunnels (Cermak et al, 1965; Snyder, 1972, 1981; Zrazhevsky and Klingo, 1971). Since the simulation of flows and pollutant dispersion under conditions of complex relief is one of the most attractive areas for using wind tunnels, many investigations have been made on this subject. Two basic approaches exist. The first is the investigation of specific topographic sites. Such "specific" studies are usually requested by an industrial company or by a controlling air-protection organization. The second category, "generic" studies, focuses on idealized situations to obtain fundamental understanding of the principal governing parameters and the physical processes involved. Such investigations have been developing in recent years in EPA's Fluid Modeling Facility and in the U.S.S.R. (Gorlin and Zrazhevsky, 1968; Berlyand, 1975). The generic approach is the more scientific, although more demanding of time and effort. Generic studies are most useful when combined with theoretical modeling in that theory and experiments serve to direct each other. To simplify the investigation, one frequently considers two-dimensional relief and neutral stratification of the flow. This is, of course, an important step in elucidating the problem, but numerous questions remain. Three-dimensional relief and non-neutral stratification are equally, perhaps more, important, and inroads have also been made in these areas (Hunt et al, 1978; Hunt and Snyder, 1980; Snyder et al. 1979; additional references are contained in these works).

Up until this time, most generic studies of flow and dispersion in complex terrain have been concerned with hills of either very small or quite

large slopes. Studies by Courtney (1979) and Britter et al (1981) exemplify small-slope studies where separation on the lee slope was not expected to occur. The works of Huber et al (1976), Arya and Shipman (1979, 1981), and Wilson et al (1979) exemplify large-slope studies, where separation from the lee slope was definitely expected. A few hills with moderate slopes have been investigated, but these have been conducted in short wind tunnels where the boundary layer was relatively thin and external turbulence was generated by a grid (Zrazhevsky et al, 1968).

Flow structure over such hills is both interesting and important from the points of view of obtaining fuller scientific knowledge and for using the results in the practical prediction of air quality. The work reported here is concerned with hills with slopes ranging from small to large. This work attempts to further the contributions made in this field thus far, both to generate new experimental information and to compare the results of the wind tunnel measurements with calculations based on previous mathematical models (Berlyand et al, 1968; 1975).

Computer programs that calculated pollutant concentrations using the above mentioned mathematical models were constructed for specific ground surface shapes. These shapes were single two-dimensional hills (or valleys) with the following parametric equations:

if

$$|\xi| \leq a$$

$$x = \frac{1}{2}\,\xi\left[1 + \frac{a^2}{\xi^2 + m^2(a^2 - \xi^2)}\right],$$

$$z = \frac{1}{2}\,m\sqrt{a^2 - \xi^2}\left[1 - \frac{a^2}{\xi^2 + m^2(a^2 - \xi^2)}\right];$$

if (1)

$$|\xi| > a$$

$$x = \frac{1}{2}\,\mathrm{sign}(\xi)\left[|\xi| + m\sqrt{\xi^2 - a^2} + a^2\left(|\xi| + m\sqrt{\xi^2 - a^2}\right)^{-1}\right],$$

$$z = 0$$

where

$$m = \frac{h_o}{a} + \sqrt{\left(\frac{h_o}{a}\right)^2 + 1},$$

h_o = height of hill, a = half-width of hill, and ξ = arbitrary parameter. x is directed along the approach flow direction (origin at hill center), and z is directed vertically upwards. Since the surface is two-dimensional, the equation does not include the y variable. When $h_o < 0$, these equations, of course, describe a valley. The hills (or valleys) described by Eq. 1 have smooth forms that are symmetric about the z-axis and smoothly merge into a flat plane at the points $x = \pm a$. These equations describe not a single surface but a two-parameter family of surfaces, the parameters being the height h_o and aspect ratio $n = a/h_o$.

The hills studied in the wind tunnel had shapes described by Eq. 1 and aspect ratios of n = 3, 5 and 8 (maximum slope angles of 26°, 16°, and 10°, respectively). The working program consisted of:

a) Wind tunnel measurements of mean and fluctuating velocities of the neutrally stable flow in the presence of rough hills as well as pollutant concentrations from elevated point sources located in different positions relative to the hills;

b) Wind tunnel measurements of concentrations from an elevated point source located over the rough flat floor;

c) Numerical calculations of surface concentrations in the presence of the hills (as well as for the flat ground surface) on the basis of the theoretical models, and comparisons of these results with the experimental data.

2. SUMMARY AND CONCLUSIONS

Wind tunnel measurements were made of the concentrations fields downwind of elevated point sources located at different positions relative to two-dimensional hills. Three hill shapes, with aspect ratios n of 3, 5 and 8, were used. For reference purposes, measurements were taken over the flat wind tunnel floor. To aid in interpretating and understanding the concentration fields thus produced, mean and turbulent velocity fields were also measured. These experimental results were compared with predictions of theoretical models developed in the U.S.S.R.

Wind and concentration measurements within the artificially-thickened, rough-wall boundary layer showed it to be a reasonable simulation of the neutral atmospheric boundary layer. The following points of agreement were demonstrated:

1. Lateral plume growth rates with Taylor statistical theory when a particular value of the Lagrangian integral scale was assumed;
2. Vertical growth rates for ground-level sources with Lagrangian similarity theory (previously shown);
3. Rate of decay of ground-level concentration at large downwind distances with gradient diffusion theory ($C \propto x^{-3/2}$).

Comparisons of numerical models with experimental data have shown satisfactory agreement (generally, within 10 to 15%) in predicting the locations and values of maximum surface concentrations as the stack height was varied; further improvements may be expected when values of lateral and vertical diffusivities more precisely corresponding to the wind tunnel boundary layer are input to the model.

The flow over the steepest hill (n = 3) separated on the lee slope and formed a recirculation zone or cavity. This cavity extended to 6.5 hill heights downwind of the crest. Within the cavity, the reversed mean flow

was found to have a mean speed of about 20% of the free-stream velocity. The flows over hills 8 and 5 did not separate, but the mean streamline patterns were noticeably asymmetric in contrast with potential theory. The horizontal mean wind velocity near the downwind base of hill 5 was very small: about 10% of the velocity in the absence of the hill at a height of $0.2h_o$; but the longitudinal turbulence intensity was extremely large: twice the mean velocity at $0.2h_o$. Even though the flow was not observed to separate in the mean, instantaneous flow reversals were frequently observed through smoke visualization. Probability density distributions measured with a pulsed-wire anemometer showed that the flow was negative up to 40% of the time, and that the mean was small but positive. Changes in the turbulence structure due to the presence of hill 8 were not highly significant, whereas changes over hills 3 and 5 were quite strong. The speed-up of the flow over the tops and the slow-down on the lee sides were observed to be larger over the steeper hills.

The dispersion characteristics were also, of course, changed by the presence of the hills. The existence of a cavity region drastically influenced the shapes of the vertical concentration profiles and the values of the surface concentrations within the cavity. Concentrations within the cavity region were essentially uniform with height. Surface concentrations were sometimes greatly increased, sometimes somewhat decreased when compared with values over flat terrain. These variations depended upon the stack height and location with respect to the hill center. Instead of being smoothly varying functions of downwind distance, some surface concentration profiles contained characteristic dips that identified the beginning and end of the cavity region.

For hill 8, the deviations of the diffusion patterns from those over flat terrain were much less significant. Changes in the concentration fields were apparently not as much influenced by changes in turbulence structure as by changes in the mean flow field, i.e., the convergence and divergence of streamlines.

The terrain correction factors for the values and locations of maximum surface concentration obtained from the wind-tunnel measurements were compared with factors calculated using a quasi-potential model. Rather

satisfactory agreement between theory and experiment was obtained: 80% of the calculated values were within 25% of the measured values when the stack was located at the upwind base or top of hill 8. When the stack was located at the downwind base, the theory significantly underpredicted the experimentally observed concentration values. This disparity is apparently related to the inability of the quasi-potential model to account for the asymmetry of the flow over the hill.

For hills 3 and 5, there was, as expected, a large disparity between calculated and experimental values when the stack was located at the downwind base of the hills caused by the presence of the recirculation zone and the zone of extremely low wind velocity. In these zones, streamwise diffusion may not be neglected. Nevertheless, there was a certain amount of agreement when the stack was located at the top or upwind base: 70% of the calculated values were within 25% of the measured values.

A comparison was also made between results of a numerical model and experimental measurements for values and locations of maximum surface concentration. Input to the numerical model were wind-tunnel data on the mean and turbulent flow fields over hill 8. The comparisons of maximum surface concentrations showed relatively good agreement (all calculations within 30% of measurements) when the stack was located at the upwind base or top of the hill, and satisfactory agreement (all within 40%) when it was at the downwind base. Further refinement of the technique used for producing the wind field and the application of more appropriate models for eddy diffusivities should improve the agreement with experimental data.

Additional tests showed the flow structure (including separation) to be insensitive to Reynolds number over a limited range, but it is not known for certain that the relatively low-Reynolds-number wind-tunnel flow simulates the very large-Reynolds-number flow in the atmosphere. Nevertheless, it is important that theoretical models be developed to predict separated flows such as this wind tunnel flow, since separation definitely occurs on the lee sides of steep-enough full scale hills.

3. THEORETICAL MODELS

3.1. Diffusion Calculations Over Flat Terrain in Wind Tunnel

Calculations were made of pollutant concentrations from an elevated point source located over flat terrain. These concentrations were calculated with numerical solutions of the diffusion equation using a finite difference method.

The diffusion equation in the case of flat terrain may be written in the following form:

$$u \frac{\partial c}{\partial x} = \frac{\partial}{\partial y} k_y \frac{\partial c}{\partial y} + \frac{\partial}{\partial z} k_z \frac{\partial c}{\partial z} \quad , \tag{2}$$

where u = wind velocity (it is supposed the wind blows along the x-axis) and k_y, k_z = horizontal and vertical components of turbulent diffusivity, respectively.

If $k_y = k_o u$ (here k_o may be constant or a function of x), a separation of variables may be performed. As a result, Equation 2 can be solved by solving the diffusion equation for concentration c' from a line source. In these studies, the equation for c' has been solved with a numerical method. It has the following form

$$u \frac{\partial c'}{\partial x} = \frac{\partial}{\partial z} k_z \frac{\partial c'}{\partial z} \, . \tag{3}$$

The boundary conditions were as follows (assuming that source coordinates are $x = 0$, $y = 0$, $z = z_s$):

$$\begin{aligned} &\text{at } x = 0, \; c' = [Q/u(z_s)]\delta(z - z_s); \\ &\text{at } z = 0, \; k_z \, \partial c'/\partial z = 0; \\ &\text{and when } z \to \infty, \; c' \to 0. \end{aligned} \tag{4}$$

Here Q = source flow rate and δ = Dirac delta function. The transformation from c' to c is determined along y = 0 by the expression:

$$c(x,0,z) = c'(x,z)/2\sqrt{\pi G}\ , \tag{5}$$

where $G = \int_0^x k_0(\xi)d\xi$.

It was also assumed that

$$u = \begin{cases} \frac{u_*}{k} \ln(1 + \frac{z}{z_0}) & \text{when } z \leq h \\ \frac{u_*}{k} \ln(1 + \frac{h}{z_0}) & \text{when } z > h \end{cases} \tag{6}$$

and

$$k_z = \begin{cases} ku_*(z + z_0) & \text{when } z \leq h \\ ku_*(h + z_0) & \text{when } z > h \end{cases},$$

where u_* = *friction velocity*, z_0 = *roughness length*, h = *surface layer height*, and k = von Kármán's constant (0.4). Values of u_*, z_0, and h were determined in accordance with wind tunnel measurements. Different models for k_0 were used, as will be discussed in Section 5.

3.2. General Description of Models for Calculating Pollutant Dispersion Over Hilly Terrain.

To calculate concentrations of pollutant from an elevated point source located near a hill, two different models developed in the U.S.S.R. were used. Both of them are based on gradient diffusion theory (also called K-theory) and calculate pollutant concentrations by solving the diffusion equation

$$u \frac{\partial c}{\partial x} + w \frac{\partial c}{\partial z} = \frac{\partial}{\partial x} k_x \frac{\partial c}{\partial x} + \frac{\partial}{\partial y} k_y \frac{\partial c}{\partial y} + \frac{\partial}{\partial z} k_z \frac{\partial c}{\partial z}\ , \tag{7}$$

where, as usual, c = pollutant concentration, u, w = horizontal and vertical wind velocity components, respectively, and k_x, k_y, k_z = turbulent diffusivity components.

Quasi-Potential Model

The first model was described by Berlyand et al (1968) and further developed by Berlyand and Kisselev (1973) as well as by Berlyand et al (1979). It was intended for application to atmospheric flows with neutral stratification. It assumes there is no flow separation in the lee of the hill.

In the presence of a hill, the domain in which pollutant diffusion occurs is curvilinear. This domain can be transformed to an upper semiplane using conformal mapping. For a hill having a shape determined by Eq. 1, this mapping is analytical, a fact that greatly simplifies the method of solution.

Let the function

$$\tau(x,z) = \phi(x,z) + i\psi(x,z) \tag{8}$$

represent this conformal mapping. ϕ and ψ can be interpreted as the velocity potential and stream function, respectively, of a potential flow in the domain under consideration. Coordinates ξ and ζ are introduced as

$$\xi = \phi(x,z)/U \ , \ \zeta = \psi(x,z)/U \ , \tag{9}$$

where U = wind speed in the approach flow far upstream.

Let us now substitute these coordinates into Equation 7 and use (ξ, ζ) instead of rectangular coordinates (x, z). With the additional assumptions that (1) the streamlines of our flow coincide with the streamlines of potential flow in the same domain, (2) $k_x = k_z = k_\zeta$, and (3) spreading of pollutant along streamlines caused by turbulent diffusion is negligible, then Equation 7 may be reduced to the following form

$$u_\xi \frac{\partial c}{\partial \xi} = \frac{1}{V_p^2} \frac{\partial}{\partial y} k_y \frac{\partial c}{\partial y} + \frac{\partial}{\partial \zeta} k_\zeta \frac{\partial c}{\partial \zeta} \ . \tag{10}$$

Here $u_\xi = v_\xi / V_p$, where v_ξ = wind velocity parallel to the streamlines and V_p = dimensionless velocity (normalized by U) module of the potential flow.

Assuming further that $k_y = k_o V_p v_\xi$ (a generalization of the assumption made in the case of flat terrain, analogous to the procedure used in Equation 2), we can separate variables in Equation 10. As a result, we shall solve the diffusion equation for concentration c' from a line source, which is much

easier than solving Equation 10.

The relation between concentrations from point and line sources is given by the following expression

$$c(\xi,y,\zeta) = \frac{c'(\xi,\zeta)}{2\sqrt{\pi G}} \exp(-\frac{y^2}{4G}) , \qquad (11)$$

where $G = \int_{\xi_S}^{\xi} k_o(\eta - \xi_S)d\eta$,

and ξ_S = the source coordinate.

The equation for c' is as follows

$$u_\xi \frac{\partial c'}{\partial \xi} = \frac{\partial}{\partial \zeta} k_\zeta \frac{\partial c'}{\partial \zeta} . \qquad (12)$$

We shall use for u_ξ and k_ζ the same formulas as Eq. 6, with ζ in place of z; thus Equation 12 is mathematically identical to Equation 3. The boundary conditions are also analogous to those in the case of flat terrain. Assuming that source coordinates are $\xi = \xi_S$, $y = 0$, $\zeta = \zeta_S$, the conditions are

$$\begin{aligned} &\text{at } \xi = \xi_S \text{ , } c' = [Q/u(\zeta_S)]\ \delta(\zeta - \zeta_s); \\ &\text{at } \zeta = 0 \text{ , } k_\zeta \partial c'/\partial\zeta = 0; \qquad (13) \\ &\text{and when } \zeta \to \infty, \ c' \to 0. \end{aligned}$$

These notations have the same sense as in Equation 4.

The problem (Eq. 12) with boundary conditions (Eq. 13) is mathematically equivalent to Equations 3 and 4 and may be solved using the same numerical methods. In practice, surface concentrations are the most frequently used pollutant dispersion characteristics; therefore, for the case of flat terrain, Berlyand (1975) has constructed approximation formulas for surface concentrations based on numerical solutions of the diffusion equation. Because of the mathematical identity between Eqs. 12 and 13 and Eqs. 3 and 4, these approximation formulas are also appropriate for the model under consideration. Using such formulas to calculate surface concentrations saves a great deal of computer time compared to the amount required for numerical solutions.

This model will be referred to henceforth as the "quasi-potential model" (QPM).

Wind-Measurement Diffusion Model

The second model used for calculations of pollutant concentrations in hilly terrain was described by Berlyand et al (1975). It incorporates data from wind tunnel measurements of wind velocities and turbulence characteristics of the flow near a hill as input to calculate the entire flow field as well as the concentration field from a source. This second model will be referred to as the Wind-Measurement-Using Diffusion Model (WMDM).

Such a "mixed" model offers advantages in investigations of pollutant spreading over complex terrain and helps to clarify the understanding of its regularities. When sufficiently developed, this approach simplifies wind tunnel modeling, since it excludes (1) concentration measurements which demand special instrumentation as well as additional time and (2) difficulties connected with these measurements (satisfying additional similarity criteria, constructing a source with or without some specified plume rise, influence of background concentrations, etc.). To apply this model and to facilitate interpretation of results obtained on concentration fields, a relatively large quantity of wind measurements are required. However, it may be noted that wind measurements are usually conducted relatively quickly. In the future, it may be possible to determine the optimal quantity of wind measurements needed to obtain reliable results of concentration calculations. This approach also offers good possibilities for testing different diffusion models for hilly terrain when the mean wind field is known.

Setting aside the questions of similarity between atmospheric flow and the corresponding flow in a wind tunnel, this model may be divided into three parts:

1) Generating a mass-consistent wind field on the basis of wind tunnel data;
2) Calculating the turbulent diffusivity on the basis of measurements and theoretical assumptions;
3) Numerical solution of the diffusion equation.

Details of these parts are discussed in the following sections.

3.2.1. Generation of a mass-consistent wind field

The generation of a mass-consistent wind field is the most important part of the problem. In recent years the question of producing a mass-consistent wind field using wind measurements has been studied by a few American scientists (Dickerson, 1978; Sherman, 1978; Pepper and Baker, 1979). Their technique, developed on the basis of the works of Sasaki (1958, 1970a, 1970b), is quite similar to the present model, but the area of application is rather different. Their wind-field models are used to predict regional or meso-scale pollutant transport. For input, they use available meteorological data in the regions being investigated.

Complementary mathematical/wind-tunnel modeling has good possibilities for further development of mass-consistent wind-field models because the experiments are well-controlled and the data are more accurate, allowing better comparisons with calculations. This approach makes it easier to determine the influence of the wind-field-producing technique on the final results and to test virtual improvements of the techniques, for example, the use of more sophisticated methods of interpolation and differentiation of the measured wind field.

Calculation of the entire mass-consistent wind field is necessary to solve the diffusion equation. Before making such an attempt, it is useful to examine the equation again.

If only smooth obstacles are considered, the diffusion equation can be used in the following form:

$$u \frac{\partial c}{\partial x} + w \frac{\partial c}{\partial z} = \frac{\partial}{\partial y} k_y \frac{\partial c}{\partial y} + \frac{\partial}{\partial z} k_z \frac{\partial c}{\partial z} . \qquad (14)$$

Assuming again that $k_y = k_o u$, we can again separate variables and reduce the problem to solving for concentration c' from a line source. This equation is as follows

$$u \frac{\partial c'}{\partial x} + w \frac{\partial c'}{\partial z} = \frac{\partial}{\partial z} k_z \frac{\partial c'}{\partial z} . \qquad (15)$$

The relation between concentrations from point and line sources is expressed analogously as in Equation 5.

The problem of calculating diffusion in hilly terrain is that the area of diffusion in coordinates (x, z) is not rectanglular. To apply numerical methods, it is easier to make a substitution of variables in Equation 15 in order to transform the domain of its solution to a half-plane. If it is known that the perturbation of air flow due to the influence of irregularities in the underlying surface does not exceed level z = H, this transformation can be performed using the following substitution of variables

$$x' = x;\ z' = \frac{H(z - h(x))}{H - h(x)}\ , \tag{16}$$

transforming the area $(-\infty < x < \infty)\ x\ (h(x) \leq z \leq H)$ to the strip $(-\infty < x' < \infty)\ x\ (0 \leq z' \leq H)$. Within strip $0 \leq z' \leq H$, Equation 15 can be rewritten as

$$\hat{u}\frac{\partial c'}{\partial x'} + \hat{w}\frac{\partial c'}{\partial z'} = \frac{\partial}{\partial z'}\hat{k}_z\frac{\partial c'}{\partial z'}\ , \tag{17}$$

where

$$\hat{u} = \frac{H - h(x)}{H} \cdot u,$$

$$\hat{w} = w + \frac{z' - H}{H} \cdot u \cdot \frac{dh}{dx}\ , \tag{18}$$

and

$$\hat{k}_z = \frac{H}{H - h(x)}\,k_z.$$

Note that the quantities $\hat{u}$ and $\hat{w}$ are defined such that they satisfy the continuity equation

$$\frac{\partial \hat{u}}{\partial x'} + \frac{\partial \hat{w}}{\partial z'} = 0\ , \tag{19}$$

when the initial components of velocity u and w satisfy the equation $\partial u/\partial x + \partial w/\partial z = 0$.

The problem of producing a mass-consistent wind field for the specific case at hand can be formulated as follows. In the rectangle $R = \{0 \leq x' \leq L;\ 0 \leq z' \leq H\}$, the functions a(x', z') and b(x',z') are fixed, calculated from the measured velocity components of a flow by means of the first two relationships of Eq. 18. The quantities a(x', z') and b(x', z') have the sense of horizontal and vertical velocity components converted to the coordinate system of Eq. 16. It is necessary to construct the functions $\hat{u}(x', z')$

and $\hat{w}(x', z')$ to satisfy the continuity equation 19 such that they approximate $a(x', z')$ and $b(x', z')$.

The solution of this problem utilizes the fact that in a two-dimensional flow, a stream function $\psi(x', z')$ may be constructed. Velocity components are determined from this function using the equation

$$\hat{u} = \frac{\partial \psi}{\partial z'} \quad ; \quad \hat{w} = - \frac{\partial \psi}{\partial x'} \ . \tag{20}$$

The measured velocities a and b should be approximated (according to Eq. 20) with derivatives of the stream function in the best manner (in the mean-square sense). Next there arises the variational problem of the minimization of the functional

$$I(\psi) = \int_R \int dx'dz' \ [(\frac{\partial \psi}{\partial z'} - a)^2 + p^2 \ (\frac{\partial \psi}{\partial x'} + b)^2]. \tag{21}$$

The non-negative "weight" p^2 introduced here allows for the fact that the velocity components a and b may be determined with different accuracies. Note that the area of integration R should be selected such that at its boundary ∂R the function ψ agrees with the stream function of the approach flow $\psi^o(z')$, corresponding to the velocity $\hat{u}^o = \frac{d\psi^o}{dz'}$.

Using standard variational analysis techniques, the variational problem can be transformed to the Euler equation for the desired stream function

$$p^2 \frac{\partial^2 \psi}{\partial x'^2} + \frac{\partial^2 \psi}{\partial z'^2} = \frac{\partial a}{\partial z'} - p^2 \frac{\partial b}{\partial x'} \ . \tag{22}$$

In the simplest case (p = 1), this equation has an obvious physical interpretation. The mass-consistent wind field approximation may be fulfilled by preservation of the measured vorticity.

Let us introduce the symbols

$$\psi = \psi^o(z) + \psi'(x', z'); \ a = \frac{d\psi^o}{dz'} + a'. \tag{23}$$

The quantities of a' and ψ' represent deviations from the corresponding characteristics in the approach flow. Then Eq. 22 becomes (p = 1)

$$\frac{\partial^2 \psi'}{\partial x'^2} + \frac{\partial^2 \psi'}{\partial z'^2} = \frac{\partial a'}{\partial z'} - \frac{\partial b}{\partial x'} \ , \tag{24}$$

with the boundary condition

$$\psi'|_{\partial R} = 0. \tag{25}$$

Equations 24 and 25 can be numerically solved by a computer using finite difference methods. Mathematically, these equations are equivalent to the Dirichlet problem for the Poisson equation. Since area R is rectangular, it is convenient to utilize a direct method, the fast Fourier transform (FFT) technique (Ogura, 1969), for its solution.

3.2.2. Calculating the turbulent diffusivity

Calculating the turbulent diffusivity on the basis of measurements depends of course on what measurements are made in the wind tunnel experiments. When developing the model, the authors had data on mean velocity components and turbulence intensities only; thus, it was necessary to use a method of turbulent diffusivity calculation based on these data. In the model, the following equation for diffusivity was used:

$$k_z = kc^{1/4}\varepsilon^2 u^2 \int_{h(x)}^{z} \frac{dz}{\varepsilon u} . \tag{26}$$

This equation is a result of the differential equation for k_z suggested by Berlyand and Genikhovich (1971). Here ε is turbulence intensity (root-mean-square of horizontal velocity normalized by local horizontal mean velocity), k = von Karman's constant (0.4) and c = 0.046.

To calculate turbulent diffusivity in the atmosphere, the authors assume that similar changes in diffusivity due to the influence of irregularities in the underlying surface are seen both in the wind tunnel and in the atmosphere. In other words, the following model applies to the atmospheric diffusivity:

$$k_{atm}(x,z) = \frac{k_{wt}(x,z)}{k^o_{wt}(z)} \cdot k^o_{atm}(z) , \tag{27}$$

where k_{atm} and k_{wt} are the diffusivities in the atmosphere and wind tunnel, respectively, and the superscript "o" represents the value in the approach flow.

3.2.3. Numerical solution of the diffusion equation

Some difficulties exist in the numerical solution of diffusion equation 17 because of the presence of the term $\hat{w}\partial c'/\partial z'$. $\hat{w}$ may be either positive of negative, even at fixed x' in its dependence on z'. In this case, it is difficult to find a finite difference scheme that is absolutely stable over the entire domain of the solution. The problem may be resolved by transforming Equation 17 (Samarskii, 1977) into the following:

$$\hat{u}\frac{\partial c'}{\partial x'} = \frac{1}{f}\frac{\partial}{\partial z}\hat{f}\hat{k}_z\frac{\partial c'}{\partial z'} \quad , \tag{28}$$

which is equivalent to Equation 17. Here

$$f = \exp\left(-\int_0^z \frac{\hat{w}}{\hat{k}}\,dz'\right) . \tag{29}$$

For the above equation, there are various finite difference schemes that are absolutely stable over the entire domain. For example, the authors use an explicit-implicit scheme except for a few steps on x' near the source. It is more complicated than implicit schemes, but unlike them, it preserves the integral horizontal pollutant flux, which is desirable from a physical point of view.

All numerical calculations of pollutant dispersion over hills and flat terrain were conducted with computer programs developed in the Main Geophysical Observatory (GGO), Leningrad, U.S.S.R. by L. H. Khurshudyan and I. G. Gracheva and adjusted for use on EPA's Univac computer by L. H. Khurshudyan.

Results of these calculations are presented in Section 5.

4. APPARATUS, INSTRUMENTATION AND MEASUREMENT TECHNIQUES

The detailed features of the EPA Meteorological Wind Tunnel, the instrumentation and general procedures for velocity and concentration measurements, and the minicomputer used for the acquisition and analysis of wind tunnel data are described by Snyder (1979). Hence, only the main features of the equipment and special instrumentation or different procedures will be described here.

4.1. Wind Tunnel and Simulated Atmospheric Boundary Layer

The wind tunnel test section is 3.7 m wide, 2.1 m high and 18.3 m long. The air speed in the test section may be varied from 0.5 to 10 m/s.

A simulated atmospheric boundary layer, nominally 1 m thick, was obtained using a fence (vertical barrier) of height 15.3 cm that was placed 22.3 cm downwind of the entrance to the test section and gravel roughness covering the tunnel floor downwind of the fence. The roughness was conveniently obtained commercially as a building construction material (trade name: Sanspray), where river-washed gravel of approximately 10 mm and smaller diameter was epoxy-cemented onto 10 mm thick plywood. Previous tests showed that an equilibrium boundary layer (i.e., very slowly developing) that is a reasonable approximation of a neutral atmospheric boundary layer was established at a distance of 7 to 8 m from the fence (Arya and Shipman, 1979; Courtney, 1979). Additional measurements of the boundary layer structure and dispersion characteristics were made during the current study and are presented in section 5.

4.2. Velocity Measurements

Measurements of the boundary layer and flow structure over the hills were made with TSI, Inc. model 1054A anemometers in conjunction with model 1241-T1.5 (end-flow style) and 1243-T1.5 (boundary layer style) cross-hot-

wire probes. The output signals from the anemometers were digitized at the rate of 500 hertz and linearized and processed on the PDP 11/40 minicomputer. Sampling (averaging) times of two minutes were found to yield reasonably repeatable results--generally within ±5% on the measurement of turbulence intensity.

All measurements made previous to the current study had been done using hot-film probes (thin metallic-oxide coating on quartz fiber of 0.5 mm diameter). The sensitivity of the film probes to transverse velocity fluctuations (hence, also Reynolds stresses), however, had been found by Lawson and Britter (1981) to depend upon the mean wind speed, decreasing rather strongly in the range below about 3 m/s. Lawson and Britter derived "yaw-response" correction factors as functions of mean wind speed and probe type on the basis of specially designed experiments to compensate for this decreased sensitivity. However, their experiments did not specifically examine the response of the probe when it was not aligned with the mean wind direction. Because the normal situation when measuring flow over hills is that the probe is not aligned with the mean wind (it is normally aligned parallel to the flat wind tunnel floor), additional tests were desirable. Such additional tests were made and the results are covered in this discussion.

A special mechanism was constructed and attached to the wind-tunnel carriage. This mechanism permitted rotation of the probe through a known angle ϕ in the vertical plane (x-z), while maintaining the probe tip (the sensor itself) at a fixed position.

A simple analysis shows that the mean velocities indicated by the probe should be

$$U_p = U\cos\phi + W\sin\phi,$$

$$W_p = -U\sin\phi + W\cos\phi, \qquad (30)$$

and

$$\phi_p = \tan^{-1}\frac{W_p}{U_p} = -\phi.$$

The stresses indicated by the probe should be

$$\overline{u_p^2} = \overline{u^2}\cos^2\phi + \overline{w^2}\sin^2\phi + 2\overline{uw}\sin\phi\cos\phi,$$

$$\overline{w_p^2} = \overline{u^2}\sin^2\phi + \overline{w^2}\cos^2\phi - 2\overline{uw}\sin\phi\cos\phi, \qquad (31)$$

and

$$\overline{uw}_p = \overline{uw}(\cos^2\phi - \sin^2\phi) - (\overline{u^2} - \overline{w^2})\sin\phi\cos\phi,$$

where capital letters and overbars indicate mean values, lower case letters indicate deviations from the mean, U (or u) is the velocity component in the horizontal plane, W (or w) is the component in the vertical plane, and the subscript "p" denotes the value indicated by the probe when it is rotated from the horizontal through the angle ϕ.

The Reynolds stresses indicated by each of the probes are shown as functions of the probe rotation angle in Figure 1. Also shown for comparison on the figure is the last of Equations 31. Results from the hot-wire compare quite favorably with the corrected results (Lawson and Britter, 1981) from the hot-film at zero angle. The hot-wire results, however, are consistently closer to Equation 31 at non-zero angles.

Figure 2 shows that the angles indicated by the two probes are essentially identical, but that both underestimate the true angle by 13%. Separate tests showed that the indicated angle was independent of wind speed in the range from 2 to 8 m/s. Consequently, to a first approximation, the actual flow angle may be estimated by multiplying the indicated angle by 1.15.

Measurements of other parameters, mean velocity and horizontal and vertical fluctuating velocities, showed the hot-wire response to be slightly better than the corrected hot-film response at non-zero angles (Figures 3 to 5), so that the hot-wire probes were used exclusively for velocity measurements over the hills. End-flow probes were used wherever possible, but they could not be placed close to the hill surfaces upwind of the crests because of their physical configuration. Hence, boundary-layer style hot-wire probes were used in those regions.

Comparisons of measurements of mean velocity, longitudinal and vertical fluctuating velocities, and Reynolds stresses are made in Figures 6 through 9, respectively. Vertical profiles measured with both types of hot-wire probes at a distance of 3a (a is half-length of hill) upwind of the center of the hill with slope n = 8 are compared with profiles measured with hot-wire and hot-film probes at a corresponding position but in the absence of any hill. The hot-film measurements were taken from Courtney (1979), where the freestream wind speed was 8 m/s. Courtney's measurements were scaled to match the freestream speed of 4 m/s in the current study. In general,

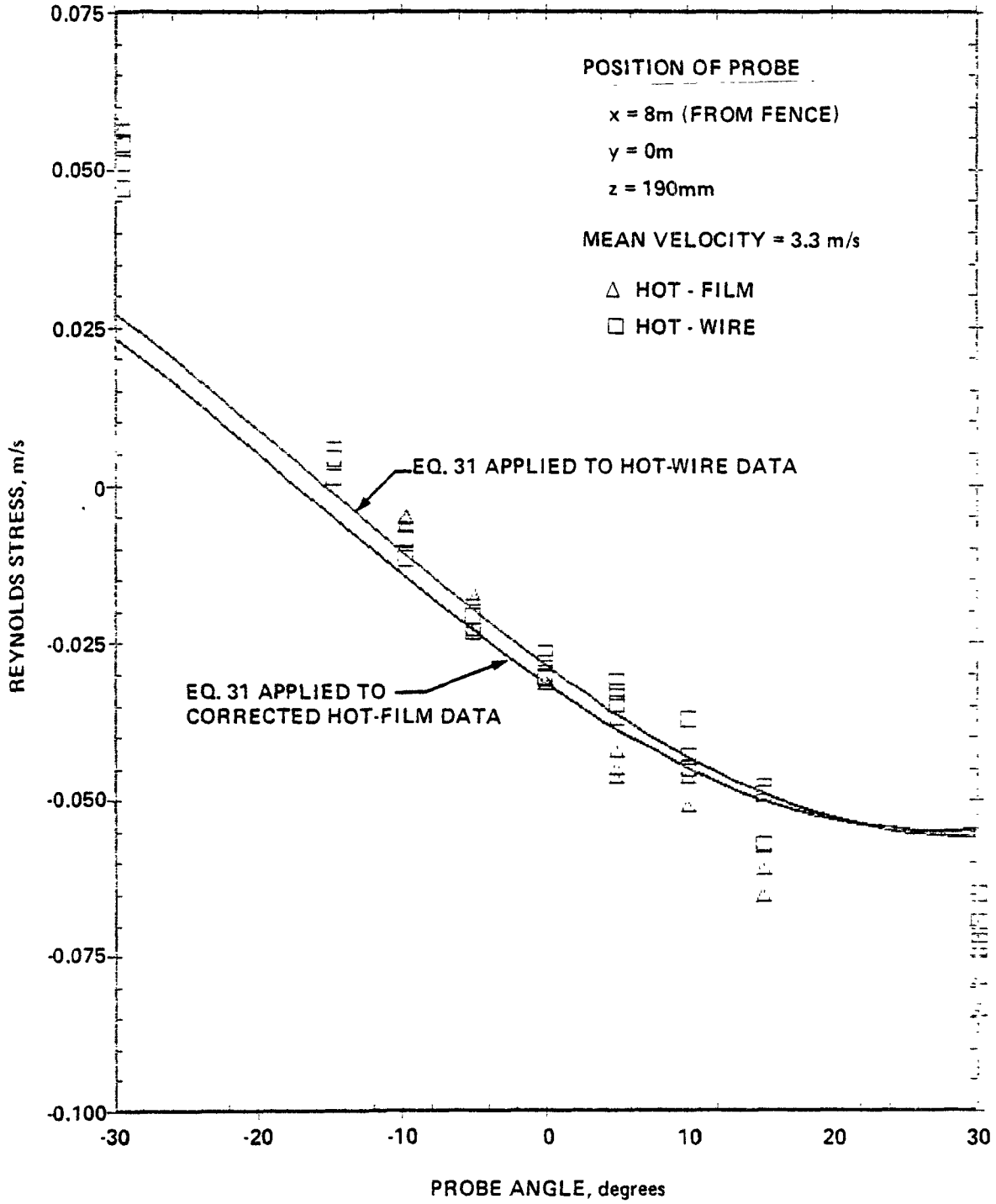

Figure 1. Reynolds stresses indicated by yawed end-flow probes.

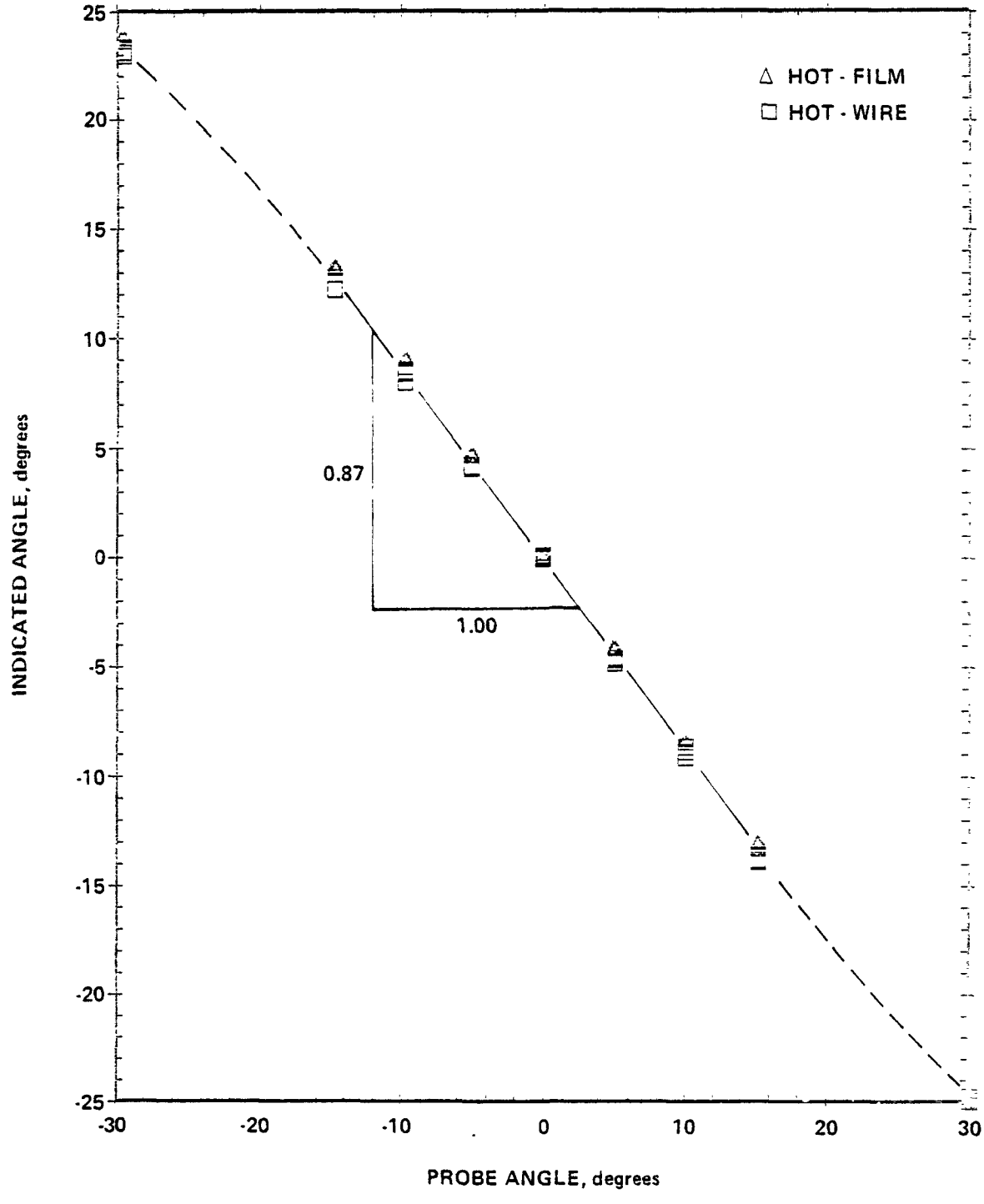

Figure 2. Flow angles indicated by yawed end-flow probes.

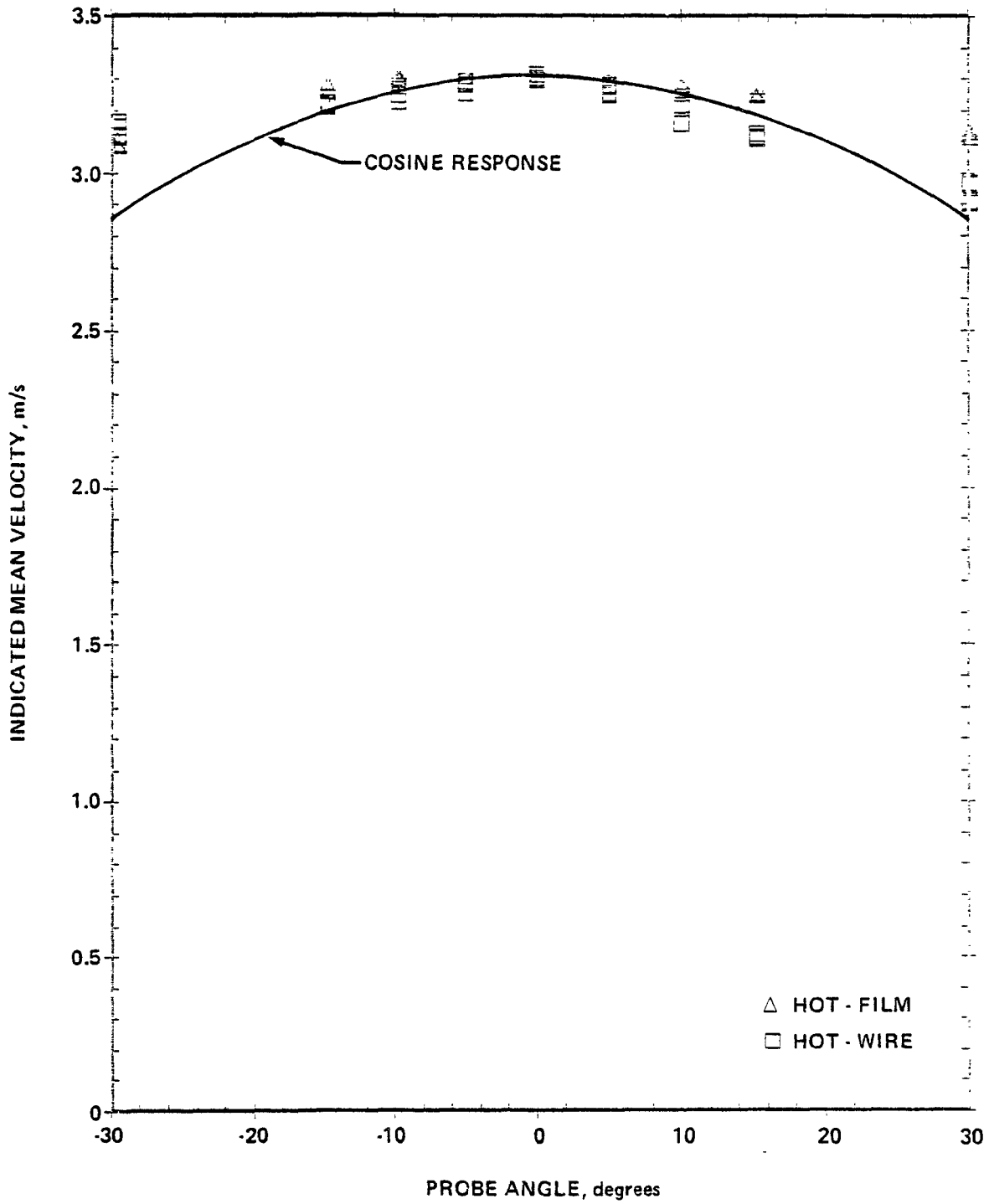

Figure 3. Mean velocities indicated by yawed end-flow probes.

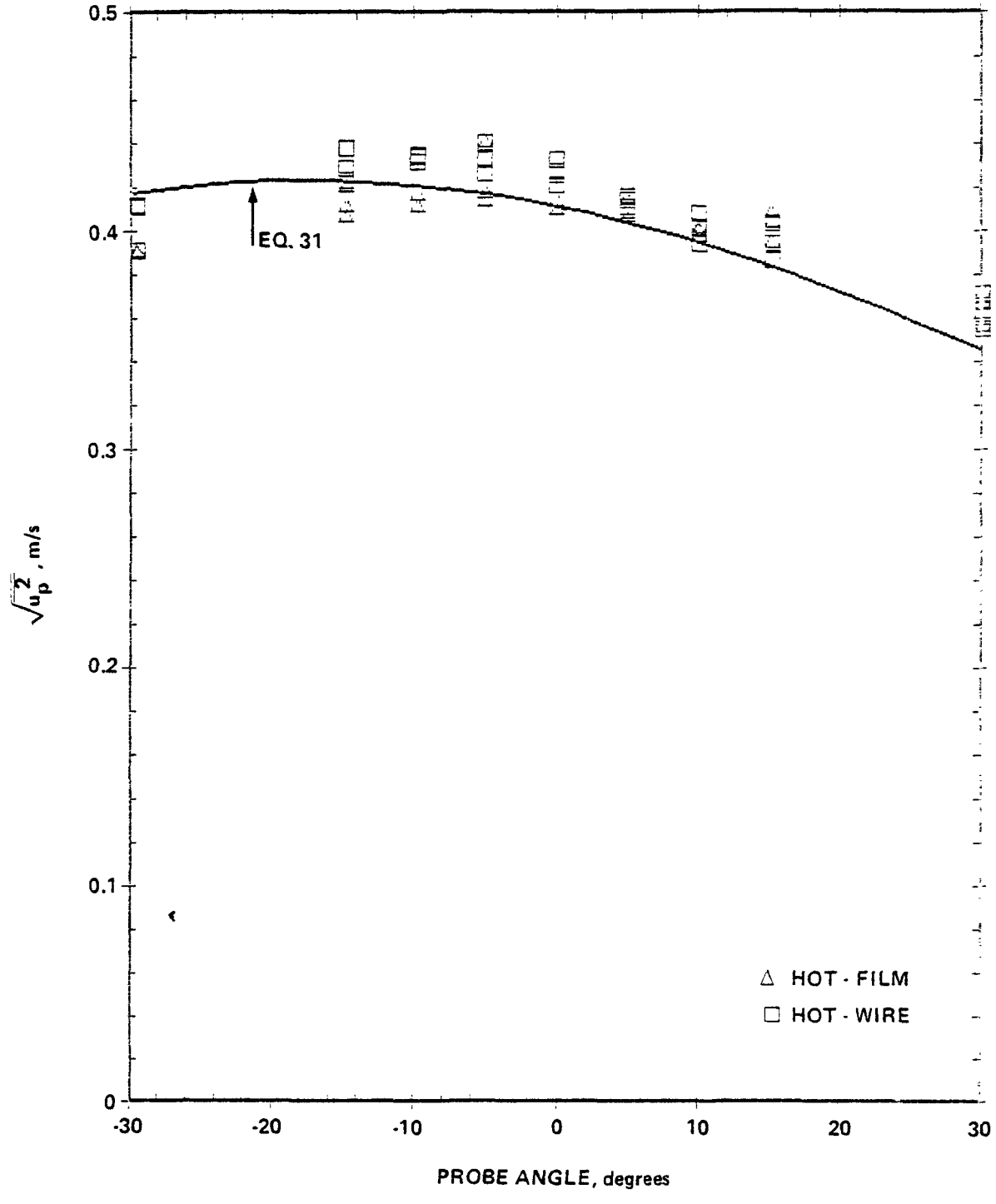

Figure 4. Longitudinal fluctuating velocities indicated by yawed end-flow probes.

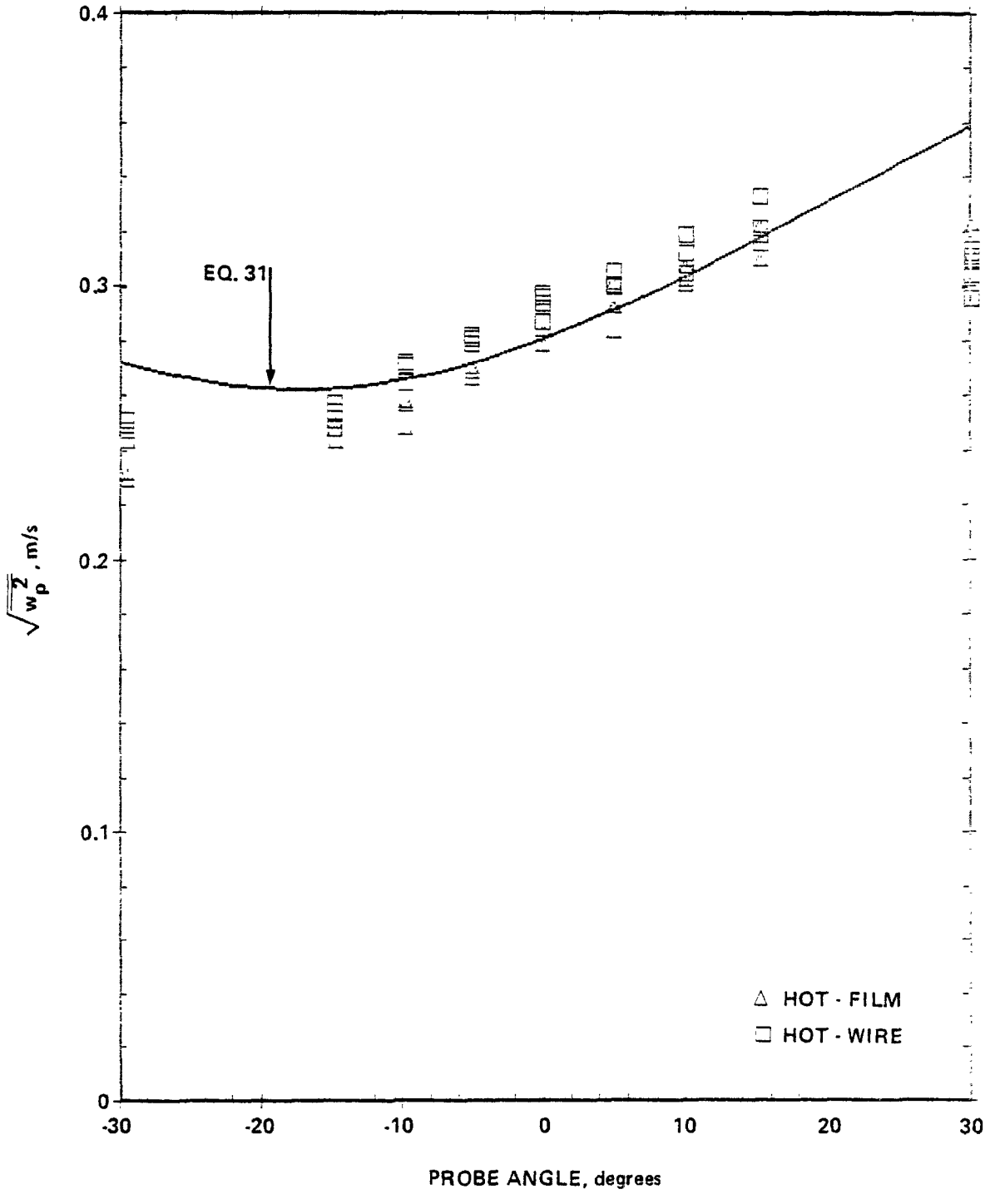

Figure 5. Vertical fluctuating velocities indicated by yawed end-flow probes.

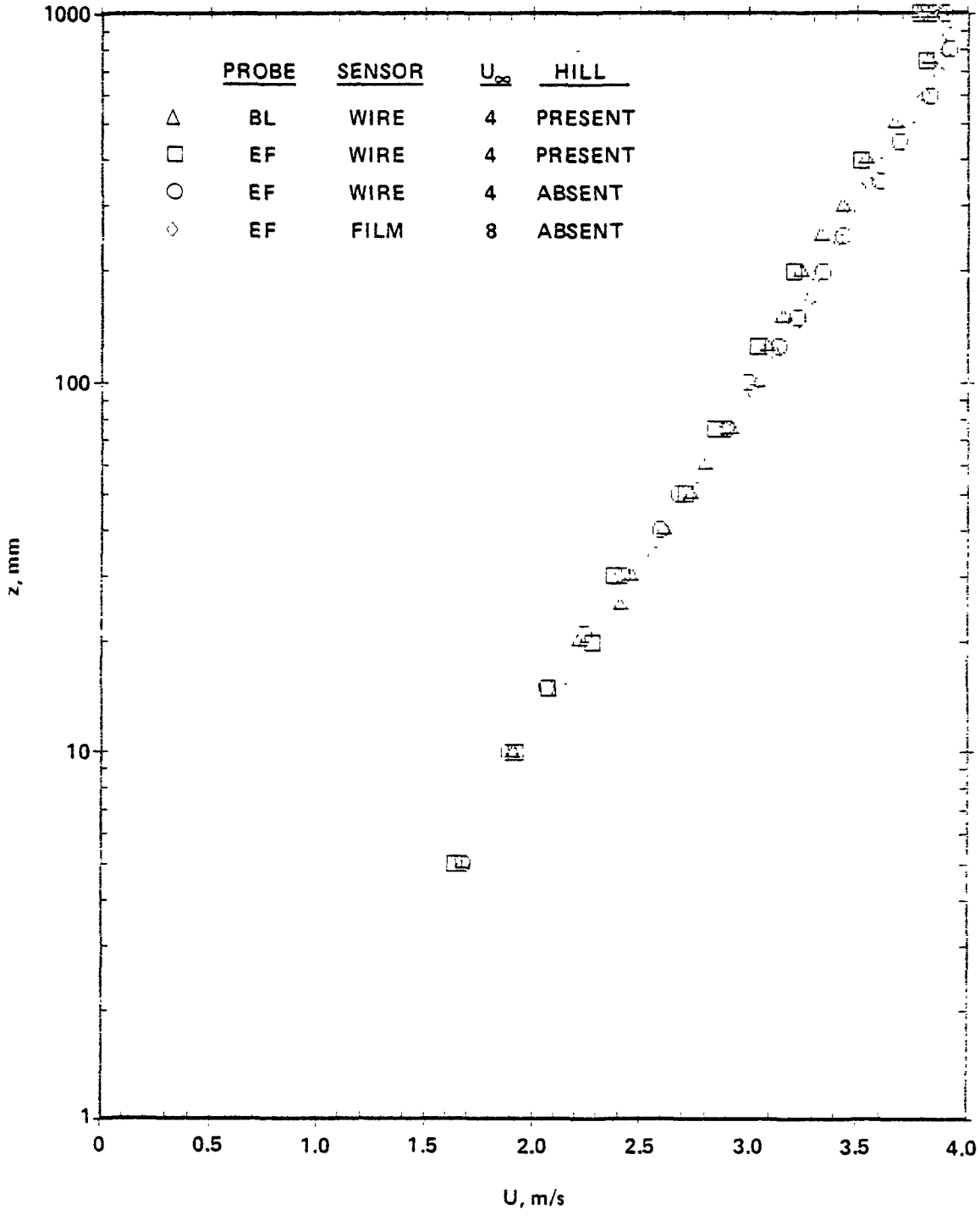

Figure 6. Comparison of mean velocities measured with different probe types.

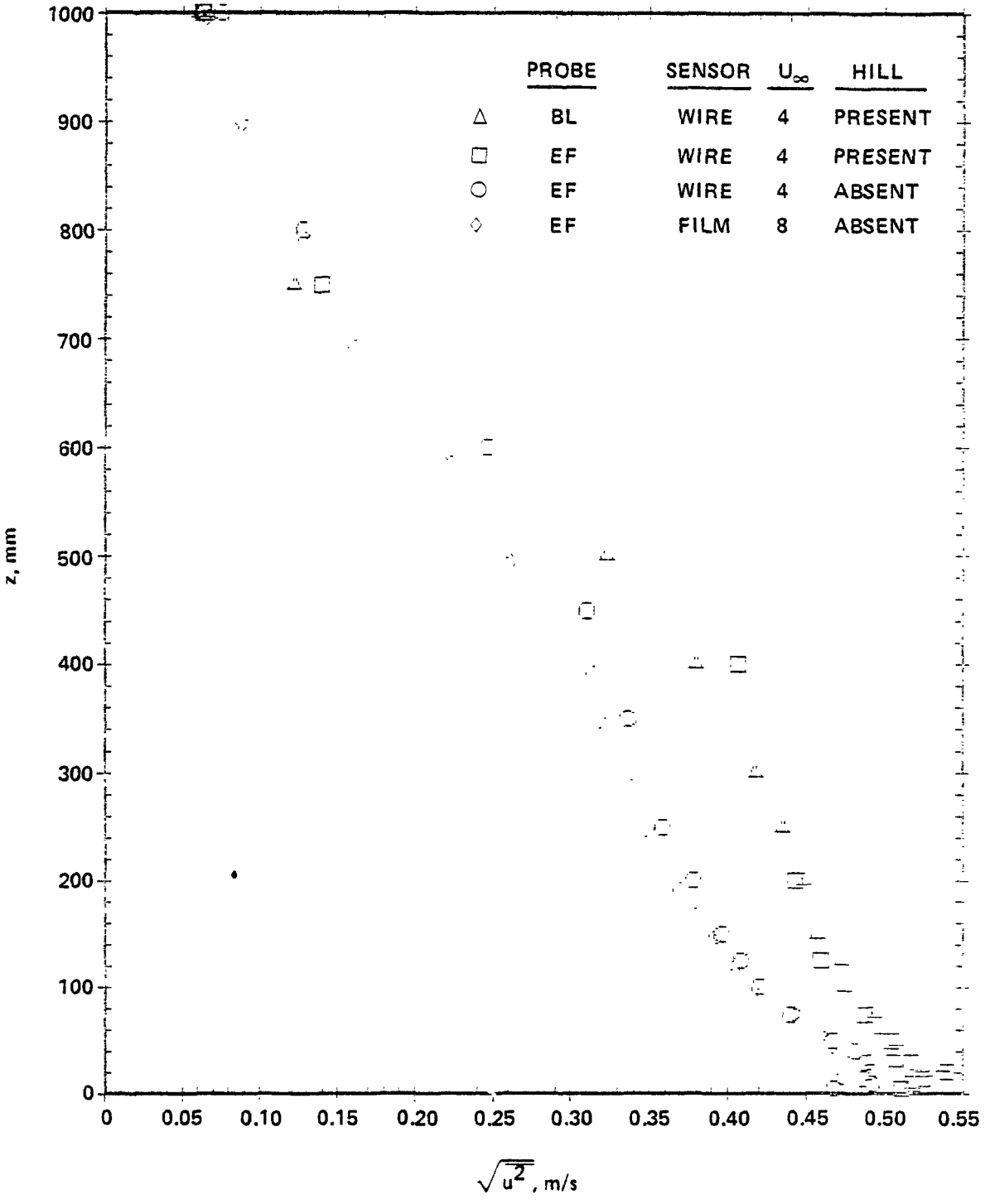

Figure 7. Comparison of longitudinal fluctuating velocities measured with different probe types.

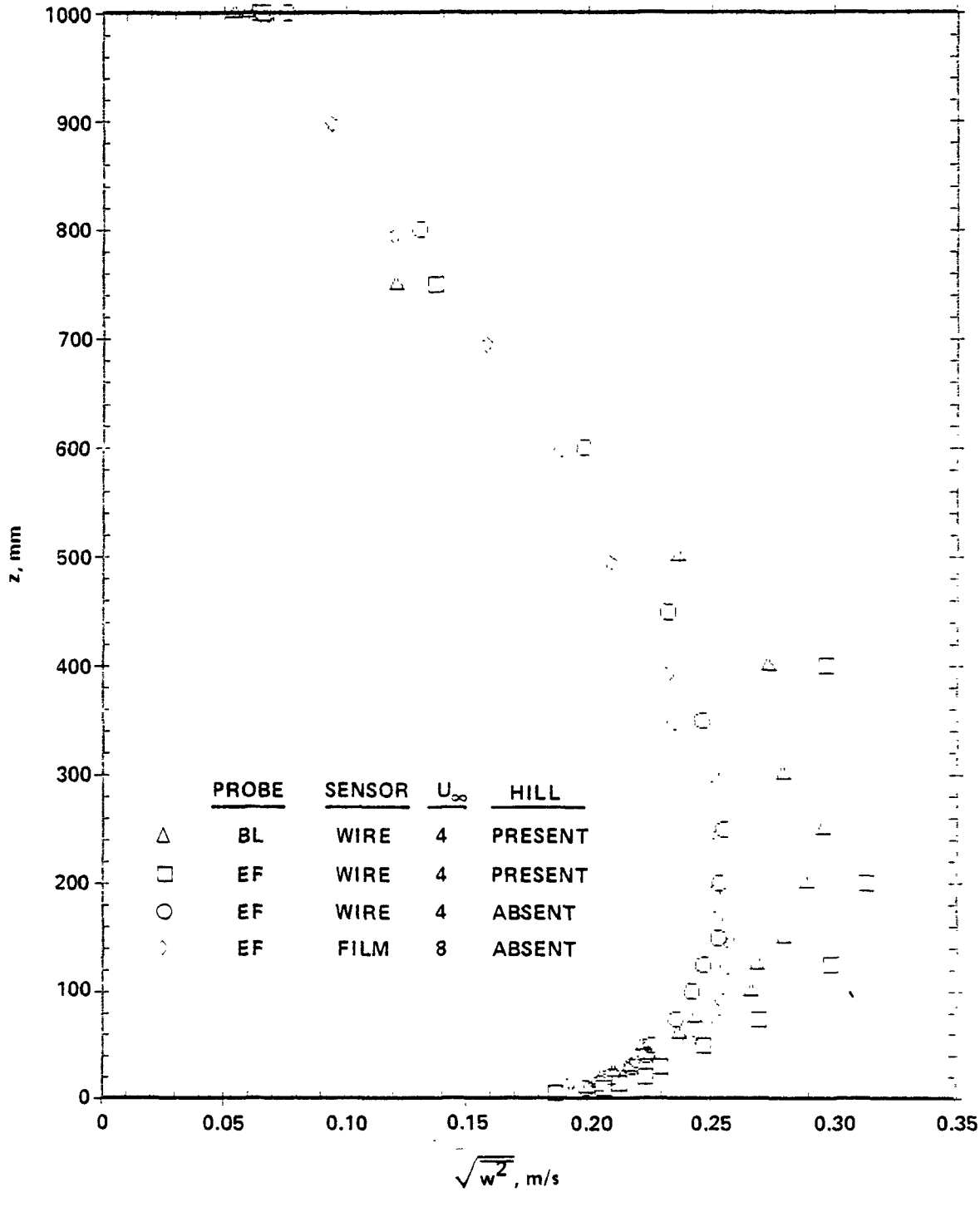

Figure 8. Comparison of vertical fluctuating velocities measured with different probe types.

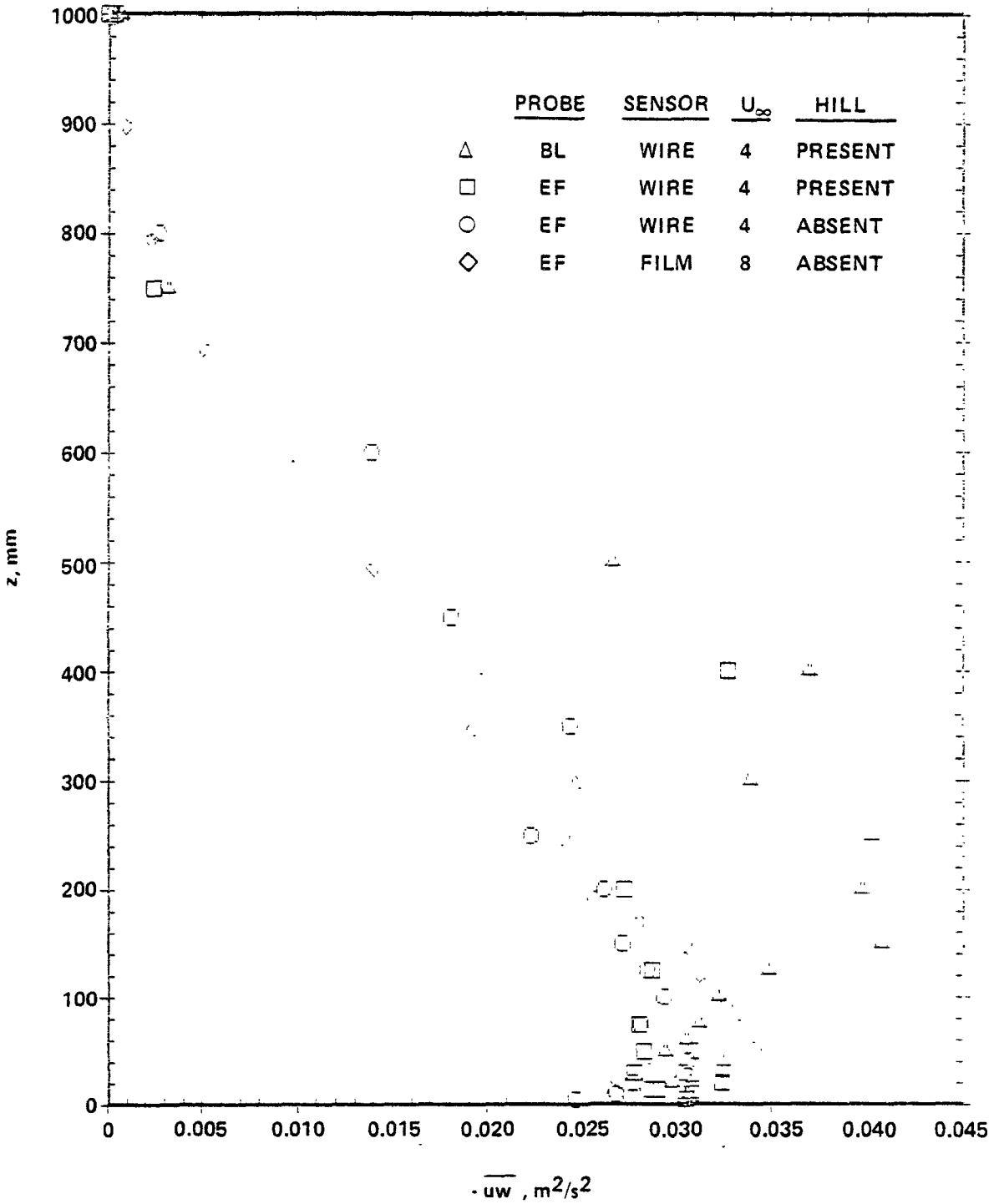

Figure 9. Comparison of Reynolds stresses measured with different probe types.

the comparisons in Figures 6 through 9 show good agreement between measurements made with various styles and sensor types. Second, they show that the boundary layer structure was Reynolds-number independent, i.e., the flow structure was independent of the free-stream velocity, at least in the range of 4 to 8 m/s. Third, the influence of the hill was seen in the Reynolds stresses and vertical fluctuating velocities, less in the longitudinal fluctuating velocities, but not-at-all in the mean velocities. Fourth, the hot-wire and corrected hot-film measurements compared quite well for end-flow probes, but some discrepancy was seen between the boundary-layer and end-flow hot-wire measurements of vertical fluctuating velocities and Reynolds stresses. This discrepancy may have been caused by improper alignment--due to poor construction of the boundary-layer style probe during calibration and subsequently during measurements, but the comparison was adequate for the purposes of the present study.

The hot-wire probes were calibrated each day of measurements and frequently more often, against a pitot-static tube mounted in the freestream of the wind tunnel above the boundary layer. The calibrations were made over the velocity range of interest, typically 5 to 7 points over the range 1 to 5 m/s, and "best-fit" to King's law

$$E^2 = A + BU^{\alpha} , \qquad (32)$$

where E = output voltage of anemometer and U = wind speed indicated by Pitot tube. A, B, and α are constants that were determined through an iterative least-squares procedure. A typical calibration curve is shown in Figure 10. Corrections for varying ambient temperatures were made according to the method of Bruun (1975).

4.3. The Models

Four model hills were constructed; all had shapes given by Equation 1, and extended across the width of the test section of the wind tunnel. Three had heights of 117 mm and aspect ratios ($n = a/h_o$) of 3, 5 and 8 (maximum slopes of 26°, 16° and 10°, respectively). The fourth had a height of 234 mm and an aspect ratio of 3. They will be referred to henceforth as hill 3, hill 5, hill 8, and big hill 3. Figure 11 shows the hill shapes to scale

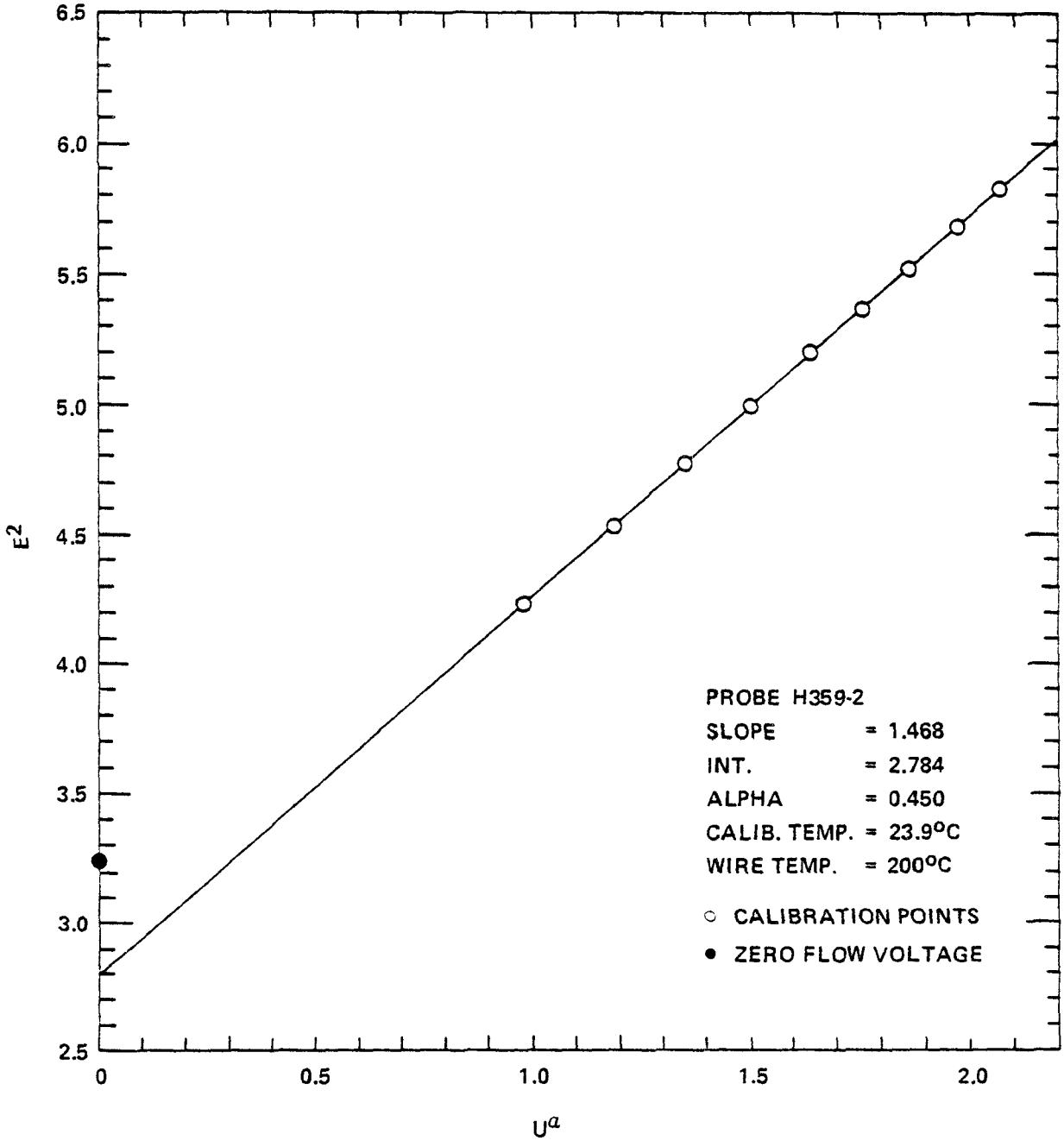

Figure 10. Typical calibration curve for hot-wire anemometer.

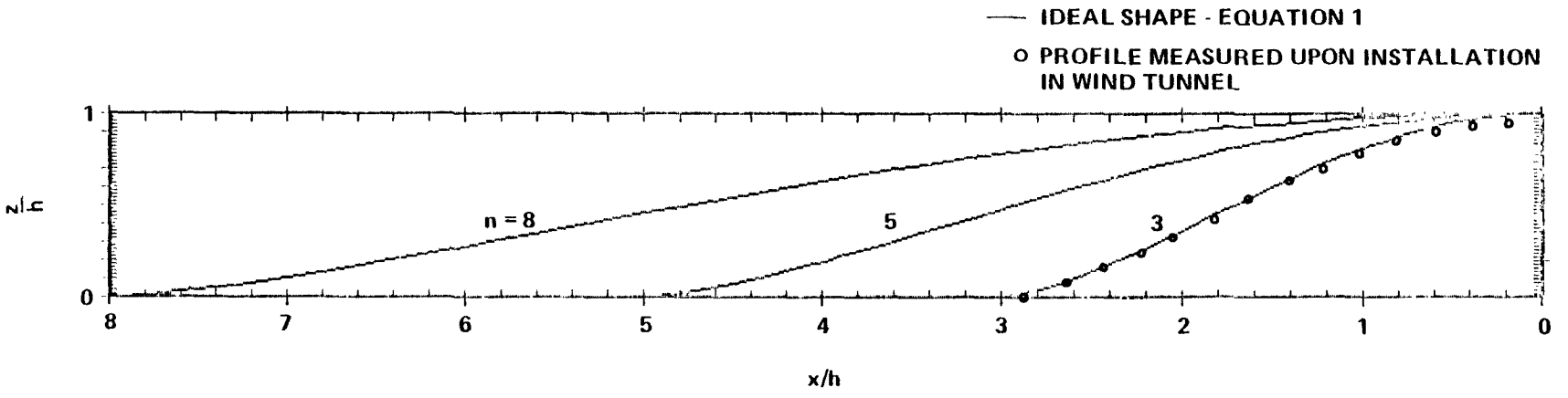

Figure 11. Shapes of model hills (to scale).

and compares the ideal shape of hill 3 with that measured after it was installed in the wind tunnel. The actual shape differed from the ideal shape by less than ±3 mm. All the models were covered with gravel to match the roughness of the wind tunnel floor (described in section 4.1). The difference between the ideal and actual shapes shown in Figure 11 is primarily due to the uncertainty of measuring to the tops of the gravel stones.

The centerlines of all hills were placed 8.7 m downwind of the fence at the entrance of the test section.

4.4. Pollutant Source

In accordance with the purposes of the present investigation, the tracer was to be neutrally buoyant and released from a point source. The tracer chosen, ethylene (C_2H_4), was emitted from a "stack" that was adjustable in height. It contained a 90° bend and a porous stone sphere as shown in Figure 12. Since ethylene is only slightly less dense than air (mol. wt. = 28; s.g. = 0.974 at 15°C) and since it was emitted at relatively small flow rates into a 2 m/s (or greater) air stream, it may be safely considered as neutrally buoyant.

In previous studies, a 6 mm dia., bent-over tube released ethylene isokinetically into the air stream. In the current study, because the wind was not always horizontal (as on the windward sides of the hills) and possibly in the reverse direction (as in the separated regions on the lee sides of the hills), a different source configuration was used. The ethylene was emitted through a porous sphere placed at the end of the bent-over tube (Figure 12). The sphere had a diameter of 15 mm; it was machined to shape from a commercially available porous stone (home aquarium aerator). Because the source flow rates were proportioned to the local wind speeds in the absence of the hills (they were equal to the isokinetic release rates as in the previous studies in order to maintain downwind concentrations within the range of the measurement devices), the surface emission velocities were reduced by a factor of 25 and hence were approximately 4% of the crosswind speed. To determine whether the source emission velocity had an influence on the downwind concentration field, a special test was run by increasing the source flow rate Q by 50%. The results, shown in Figure 13, show that the source

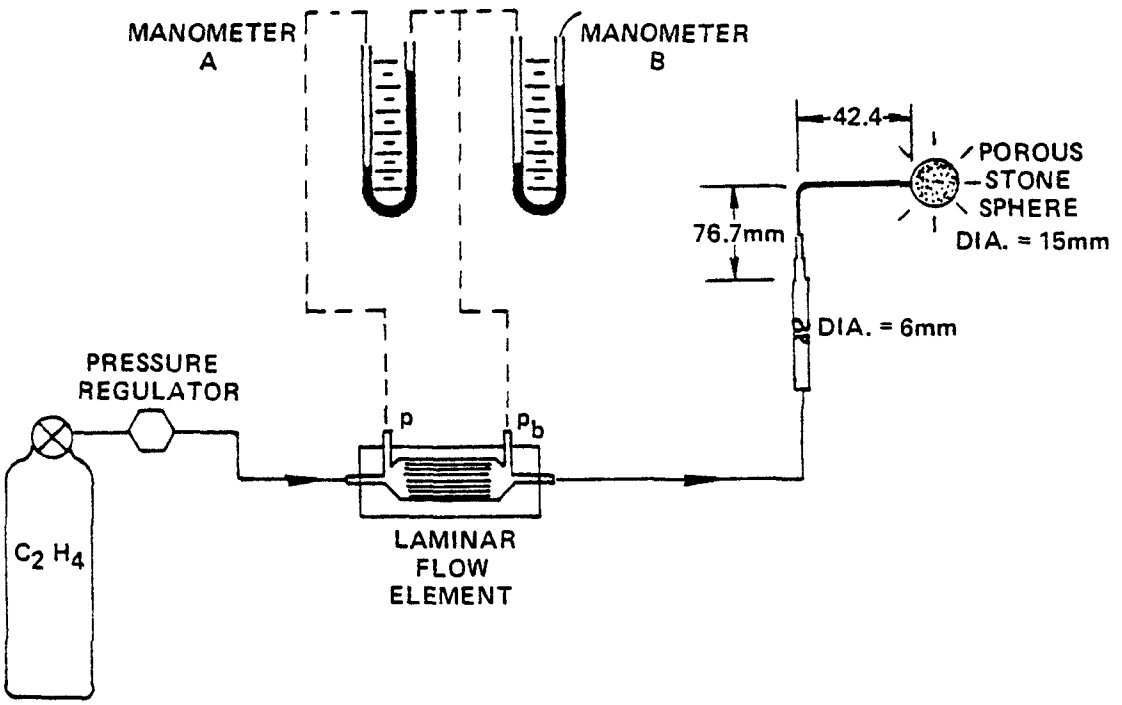

Figure 12. Diagram of source and flow measurement apparatus.

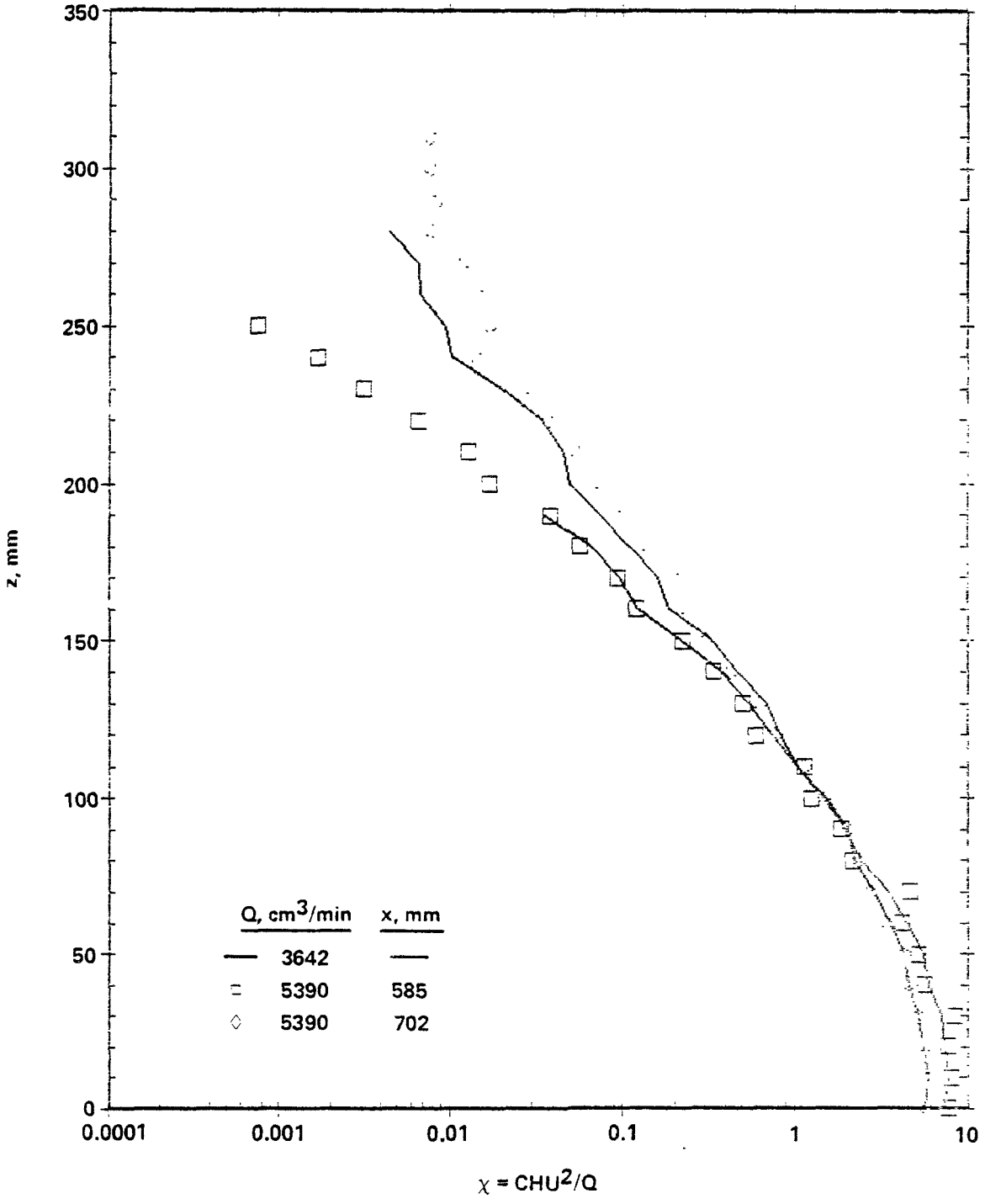

Figure 13. Comparison of concentration profiles measured under different source flow rates.

emission velocity had no influence when the concentration was normalized as $\chi = CUH^2/Q$.

Vertical concentration profiles measured downwind of the two types of sources over the flat wind tunnel floor are compared in Figure 14. It may be observed that the profiles close to the sources differ in a predictable manner because of the different source diameters, but farther downwind, such differences disappear.

Stacks were located at one of three positions such that the center of the porous sphere was above the upwind base (leading edge, x_s = (1)), the top (center, x_s = (2)) or the downwind base (trailing edge, x_s = (3)) of the hills.

4.5. Calibration of Source

The tracer was high-purity ethylene (CP grade; minimum purity of 99.5 mole percent). The ethylene flow rate Q was measured and continuously monitored using a Meriam laminar flow element (model 50MJ10-1/2) and a Meriam micromanometer (model 23FB2TM-20, null type) as shown in Figure 12.

The laminar flow element (LFE) consists of a bundle of very small diameter tubes housed within a stainless steel block containing pressure ports at the entrance and exit of the tube bundle. Under normal operating conditions, because of the small tube diameters, the flow through each tube is laminar and the pressure drop through the tubes is proportional to velocity. If the density is maintained sensibly constant, then, the volumetric flow rate through the LFE is proportional to the pressure differential, which is easily measured quite accurately with a micromanometer (Δp's are typically in the range of 1 to 20 cm of water). However, because the temperature and absolute pressure of the gas may vary from one situation to the next, and because viscosities vary from one gas to the next, the LFE should be calibrated for each set of operating conditions. This system was calibrated using a bubble meter and stop watch or a volumetric flow calibrator (Brooks model 1050A 1J1) which has a rated accuracy of 1/2%. A typical calibration curve for this system is shown in Figure 15.

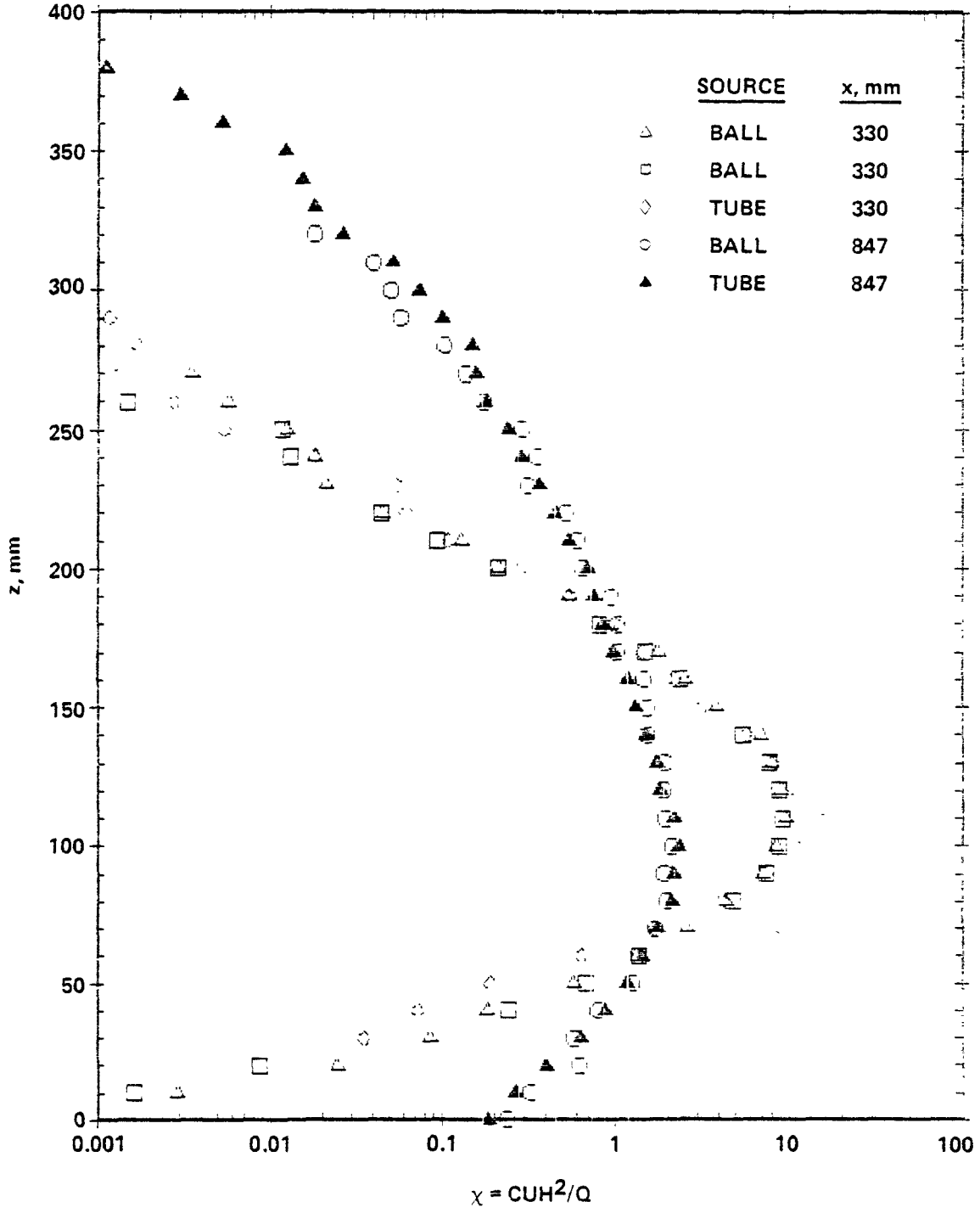

Figure 14. Comparison of vertical concentration profiles measured downwind of isokinetic release tube and porous sphere.

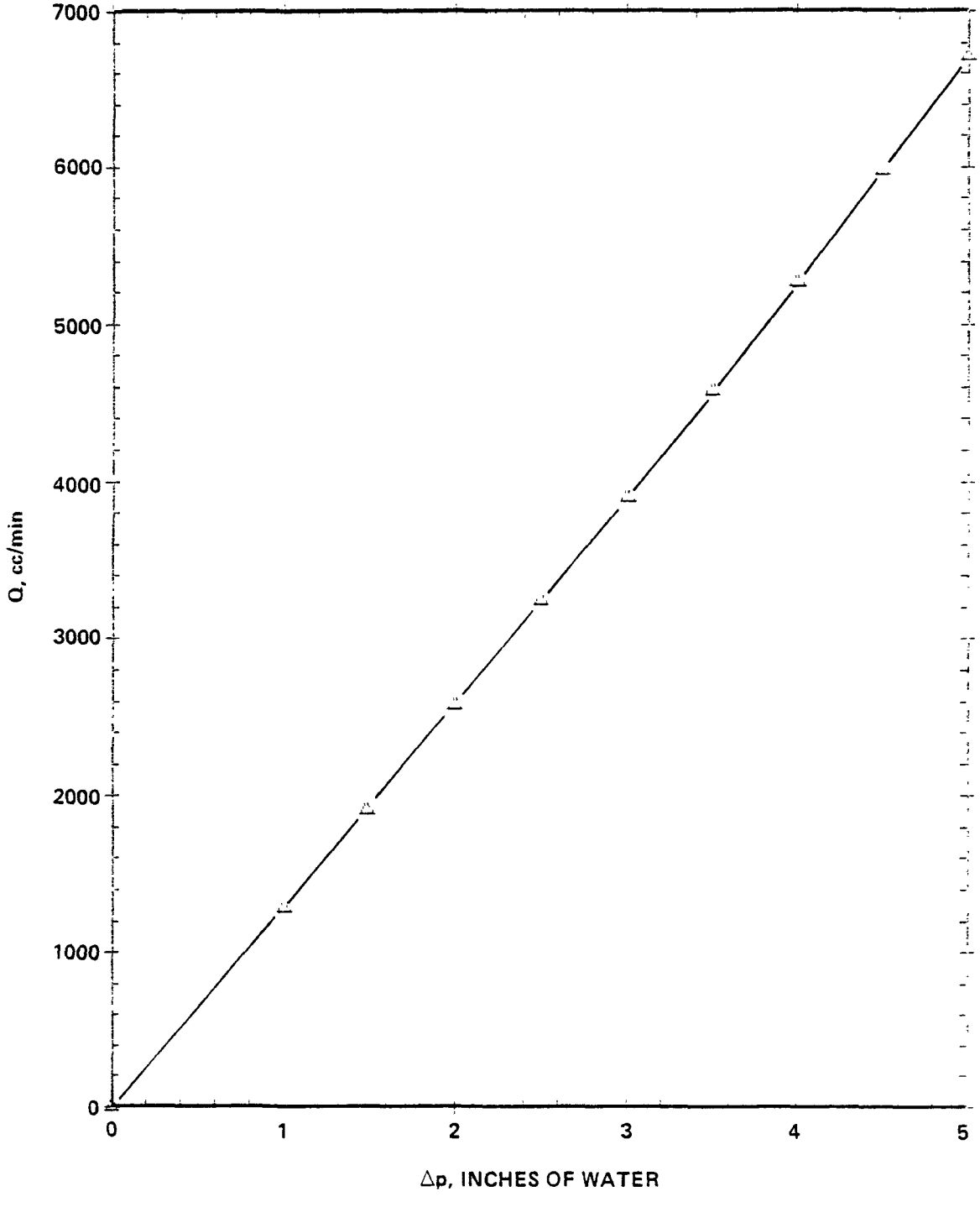

Figure 15. Typical calibration curve for laminar flow element.

Some difficulties were experienced with a shifting of the calibration of the flow rate through the porous stack, primarily during measurements for hill 3. Figure 16 shows, for example, the history of stack "P4". According to these data, the flow rate varied by 30% from one set of experiments to the next at the same pressure differential Δp across the LFE.

Special experiments were conducted to determine the cause of this discrepancy. The resistance at the outlet, hence, the back pressure p_b (relative to atmospheric) within the LFE was varied to determine its influence. These data (Figures 17 and 18) show that, whereas p_b was varied over a very wide range, the flow rate was predictable to within a few percent by Δp alone and correctable to within .05%, even at moderately large p_b. These experiments suggested that the discrepancy (Figure 16) was caused by a leak somewhere in the tubing from the LFE to the stack, even though previous searches for leakage were unsuccessful. Thereafter, both Δp and p_b were simultaneously monitored and no further difficulties were experienced.

Unfortunately, this discrepancy was discovered toward the end of the experimental period, and thus cast some doubt on the absolute accuracy of the concentration data (as they are only meaningful when normalized by the source strength Q). For example, Figure 19 shows two concentration profiles measured at the same position under the "same" conditions, but it is apparent that the source strength differed between the two runs. Suspect data were identified through a comparison of points from different profiles and by checking the mass continuity relationship:

$$Q = \int_{-\infty}^{\infty}\int CU\,dy\,dz. \tag{33}$$

Note that the profile shapes (including the standard deviations, locations of maximums, etc.) were not suspect (as verified in Figure 19)--only the magnitudes of the concentrations--and only in a relatively few files. All suspect data have been identified, additional measurements were made, and faulty data have been replaced.

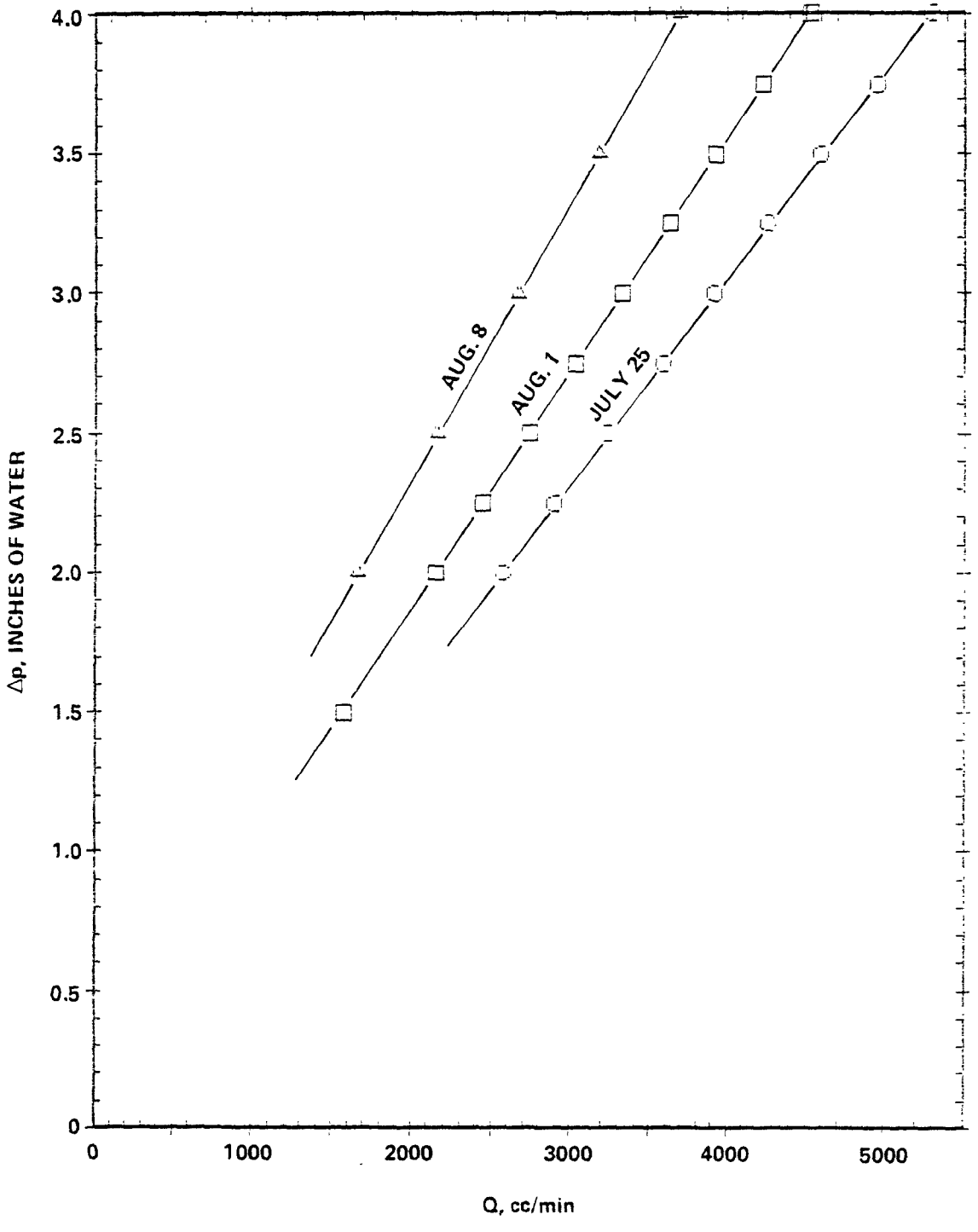

Figure 16. History of calibration of stack "P4".

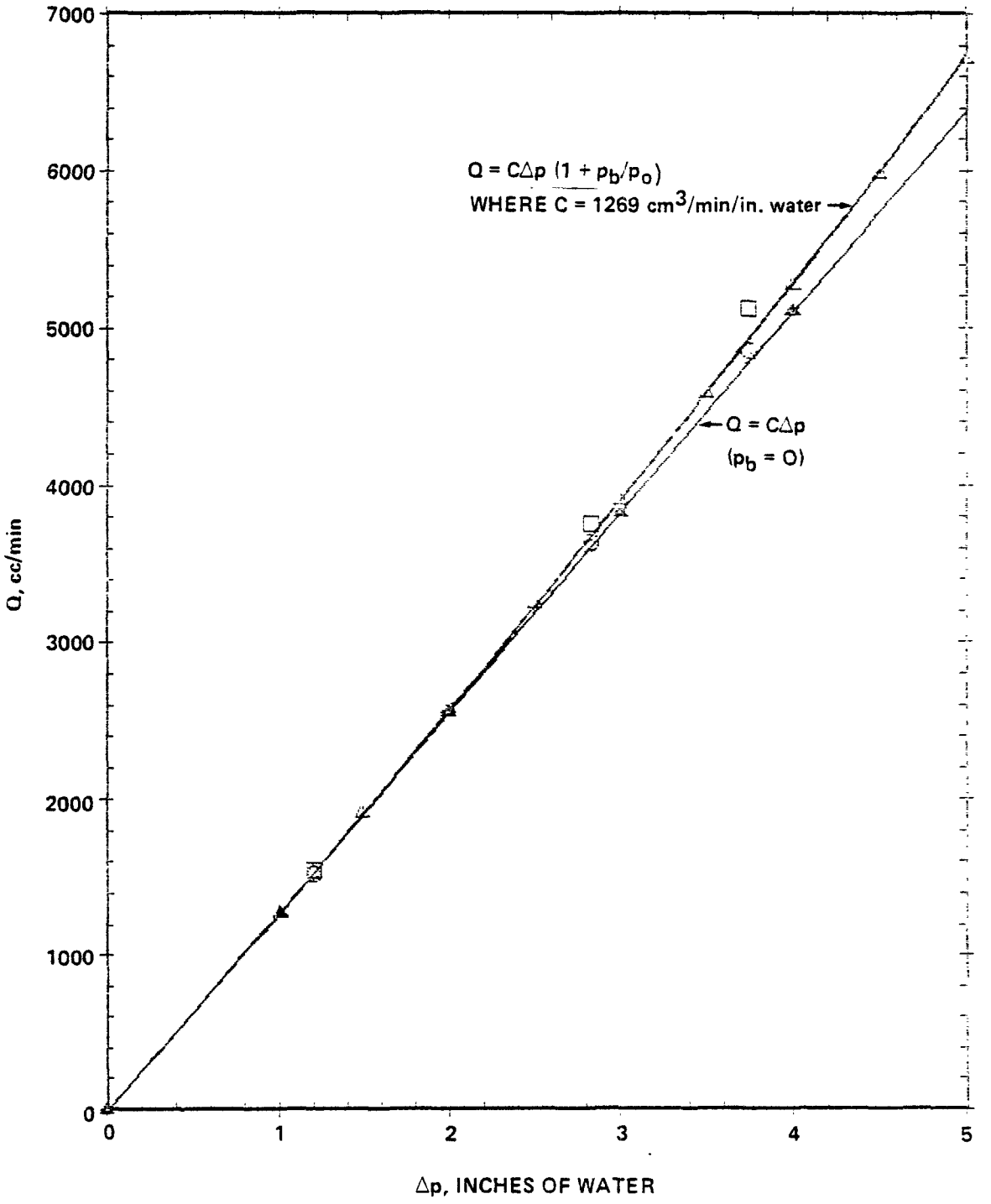

Figure 17. Results of experiments to determine influence of back pressure on laminar flow element: flow rate versus pressure differential.

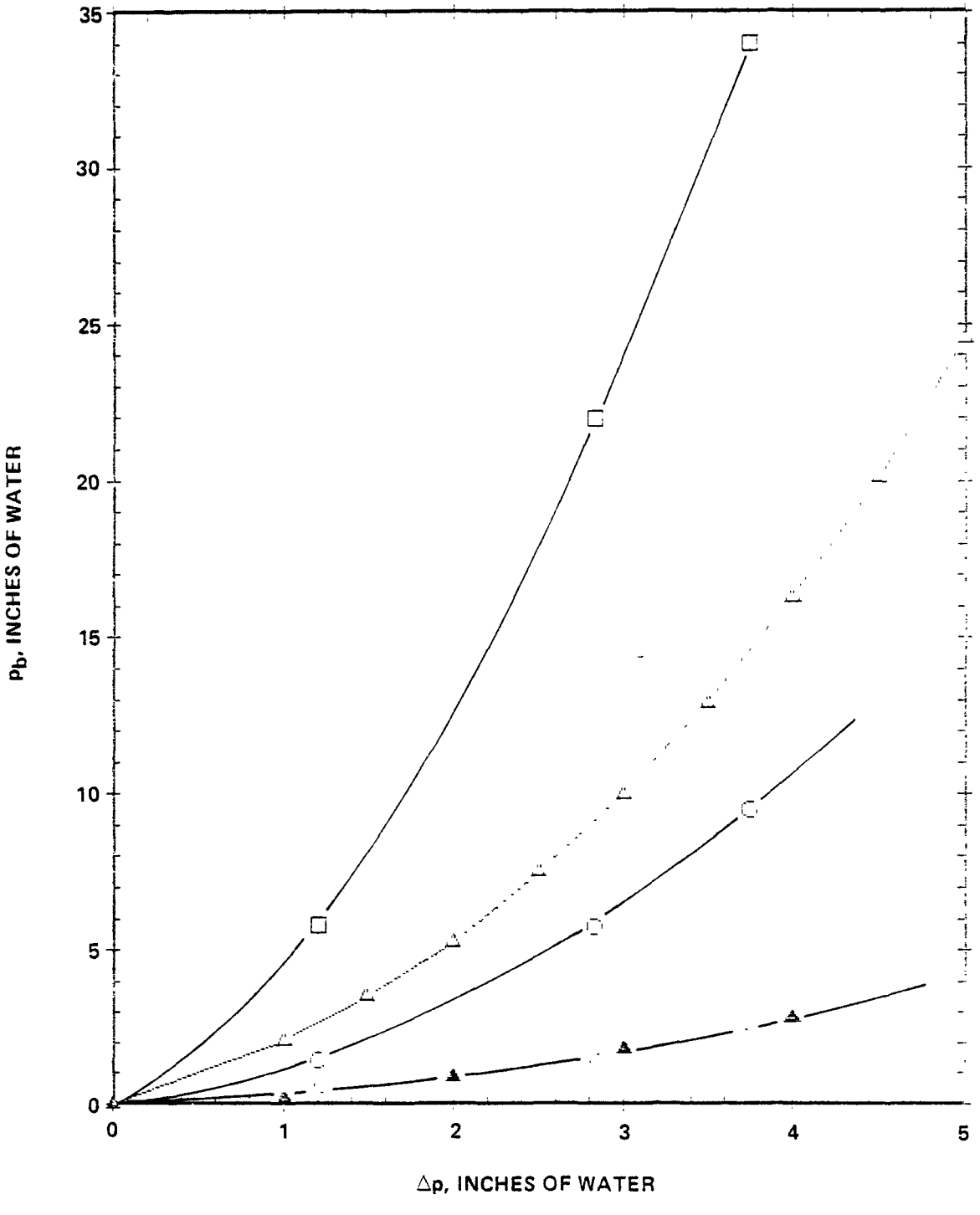

Figure 18. Results of experiments to determine influence of back pressure on laminar flow element: back pressure versus pressure differential.

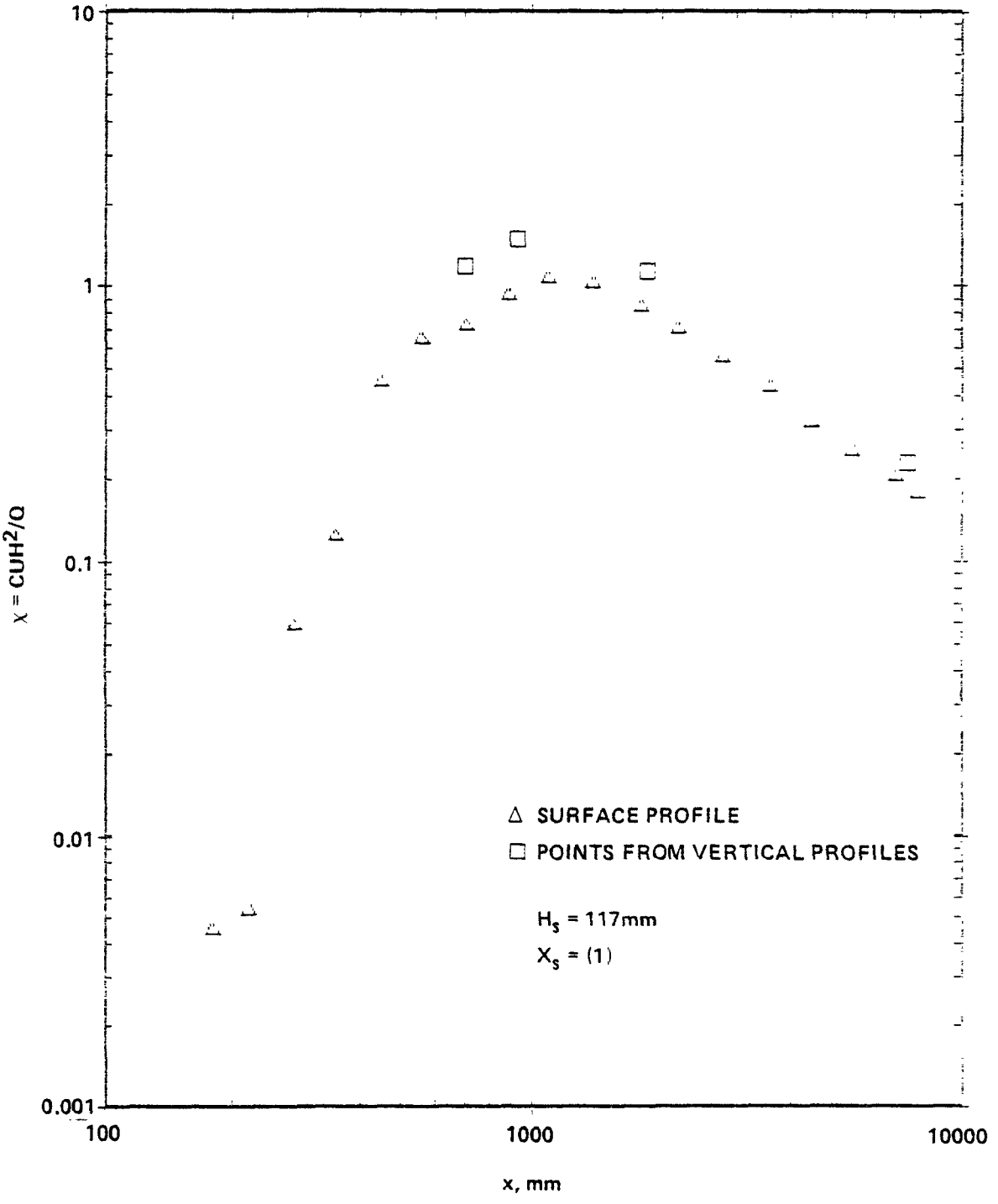

Figure 19. Comparison of concentration profiles measured under same apparent conditions indicating difficulties with source-calibration.

4.6. Concentration Measurements

Concentration profiles were obtained by collecting samples through 1.6 mm OD tubes that were fastened to the instrument carriage. These samples were drawn through Beckman model 400 hydrocarbon analyzers (flame ionization detectors, FIDs) operating in the continuous sampling mode for analysis. As many as 4 FIDs were used simultaneously in conjunction with sampling rakes which contained sampling tubes of fixed spacing.

The FIDs were initially calibrated and checked for linear response using certified gases of (nominally) 1, 0.5, 0.05, and 0.005% ethylene in hydrocarbon-free air from Scott Environmental Technology, Inc. A typical calibration curve is shown in Figure 20.

The "span" (full scale) and "zero" settings were adjusted before beginning measurements and checked after finishing measurements each day. Background (room) hydrocarbon level measurements were made at the beginning and end of each profile and frequently more often. The computer program HCA subtracted a background level from each sample measurement by assuming a linear change in background with time between sequential background measurements. Typical background levels were 5 ppm at the beginning and 30 ppm at the end of the day.

The output signals from the FIDs were digitized at the rate of 1 hz (each unit) and processed on the PDP 11/40 minicomputer. The HCA computer program controlled the sampling, processed the data (scaling, averaging, etc.), and stored the data from each of the four instruments in separate files.
A typical concentration profile is shown in Figure 21. It was evident from examination of figures such as this whether or not a particular FID was malfunctioning; for example, it is probable that FID number 4 (Figure 21) was indicating low concentration near the ground, as those points are not in line with the others. Lateral and vertical profiles were obtained from four FIDs operating simultaneously, but, because of possible probe interference, only one analyzer was used for measuring surface (streamwise along the ground) profiles.

The "corrected" concentrations (i.e., with background subtracted) were normalized by

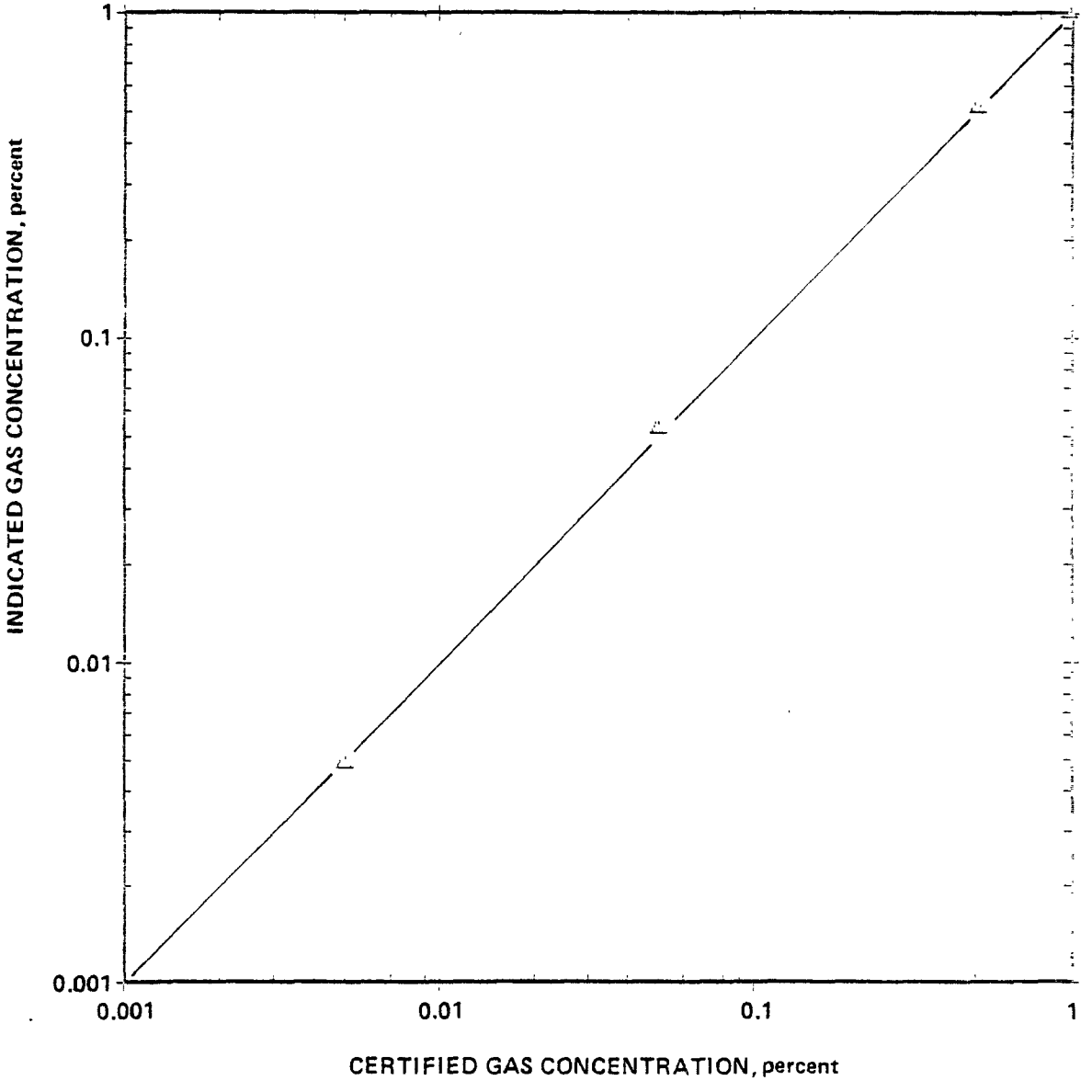

Figure 20. Typical calibration of flame ionization detector with ethylene.

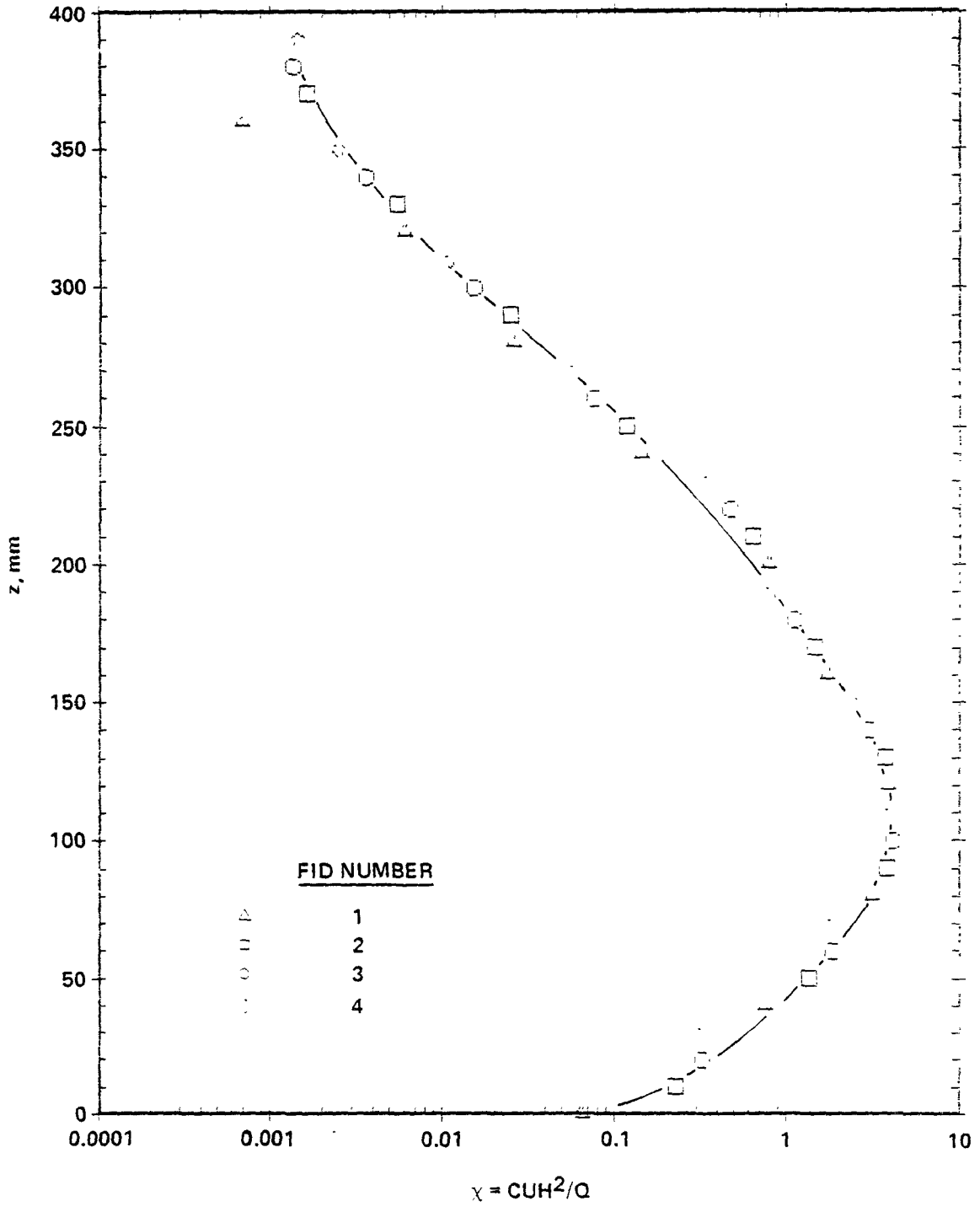

Figure 21. Typical concentration profile measured with four FIDs.

$$\chi = CU_\infty H^2/Q \ , \qquad (34)$$

where χ is the normalized concentration (used in all graphs), C is the corrected concentration (in parts per million by volume), U_∞ is the free stream velocity (normally 4 m/s), H is a convenient length scale (H = 234 mm was used throughout this study, since it is the height of the large hill), and Q is the ethylene flow rate.

Two minute sampling (averaging) times were found to yield reasonably repeatable values of concentration--generally within ±5% on mean concentrations.

For each stack height, each stack position, and each hill (also in the absence of the hills), vertical, lateral (cross-wind) and surface (streamwise approximately 5 mm above the top of the gravel) profiles of concentration were measured. Four primary stack heights were used: 29, 59, 117, and 176 mm; more limited measurements were made at other stack heights. As mentioned previously, stacks were placed at the upstream base, top and downwind base of the hills.

4.7. FID Response Characteristics

A few experiments were conducted to determine the response characteristics of the FIDs. The responses of the FIDs to step changes in concentration and to square waves are shown in Figures 22 and 23, respectively. To a first approximation, the response of the analyzer may be described as a delay-line in series with a first order filter (see Mage and Noghrey, 1972) with a time constant $\tau_c \sim 1.2$s. The delay time depends upon external parameters such as the length of the connecting tubes (about 10 m in these experiments), their diameter, the sample flow rate, and the internal volume of the sampling pump, as well as internal parameters, i.e., individual properties of each FID. From Figure 22, for example, even though the external parameters were ostensibly the same, the delay time was 9s for one FID and 13s for the other.

The root-mean-square error σ_m in the measurement of a mean concentration m may be estimated as

$$\frac{\sigma_m}{m} = \frac{\sigma}{m}\sqrt{\frac{2\tau_c}{T}} \ , \qquad (35)$$

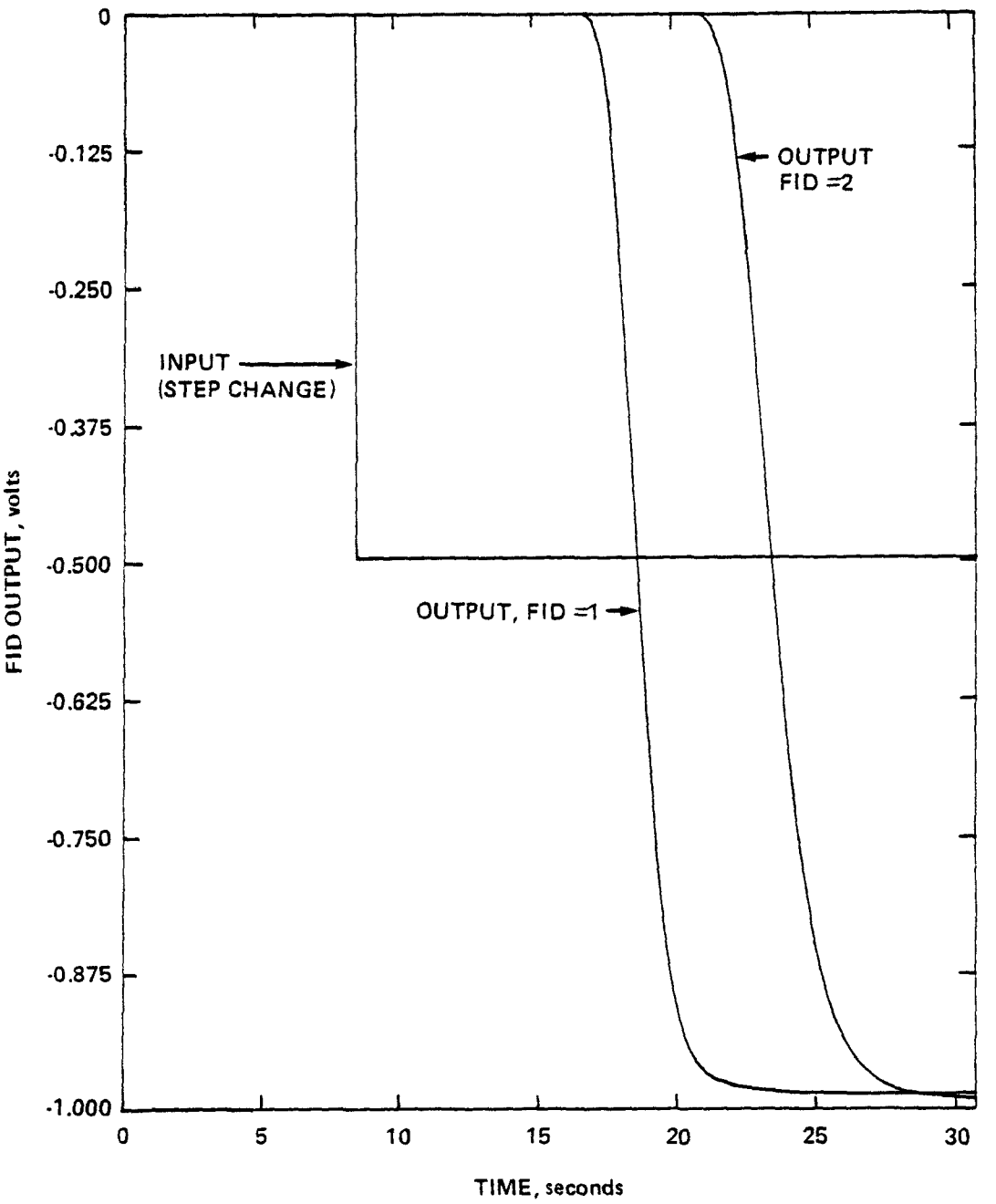

Figure 22. Response of FID's to step change in concentration.

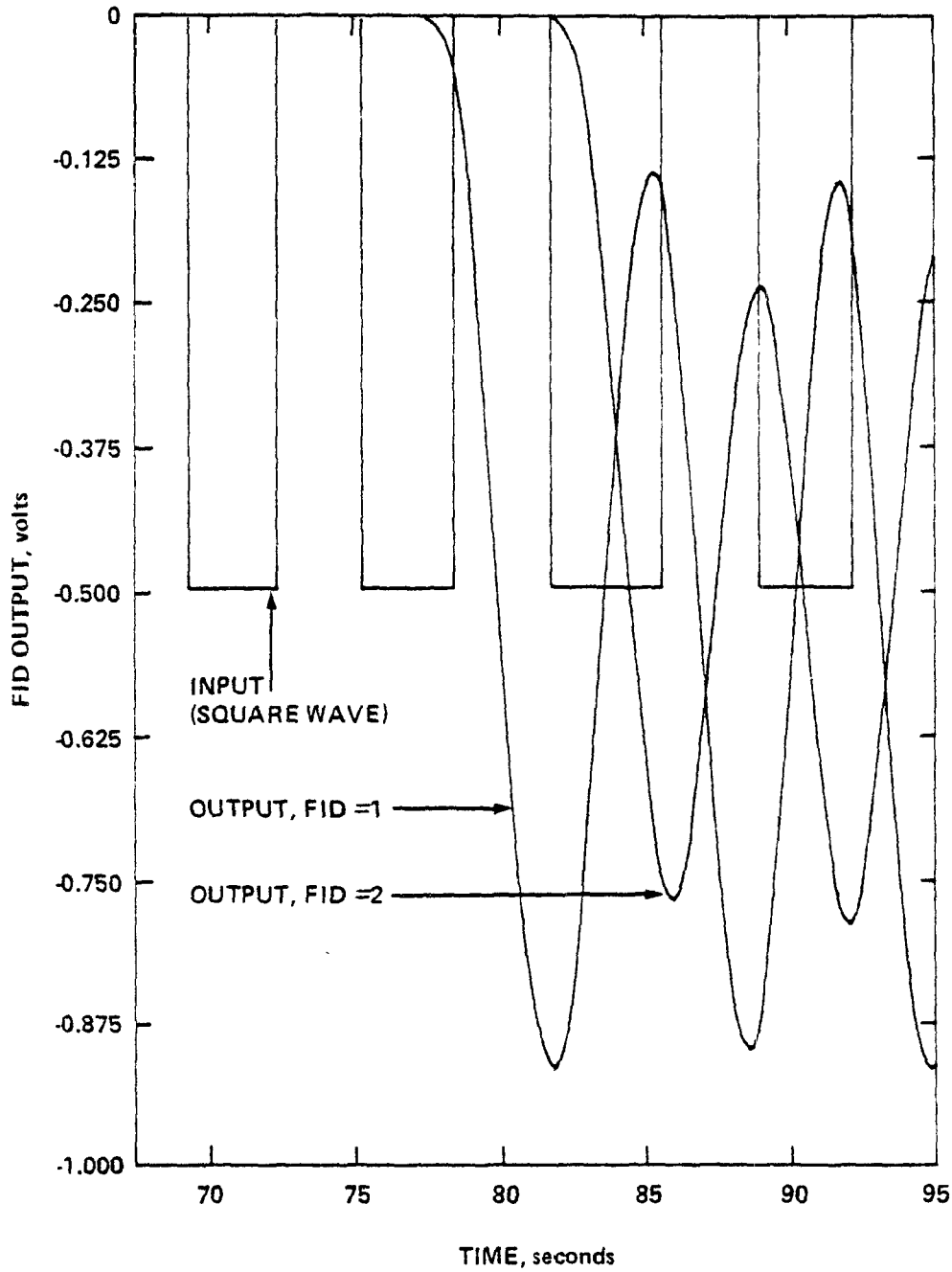

Figure 23. Response of FID's to square wave input.

where σ is the standard deviation of concentration fluctuations at the output of the FID, τ_c is the integral time scale (correlation time) of the concentration fluctuations (also at the output of the FID), and T is the sampling period (120s). Neither τ_c nor σ were evaluated directly, but it is evident that $\tau_c > 2\tau_o$. Subjective judgements made from observing the signals on the oscilloscope indicated that $\tau_c \sim 4$ sec and $0.2 < \sigma/m < 1$. (The ratio σ/m depends strongly upon the measurement point relative to the plume axis; typical values are given here). Hence, the errors σ_m/m indicated by Equation 35 range from 4 to 20% for an individual point. This range agrees quite well with the experimental observations.

4.8. Adjustment of Height of Wind Tunnel Ceiling

As discussed by Snyder (1981), it was necessary to locally raise the ceiling of the wind tunnel above the hills in order to minimize "blockage" effects which would, of course, be absent in the atmosphere. The ceiling height was adjusted by a trial and error procedure until the freestream velocity (1.6 m above the wind tunnel floor) was constant, i.e., independent of longitudinal position. This procedure ensures that the longitudinal pressure gradient will be zero, which appears to be the most natural criterion to apply in simulating full-scale conditions. Typical maximum adjustments were half the hill heights.

5. PRESENTATION AND DISCUSSION OF RESULTS AND COMPARISON WITH THEORY

5.1. Flat Terrain

5.1.1 The boundary layer structure

Additional measurements of the boundary layer structure made in the current study confirmed the results of previous studies. As seen in Figure 24, the mean velocity profile is essentially independent of downwind distance in the range of 7 to 15 m downwind of the fence (-2 to 6.5 m from the hill centers). It may be approximated very closely by

$$U/u_* = (1/k)\ln((z - d)/z_0)$$

to a height of 600 mm, where k is the von Karman constant (0.4), u_* is the friction velocity, d is the displacement height and z_0 is the roughness length. The mean velocity profile may thus be characterized by $u_* = 0.185$ m/s, $d = -0.5$ mm and $z_0 = 0.157$ mm. The displacement height is negative (but is indeed very small) because z was measured from the tops of the gravel stones. The roughness length is quite close to the 0.13 mm measurement by Courtney (1979) under the same physical arrangement, but at a freestream wind speed of 8 m/s. The overall boundary layer depth δ is approximately 1 m.

The Reynolds stress profiles, plotted in Figure 25, show considerable scatter near the surface, but there is a slight tendency for the surface shear stress to decrease with downwind distance. The turbulence structure thus reached equilibrium more slowly than did the mean flow.

Strictly speaking, a "constant stress" layer did not exist, as the vertical distribution may be conveniently approximated as a linear decrease with height from its surface value to zero at $z = \delta$:

$$\overline{uw}(z) = u_*^2(1 - z/\delta).$$

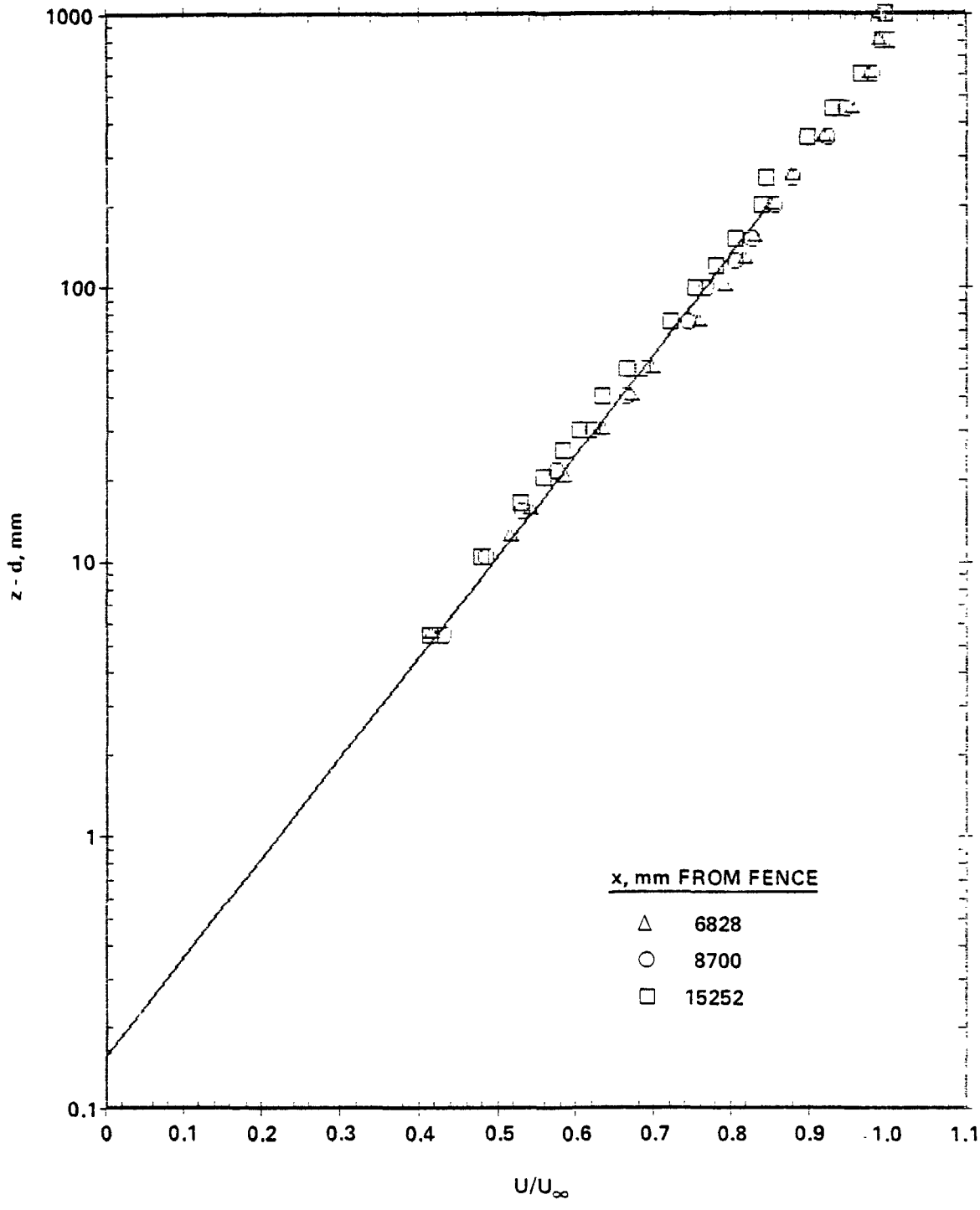

Figure 24. Typical mean velocity profiles in flat terrain.

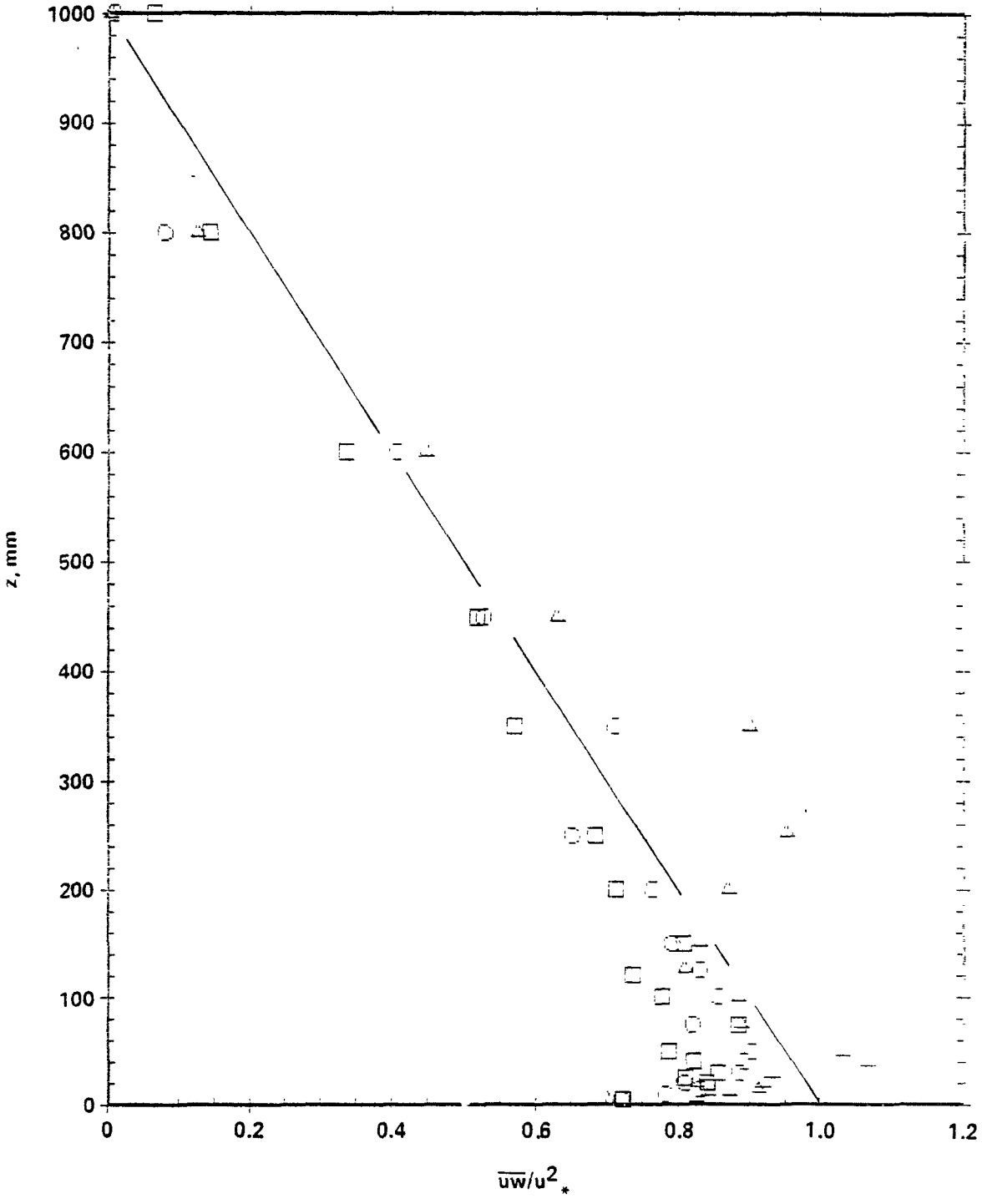

Figure 25. Typical Reynolds stress profiles in flat terrain.

This is similar to high-Reynolds-number wind-tunnel boundary layers, e.g., Zoric and Sandborn (1972). (A plot of their data is also shown as Figure 15 in Snyder, 1981). For practical purposes, however, the lowest 200 mm of the boundary layer may also be considered as a "constant stress" layer.

Longitudinal, lateral and vertical turbulence intensity profiles are shown in Figures 26 and 27. They also indicate a decay of energy with downwind distance, especially the vertical component, but the rate of decay obviously decreased. Note that the u_* used for normalization of these intensities was obtained from the slope of the mean velocity profile (Figure 24) and that near the surface, $\sigma_u/u_* \sim 2.5$, $\sigma_w/u_* \sim 1.2$, and $\sigma_v/u_* \sim 1.8$, in good agreement with other investigations of simulated and atmospheric boundary layers (Hunt and Fernholz, 1975; Counihan, 1975). Similarly, $u_*/U_\infty = 0.047$ is quite reasonable.

A brief discussion is in order concerning the scaling relationship between this wind tunnel boundary layer and the atmospheric boundary layer. In accordance with Counihan (1975), the average depth of the neutral atmospheric boundary layer is $\delta = 600$ m. Proceeding from this figure, on the basis of geometric similarity ($(z_o/\delta)_m = (z_o/\delta)_f$), $z_o = 10$ cm is obtained for the corresponding atmospheric boundary layer.

Another method of deriving a scaling relationship would be to use the measured value of u_*/U_∞ and the geostrophic drag laws or empirical means to obtain an estimate of the corresponding full-scale roughness length. This method was avoided here since even small measurement errors in the values of u_*/U_∞ can lead to largely different estimates of the corresponding roughness length. As remarked earlier, there was a slight tendency for the surface shear stress to decrease with downwind distance because the boundary layer was slowly developing; a fully-developed (equilibrium) boundary layer would undoubtedly exhibit a somewhat smaller shear stress. It is also noted that the literature presents highly contradictory relations between values of z_o and u_*/U_∞. Counihan (1975) surveyed a great quantity of published experimental data as well as model predictions. His summary shows that the value of $u_*/U_\infty = 0.047$ corresponds to the value of $z_o = 10$ cm, as obtained above from geometric similarity. The method of Clarke and Hess (1974), however, would suggest values of z_o between 40 and 90 cm. Hence, the most

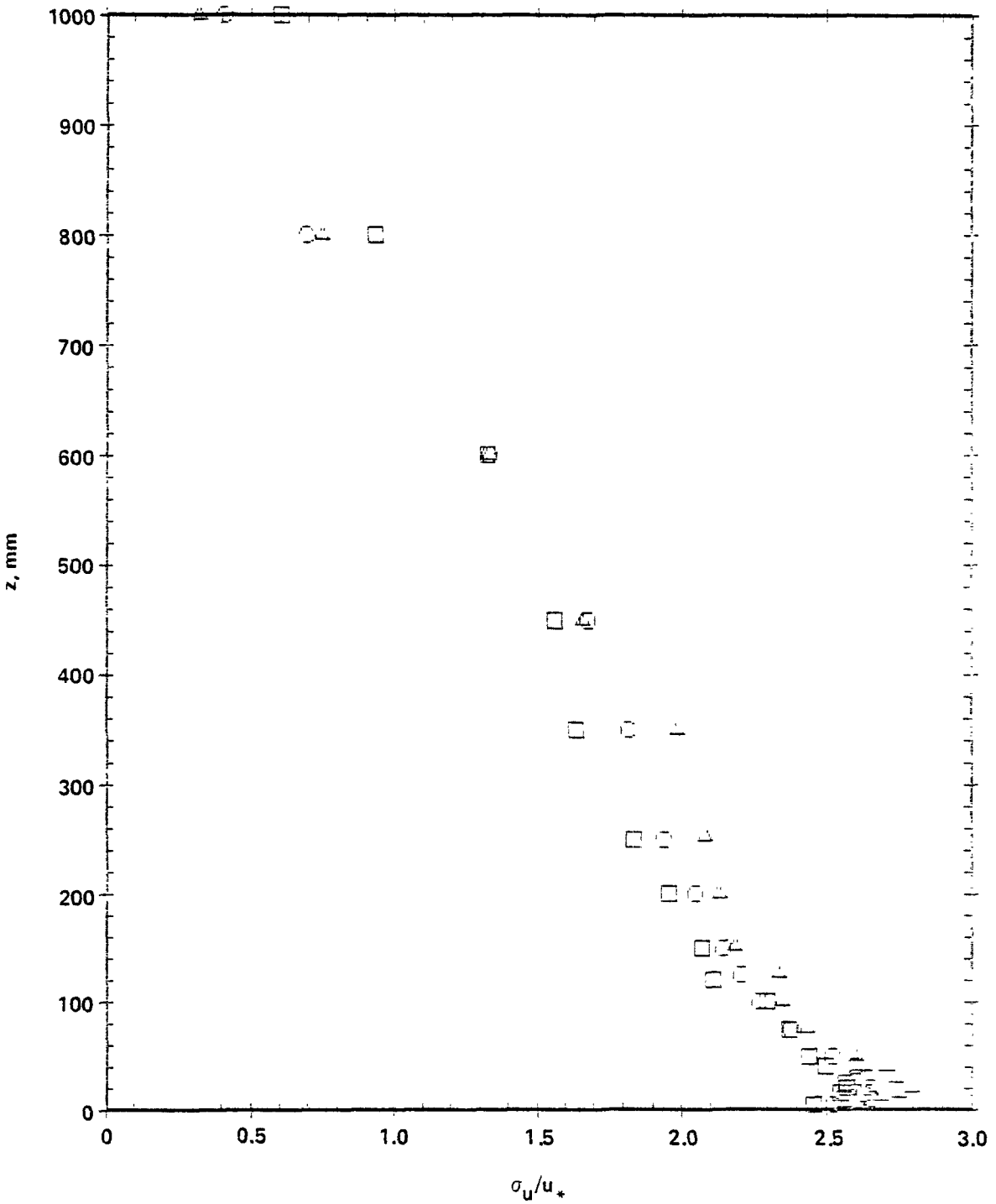

Figure 26. Typical longitudinal turbulence intensity profiles in flat terrain.

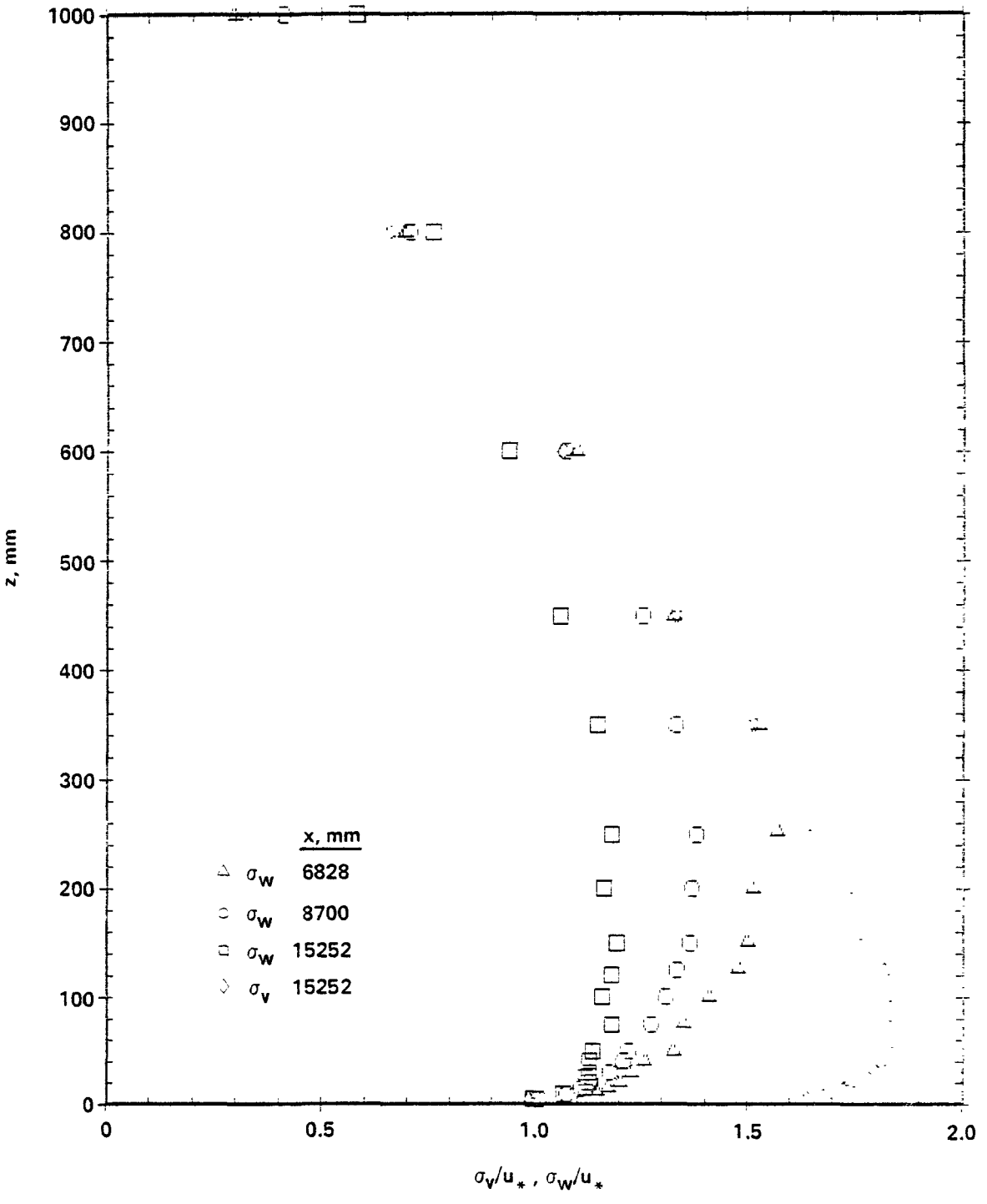

Figure 27. Typical vertical and lateral turbulence intensity profiles in flat terrain.

direct application of geometric similarity appears to be the best method under the circumstances.

It is concluded that even though this boundary layer is slowly developing, it provides a reasonable simulation of the neutral atmospheric boundary layer.

5.1.2. Dispersion characteristics of the boundary layer

Surface concentration profiles measured for source heights of 29, 59, 117, 176, 234, and 351 mm are shown in Figure 28. These source heights correspond to $h_o/4$, $h_o/2$, h_o, $3h_o/2$, $2h_o$ and $3h_o$, where h_o is the small hill height. As expected, the maximum surface concentration χ_{mx} decreased and the distance to the point of maximum concentration x_{mx} increased as the stack height h_s increased. All profiles converged asymptotically far downwind where the surface concentration decreased with the -3/2 power of x, i.e., $\chi \propto x^{-1.5}$. Such behavior is also predicted by the theory of Berlyand (1975) if it is assumed that the lateral diffusivity k_y is independent of x or, equivalently, that the lateral plume width grows as the 1/2 power of x, i.e., $\sigma_y \propto x^{0.5}$.

Similarity in the shapes of these profiles is shown in Figure 29, where normalized concentrations C/C_{mx} are plotted as functions of distance from the source normalized by distance to the point of maximum concentration x/x_{mx}. Also plotted for comparison is the analytical solution of the diffusion equation 2. This solution was obtained by Beryland (1975) using the assumptions that $U = U_1 (z/z_1)^p$, $k_z = k_1 (z/z_1)^t$ and $k_y = k_o u$ (k_o = constant, p = 0.15 to 0.2 and $t \simeq 1$ for neutral flows, z_1 = a reference height and U_1 and k_1 are mean velocity and diffusivity at the height z_1). The solution provides a universal (independent of source height) expression for C/C_{mx} as a function of x/x_{mx} along the plume centerline y = 0:

$$C/C_{mx} = \exp\left(\frac{3}{2}\left(1 - \frac{x_{mx}}{x}\right)\right)\left(\frac{x}{x_{mx}}\right)^{-3/2} .$$

The experimental data collapse quite well onto the analytical expression, especially beyond the point of maximum concentration.

Lateral concentration profiles measured at various downwind distances (through the point of maximum concentration in the corresponding vertical

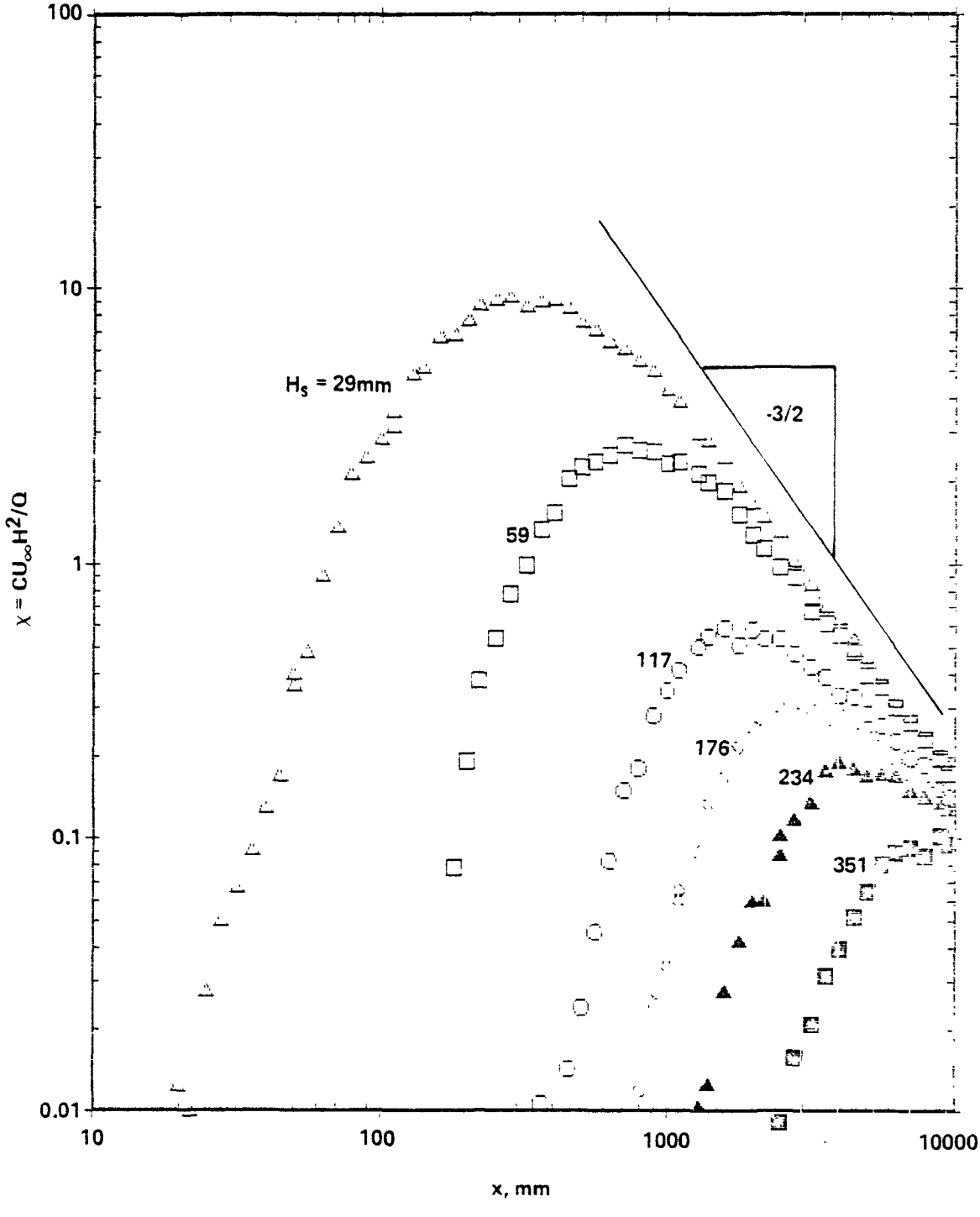

Figure 28. Surface concentrations from sources of various heights in flat terrain.

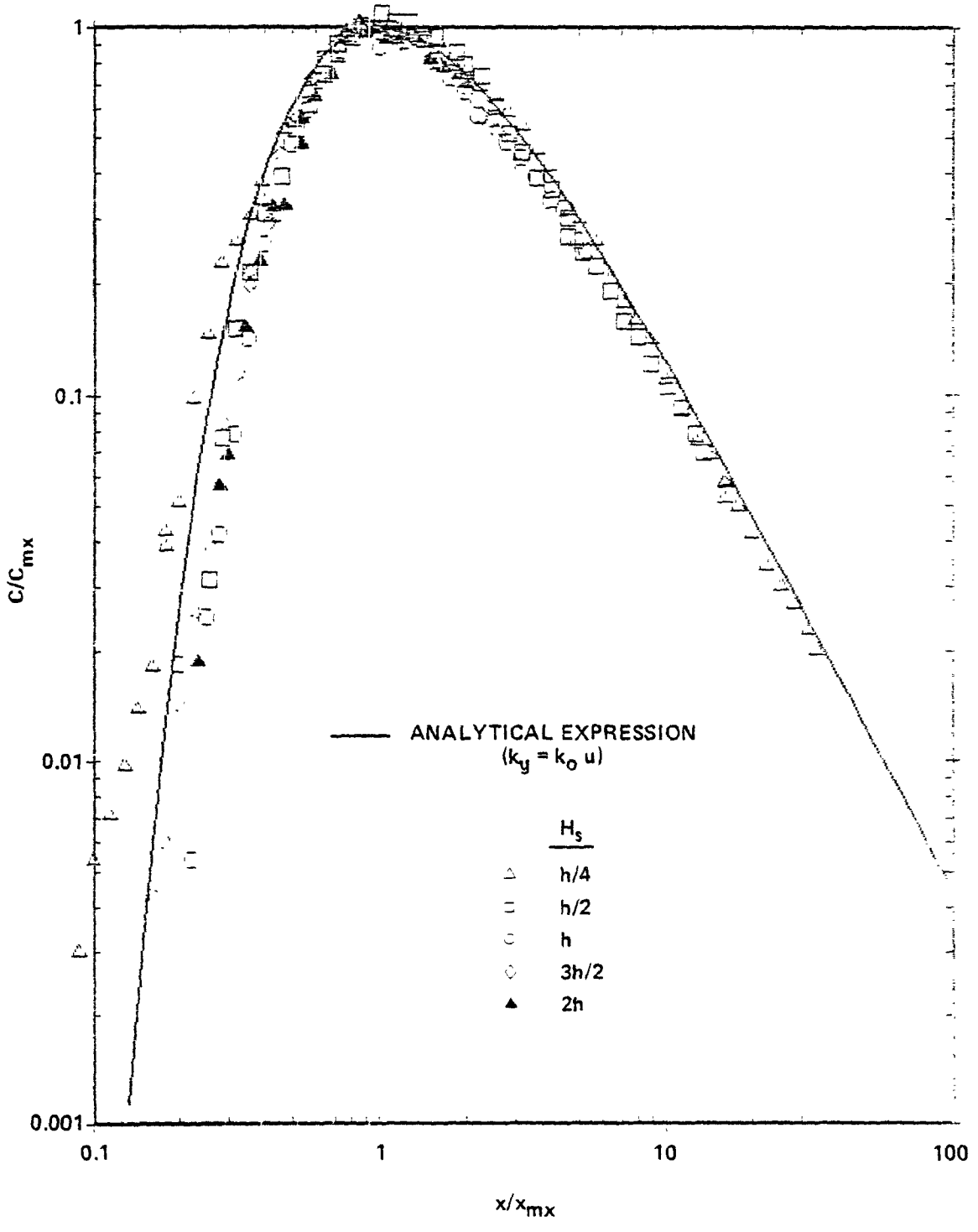

Figure 29. Similarity of surface concentration profiles in flat terrain.

profile) are shown in Figures 30 and 31 for source heights of 29 and 117 mm, respectively. All shapes are very close to Gaussian. Figure 32 shows numerous lateral profiles measured at different elevations through the plume from the source of height 117 mm. It is evident that the maximum concentration was at ground level and that close to the ground the plume width σ_y grew with height. Figure 33 shows that the plume width reached a maximum at a height of about 300 mm ($\sim 0.3\delta$) excepting the anomalous point at the ground from the elevated plume. Because of surface reflection, this profile shape was exceptionally flat. This behavior appears to be practically independent of stack height or downwind position, but firm conclusions would require more extensive measurements. This finding is contrary to Gaussian diffusion theory, wherein σ_y is independent of the elevation at which it is measured. For practical purposes, however, these differences are probably not significant.

Figures 34 and 35 show cross-sectional, isoconcentration plots from a low-level source and an elevated source, respectively. The irregularities such as in the lower left and upper right of the plume in Figure 34 are the result of scatter in the data, as no smoothing was applied.

Lateral plume widths for all plumes (and all elevations) are plotted as functions of downwind distance in Figure 36. There is no apparent variation of σ_y with stack height. For small x, $\sigma_y \propto x$, whereas for large x, $\sigma_y \propto x^{1/2}$, as predicted by Taylor statistical theory. The solid curve represents an interpolation formula assuming a Lagrangian integral scale of 400 mm. The formula agrees well with the data except for small x. The agreement could be made considerably better at small distances by assuming a virtual origin located approximately 35 mm upwind of the source, because the source was not, in fact, a point source, but rather a sphere of 15 mm diameter.

The evolution of the vertical concentration profiles is shown in Figure 37. The profile shapes are neither Gaussian nor reflected Gaussian in form, as is made more apparent in Figure 38. These latter curves are "best-fit" Gaussian, having the same standard deviations as the data set and assuming perfect reflection from the ground surface. Even relatively close to the source, before reflection from the ground becomes important, the profiles are asymmetric and

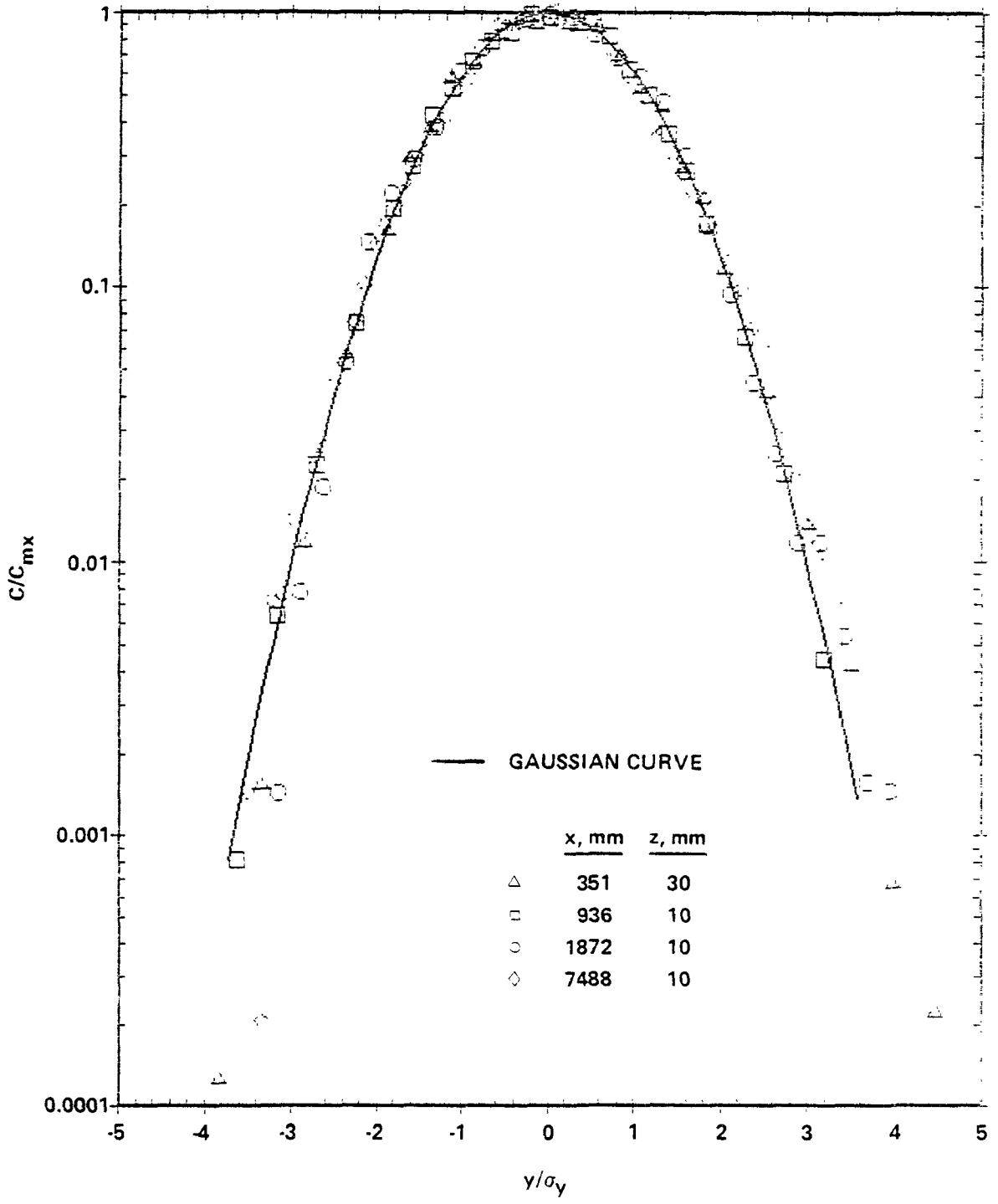

Figure 30. Similarity of lateral concentration profiles in flat terrain; H_s = 29mm.

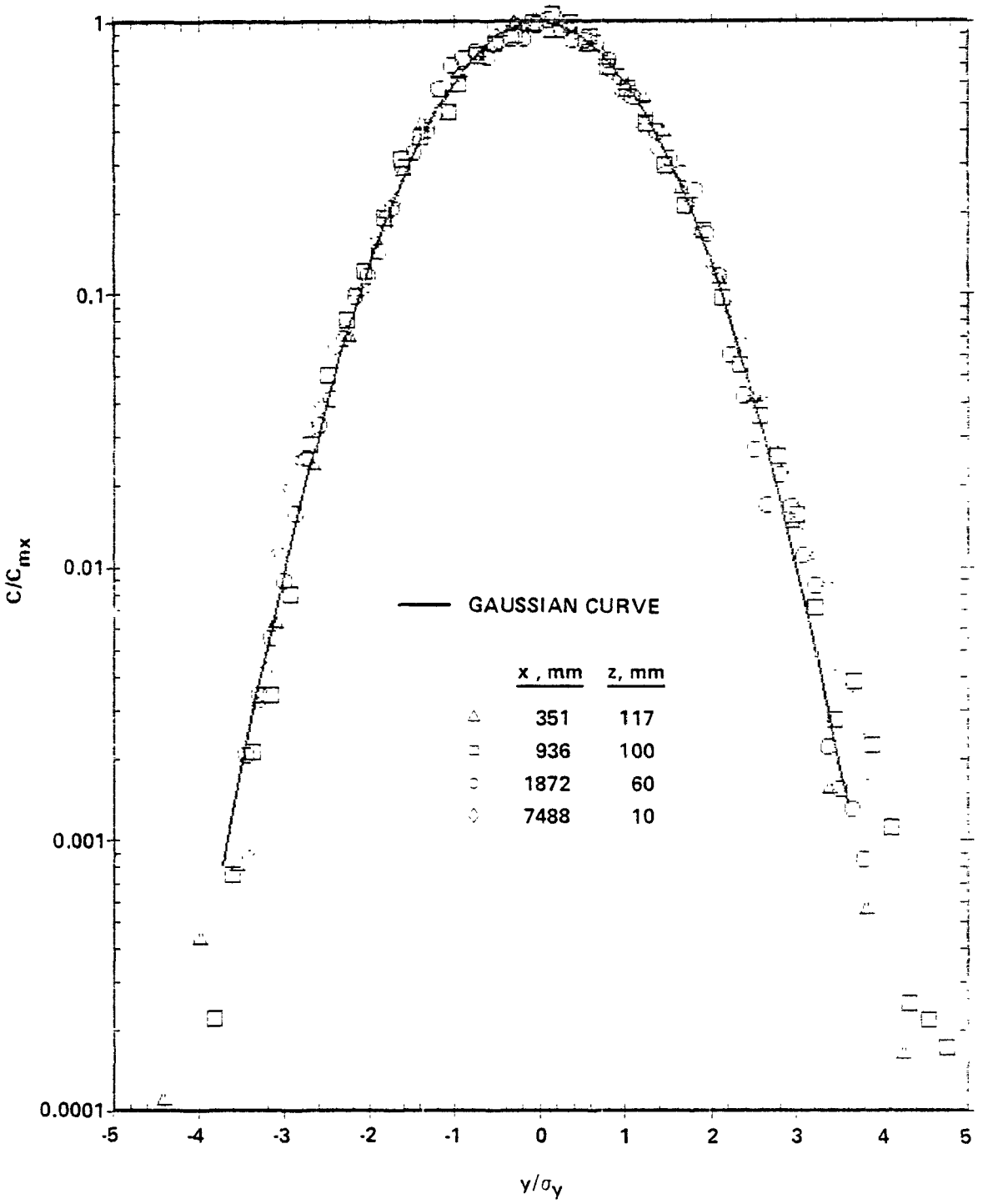

Figure 31. Similarity of lateral concentration profiles in flat terrain; H_s = 117mm.

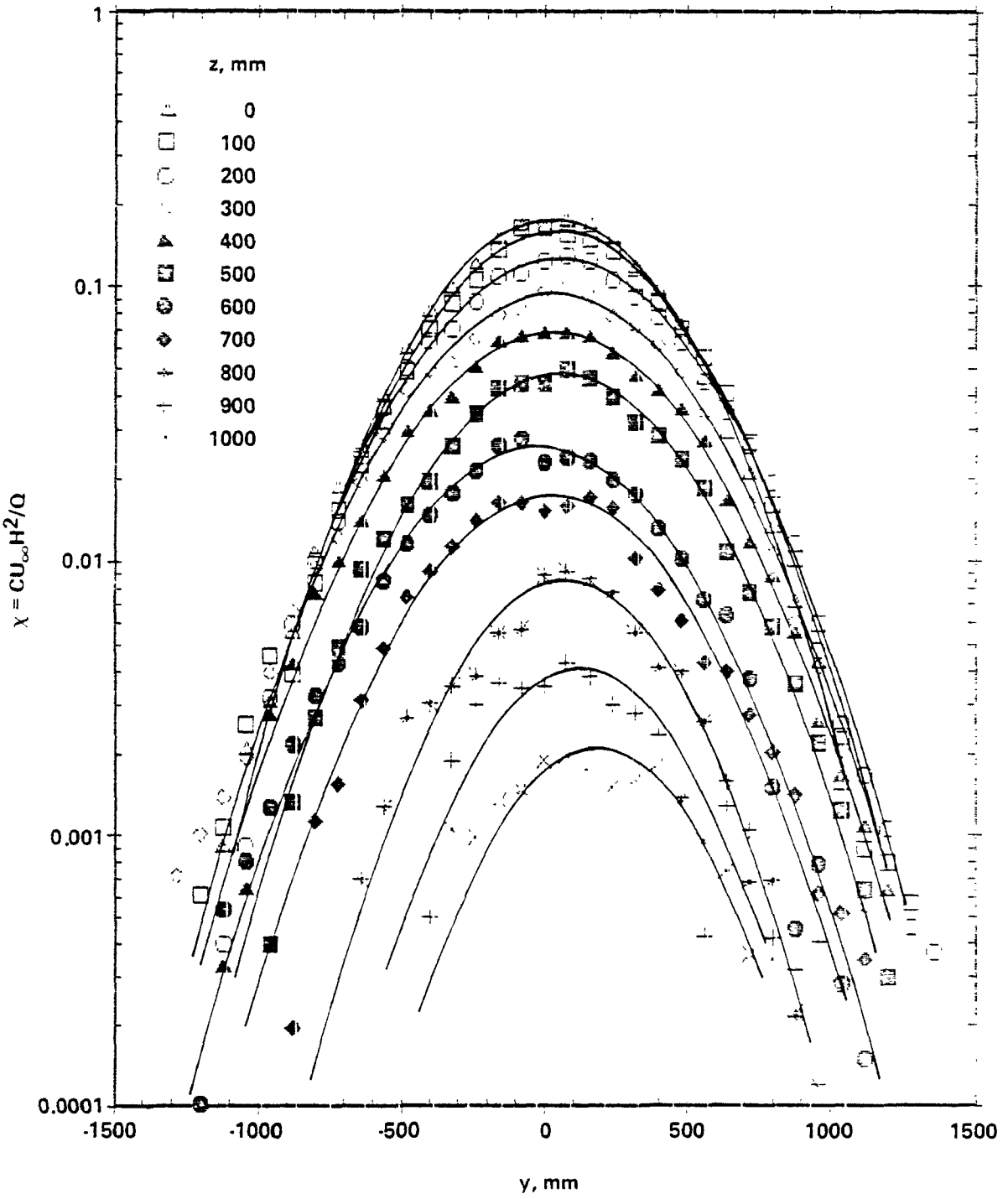

Figure 32. Horizontal profiles through plume at X = 7488mm from source of height H_s = 117mm in flat terrain.

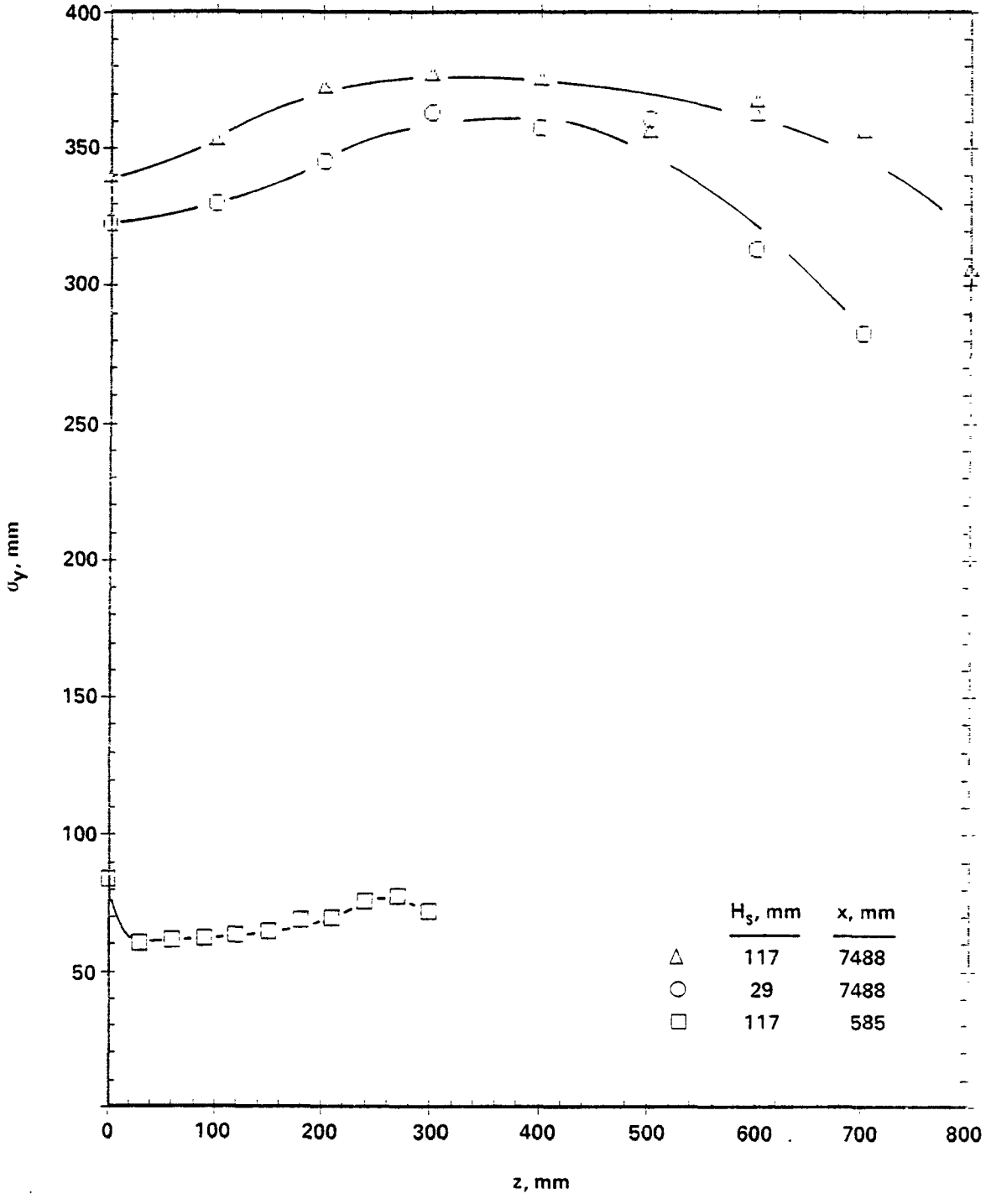

Figure 33. Lateral plume widths as functions of height above ground in flat terrain.

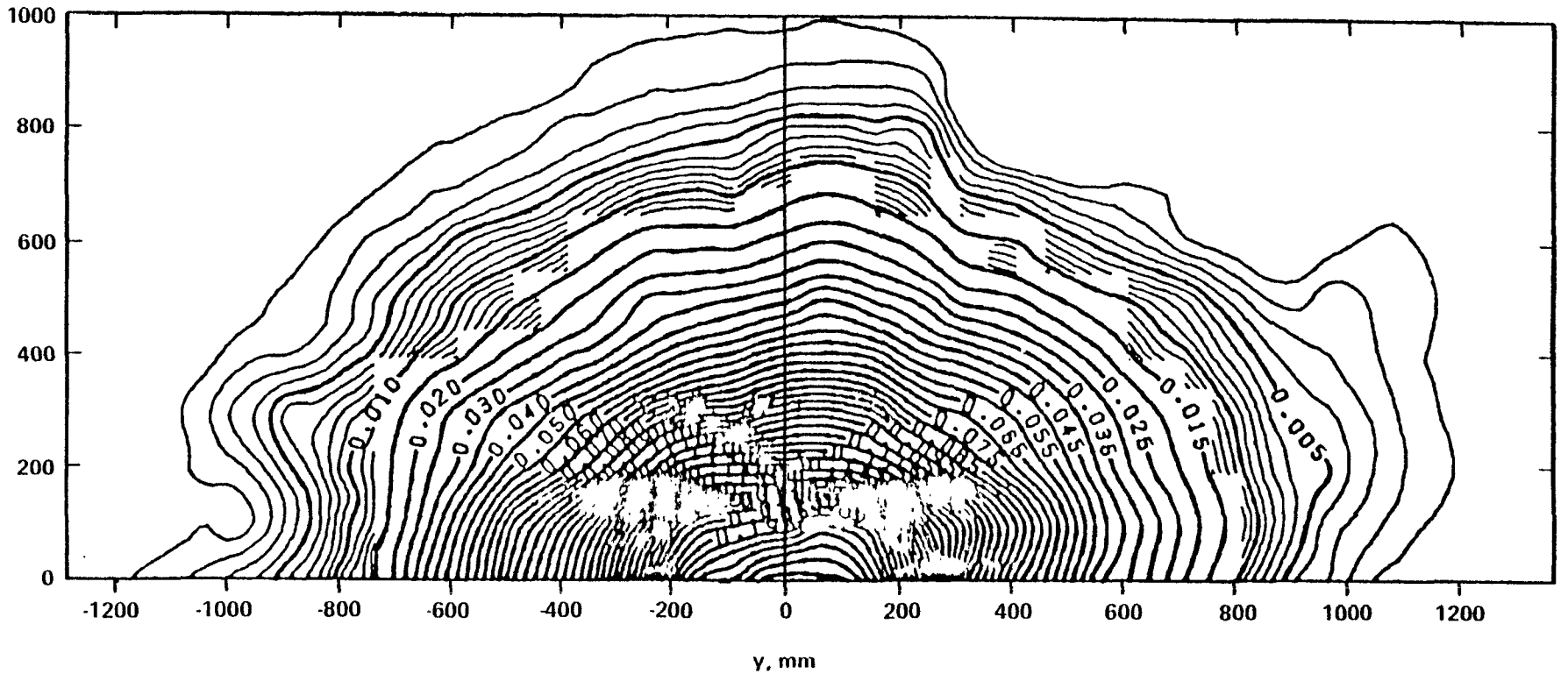

Figure 34. Isoconcentration contours of plume 7488mm downwind from source in flat terrain; H_s = 29mm.

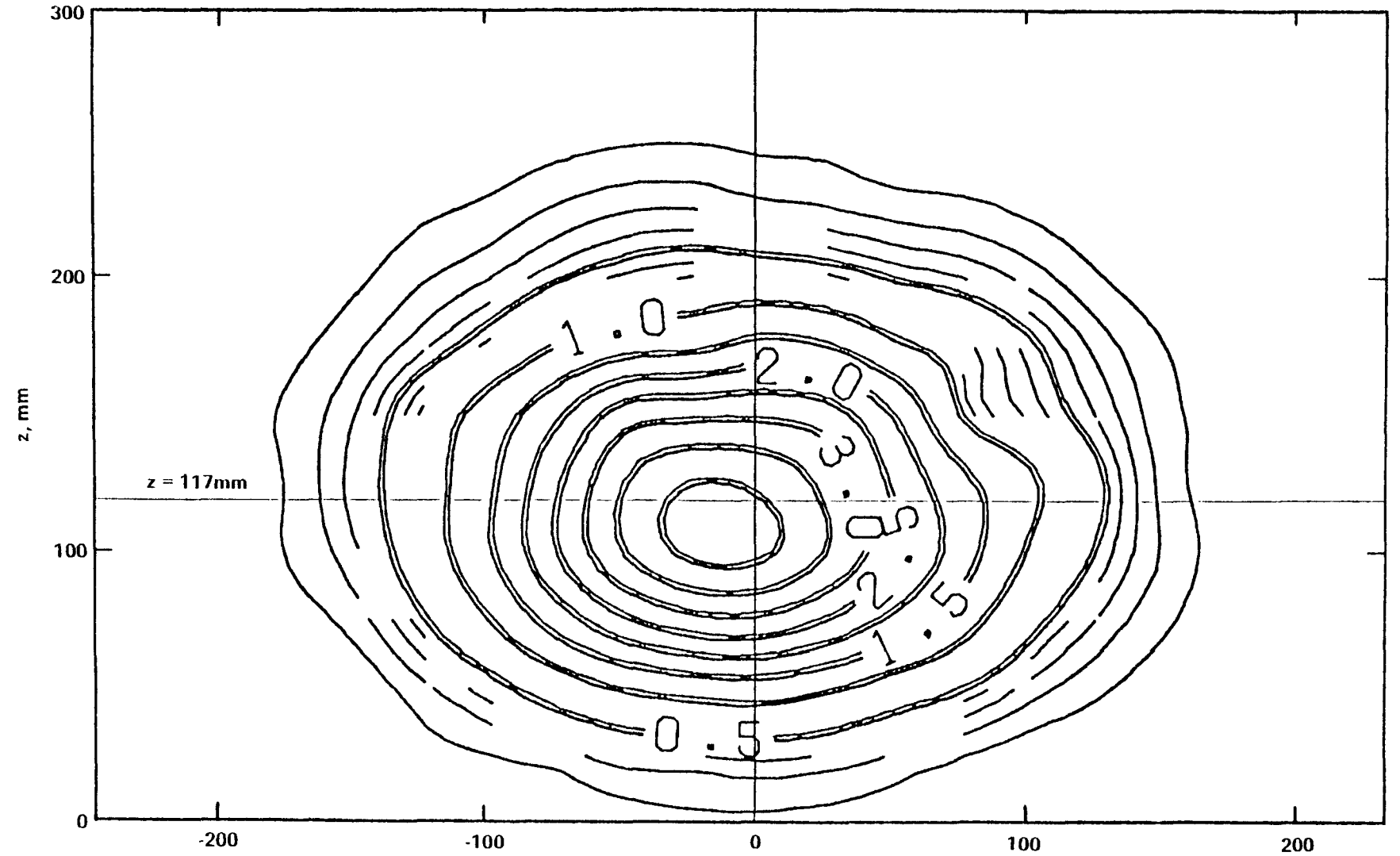

Figure 35. Isoconcentration contours of plume 585mm downwind from source in flat terrain; H_s = 117mm.

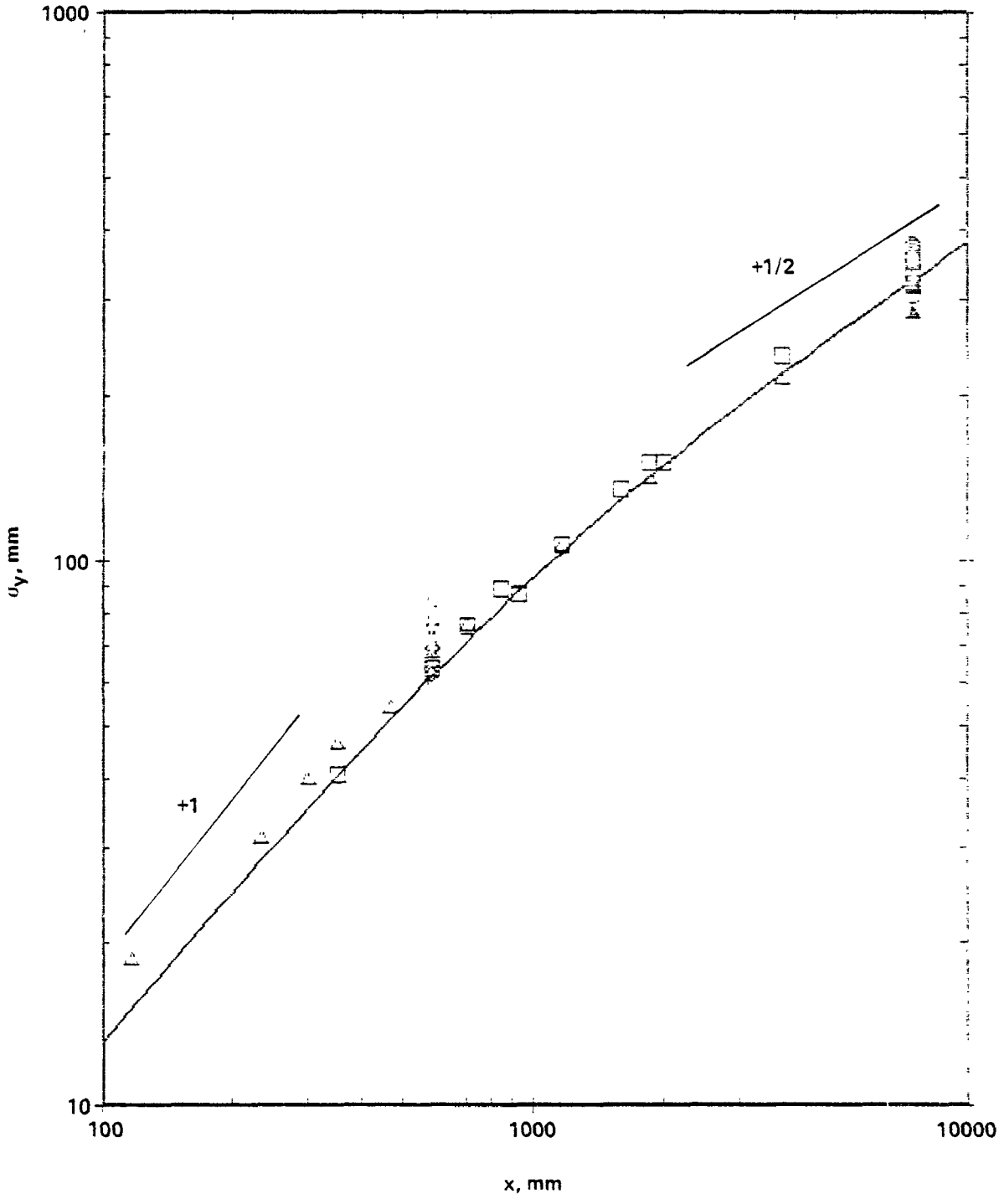

Figure 36. Growth of lateral plume width in flat terrain.

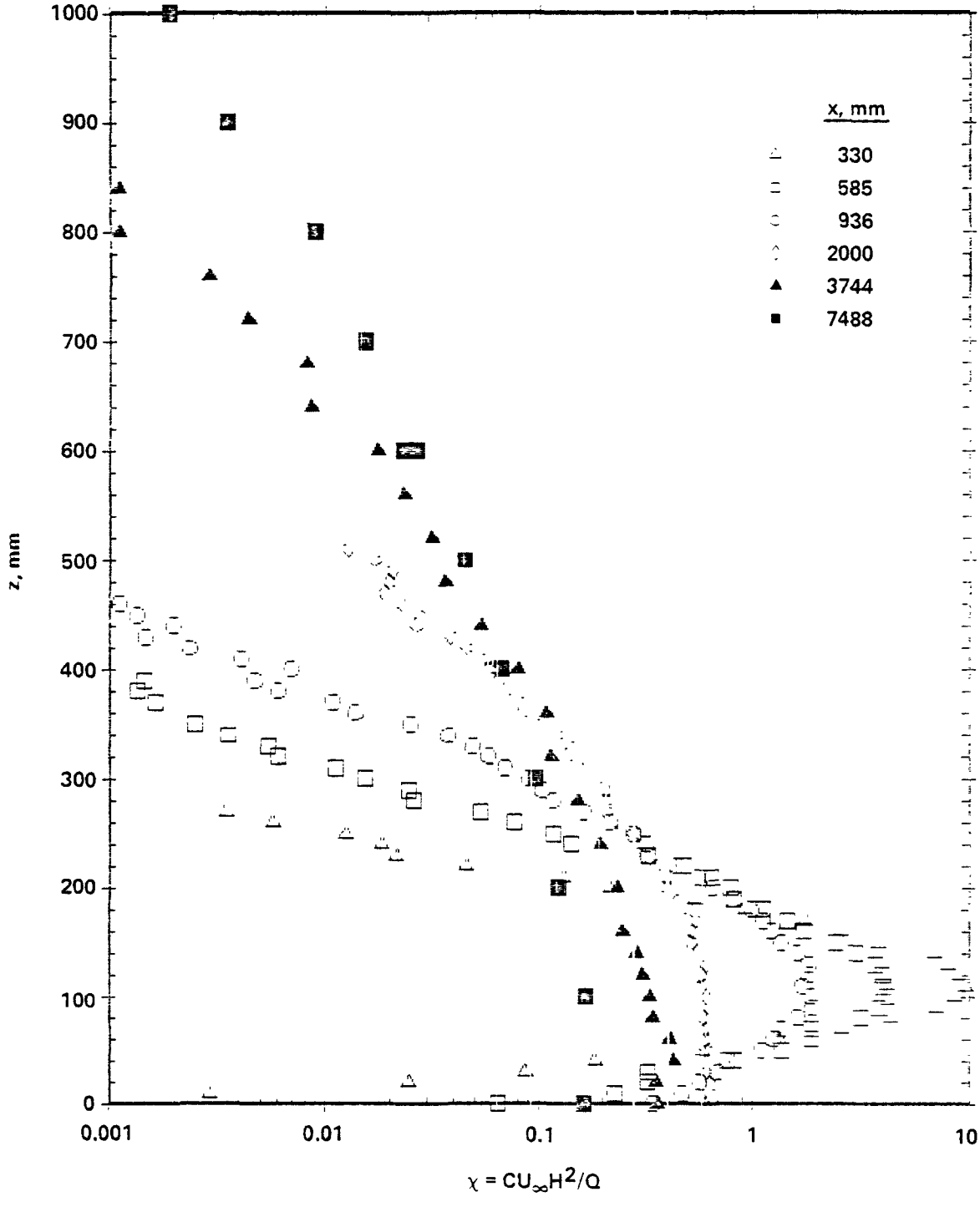

Figure 37. Development of vertical concentration profiles from source of height H_s = 117mm in flat terrain.

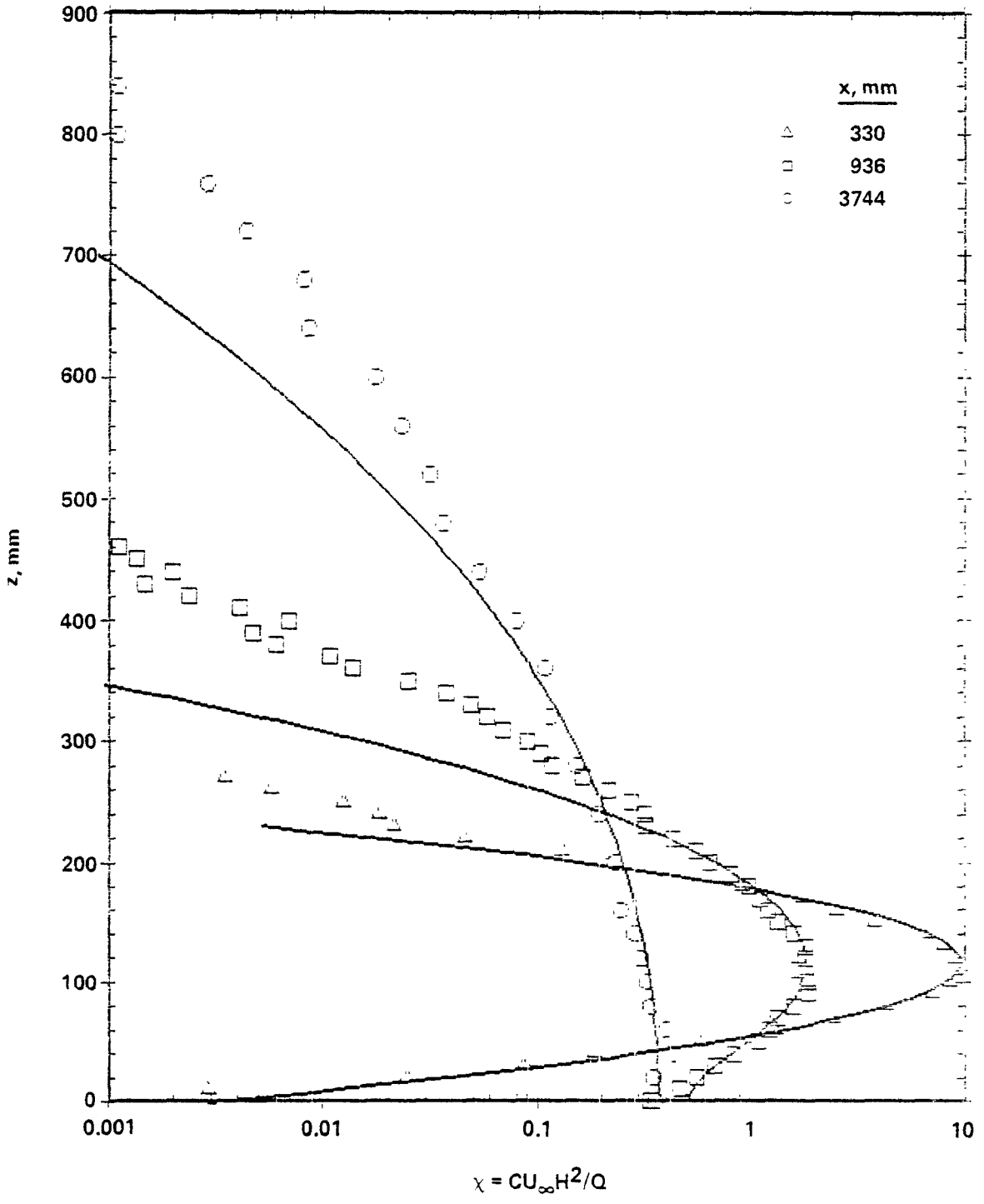

Figure 38. Reflected Gaussian fits to vertical concentration profiles; H_s = 117mm.

flatter than Gaussian--they decrease much more slowly in the tails than Gaussian curves of the same standard deviation.

It is interesting to note that at the downwind distance where the maximum surface concentration occurred (about 1900 mm for stack height 117 mm), the maximum concentration in the vertical prifile was elevated at a height of about $0.6h_s$, and its magnitude was about 25% larger than the surface value. Numerical calculations using the model described in Section 3.1 as well as Pasquill-Gifford curves (Turner, 1970) have predicted comparable results. Slightly farther downwind, the maximum in the vertical was at the surface.

Figure 39 shows the growth of the standard deviation σ_z of the vertical concentration distributions. These σ_z's are the true standard deviations about the centroids as opposed to those derived from "best-fit" reflected-Gaussian curves, because of the poor agreement between the latter and the data. However, in order to make meaningful comparisons between σ_z's, it is necessary to have some similarity in the shapes of the distributions. Since the shapes of the distributions varied with downwind distance as well as with stack height, this graph is presented with trepidation. Further work is required to find similarity functions that would allow more meaningful descriptions of the vertical growth of plumes.

5.1.3. Comparison with theory

Calculations of pollutant dispersion in the wind tunnel have been made using the model described in Section 3.1. For calculating pollutant concentrations using the solution of the diffusion equation, it was necessary to determine the lateral and vertical diffusivities k_y and k_z. It was not possible, of course, to directly measure these values in the wind tunnel. As mentioned in Section 3.1, the vertical diffusivity k_z was calculated with Equation 6, a commonly used expression for the surface layer. Although the vertical turbulent diffusivity began to decrease at large heights in the wind tunnel, it may be noted that when the source height is small compared with the boundary layer height, the behavior of k_z at the upper part of the boundary layer should have little influence on surface concentrations. This observation has been verified through additional calculations wherein k_z was prescribed as increasing linearly with height to 250 mm then linearly decreasing

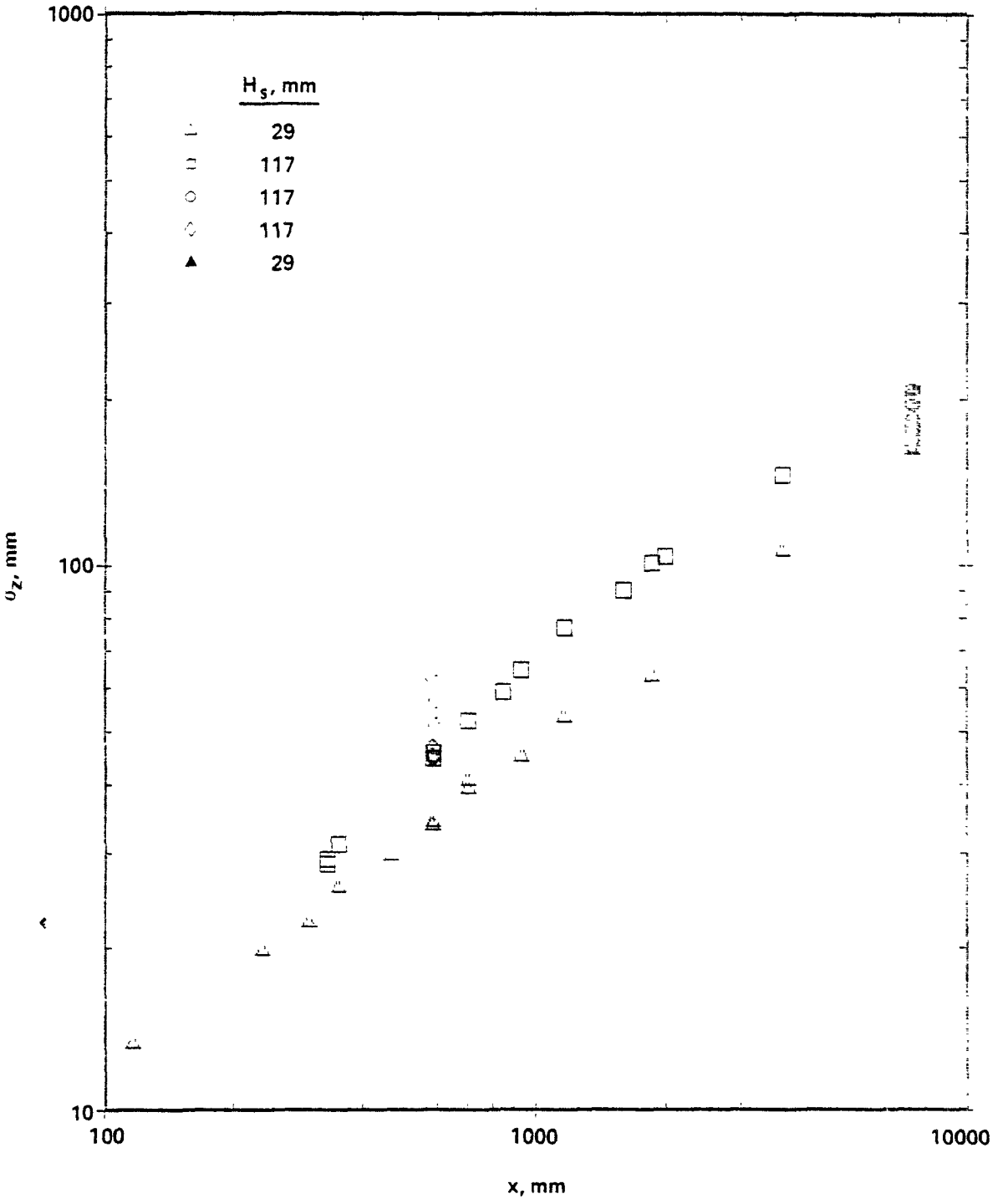

Figure 39. Growth of true standard deviation of vertical concentration distributions in flat terrain.

with height to zero at the top of the boundary layer. Discrepancies in maximum surface concentrations from sources of height up to 176 mm because of this change in the k_z profile were small.

For determining the lateral diffusivity k_y, the following hypothesis of Berlyand (1975) was used:

$$k_y = k_o U \tag{36}$$

as has also been discussed in Section 3.1.

It is possible to relate k_y and the root-mean-square lateral turbulent particle displacement σ_y through

$$k_y = (1/2)d\sigma_y^2/dt \ . \tag{37}$$

In accordance with the hypothesis of "frozen" turbulence, the above equation may be rewritten as:

$$k_y = (1/2)U\, d\sigma_y^2/dx \ , \tag{38}$$

where U = mean wind velocity and x = distance downwind of the source, i.e., t = x/U.

From Eqs. 38 and 39 follows

$$k_o = (1/2)d\sigma_y^2/dx \ . \tag{39}$$

The wind tunnel concentration data showed that σ_y had the following asymptotes

$$\sigma_y = \left\{ \begin{array}{ll} \sigma_\theta x & \text{when } x \to 0 \\ \\ \sigma_\theta \sqrt{2Lx} & \text{when } x \to \infty \end{array} \right\}, \tag{40}$$

where $\sigma_\theta^2 = \overline{v^2}/U^2$ (v = lateral turbulent velocity) and L = integral length scale of turbulence.

Consequently for k_o the equation may be written as

$$k_o = \left\{ \begin{array}{ll} \sigma_\theta^2 x & \text{when } x \to 0 \\ \\ \sigma_\theta^2 L & \text{when } x \to \infty \end{array} \right\} . \tag{41a, 41b}$$

The wind tunnel data showed that $\sigma_\theta \simeq 0.1$ and L = 400 mm (Figure 36). For the entire range of x, it is possible to approximate the behavior of σ_y by

$$\sigma_y = \left[\frac{2\sigma_\theta^2 L x^2}{x + 2L}\right]^{1/2} . \qquad (42)$$

The corresponding expression for k_o is, therefore:

$$k_o = \sigma_\theta^2 L \frac{2x(x + 2L) - x^2}{(x + 2L)^2} . \qquad (43)$$

This formula is very close to the more usual exponential formula derived using an exponential correlation function (Pasquill, 1974),

$$\sigma_y^2 = 2\sigma_\theta^2 L^2 (x/L - 1 + \exp(-x/L)).$$

Numerical calculations of the values as well as locations of maximum surface concentrations from elevated point sources of different heights were made using Equations 41a, 41b, and 43. The results are shown in Figures 40 and 41. It is immediately evident that the form chosen for k_o has a strong influence on the results. As might be expected, the smallest discrepancy between the calculations and the measured data occurred when the interpolation formula 43 was used. Equation 41a gave satisfactory results for small stack heights when the location of the maximum surface concentration was relatively close to the source. Equation 41b was satisfactory for large stack heights. Excluding the smallest stack heights, the calculations underpredicted maximum surface concentrations and overpredicted distances to the maximums. When using Eq. 43, there was an average discrepancy of 9% for the concentration, and 13% for the position. For the stack height 29 mm, the calculations gave a value for the location of the maximum surface concentration close to that measured, but overpredicted the concentration itself by about 19%.

It should be noted that in the calculation, slightly different values of u_* and z_o were used than those given in section 5.1.1. The latter values were obtained only after additional measurements had been made near the end of the experimental program.

Surface concentration distributions as functions of downwind distance from the source are known to depend upon the type of model chosen for lateral

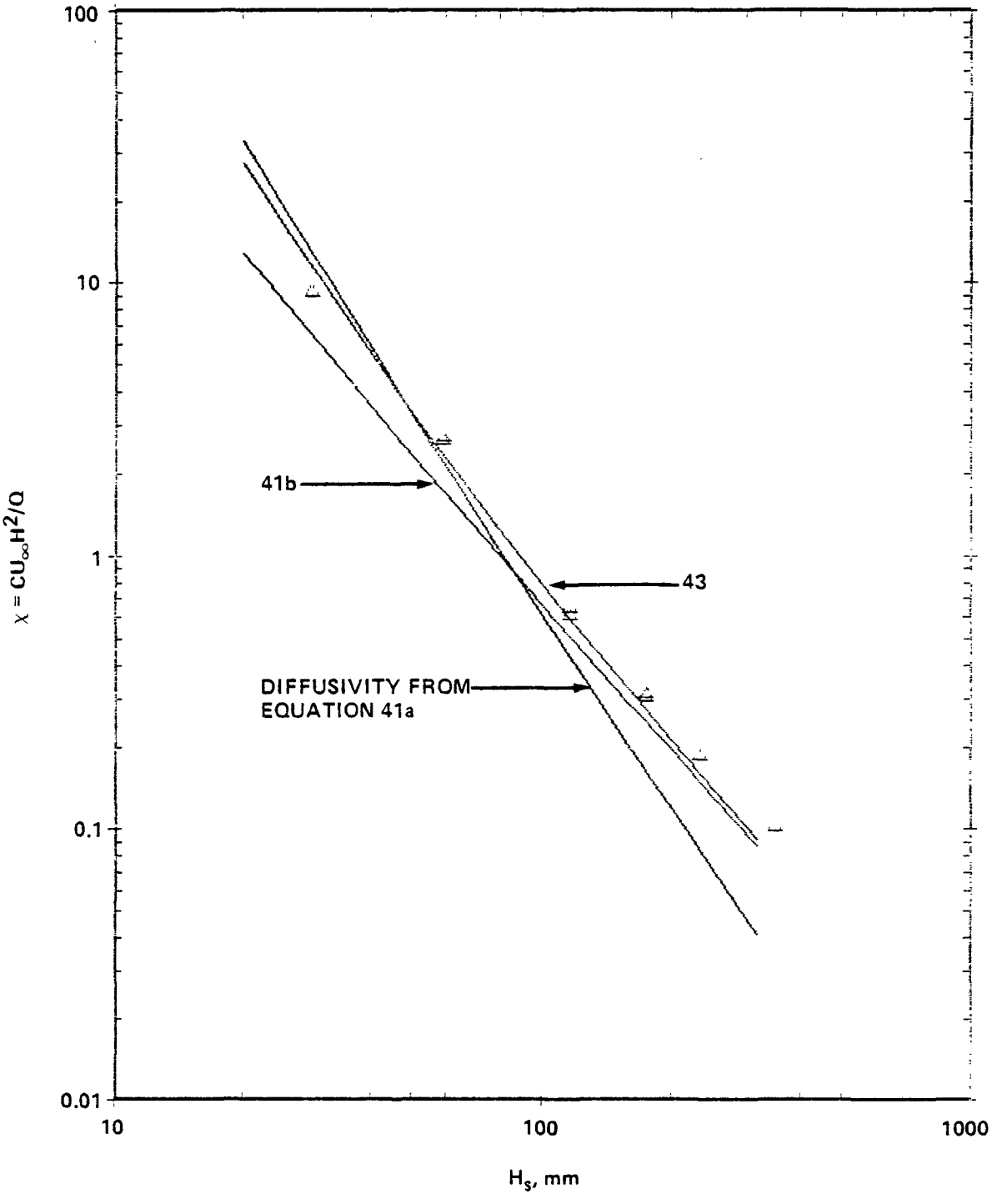

Figure 40. Comparison of numerical calculations of maximum surface concentrations with wind tunnel data in flat terrain.

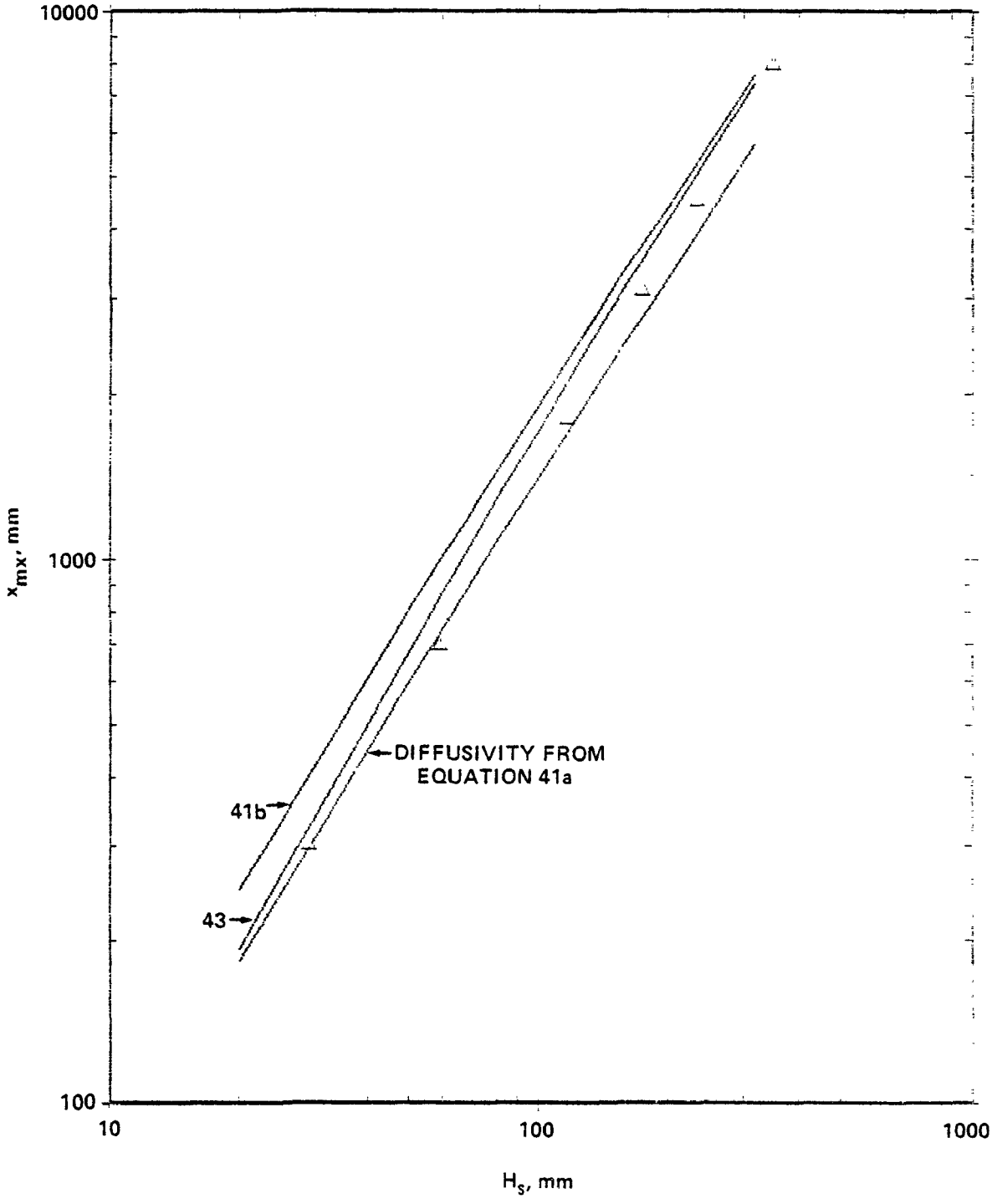

Figure 41. Comparison of numerical calculations of location of maximum surface concentration with wind tunnel data in flat terrain.

diffusion, e.g., (Berlyand, 1975). Since lateral diffusion taking place in the wind tunnel is best approximated using interpolation formula 42, it has been used to derive an expression for the surface concentration profile. The expression has the following form

$$\frac{C}{C_{mx}} = \frac{\exp(3(1 - \frac{x_{mx}}{x})/2f(p))}{\frac{x}{x_{mx}}\left[\frac{1 + f(p)/2p}{1 + \frac{x}{x_{mx}}f(p)/2p}\right]^{1/2}} \quad , \qquad (44)$$

where x = downwind distance from the source, c_{mx} = maximum surface concentration, x_{mx} = location of C_{mx}, $p = L/2x_{mx}^{o}$, $f(p) = \frac{1}{2}[1 - 8p/3 + ((1 - 8p/3)^2 + 8p)^{1/2}]$, and x_{mx}^{o} = location of maximum surface concentration predicted using Equation 41b for k_o. In Figure 42, these profiles are compared with profiles measured for different stack heights. The agreement between them is good.

Some attempts were made to calculate pollutant dispersion assuming the mass diffusivity was not equal to that for momentum, e.g., assuming the turbulent Schmidt number was 0.70 - 0.74. Comparisons with measured data on values and locations of maximum surface concentrations were not good. This question demands further, more detailed investigation of the eddy diffusivity in the wind tunnel boundary layer and the incorporation, within the numerical calculations, of models that more precisely correspond to wind tunnel conditions. Perhaps an experiment is in order to evaluate the magnitude of the turbulent Schmidt number under conditions similar to those of the present study.

5.2. Hills

5.2.1. Velocity measurements

Vertical profiles of mean and fluctuating velocities as well as Reynolds stresses were measured at numerous positions upwind, over and downwind of all model hills. Mean velocity profiles over hill 8 are shown in Figure 43. Note that longitudinal as opposed to streamwise velocities are presented; they may differ slightly near the surface, of course, because the mean velocities there are essentially parallel to the surface. Decreases in mean

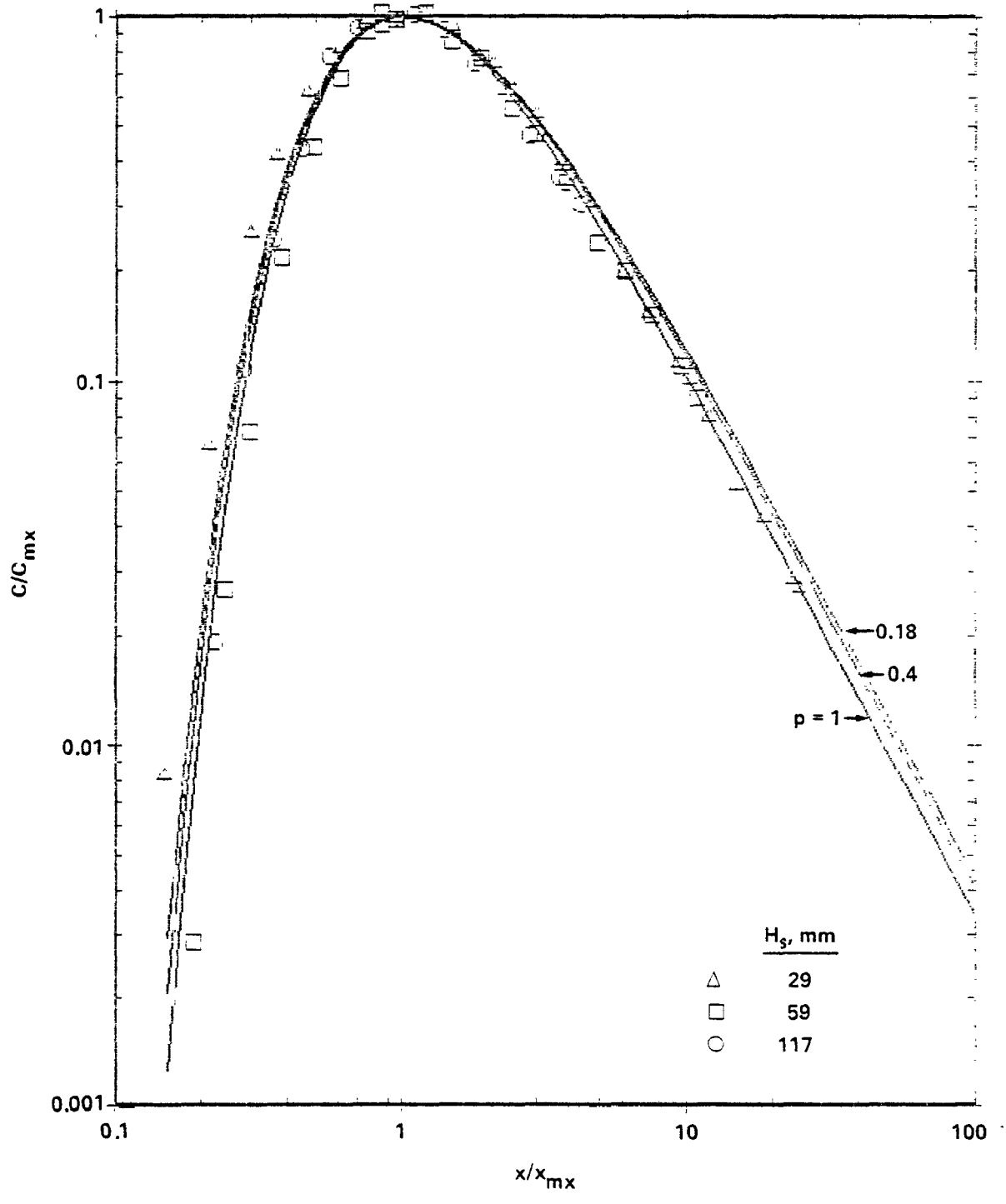

Figure 42. Comparison of surface concentrations predicted by Equation 44 with wind tunnel data in flat terrain.

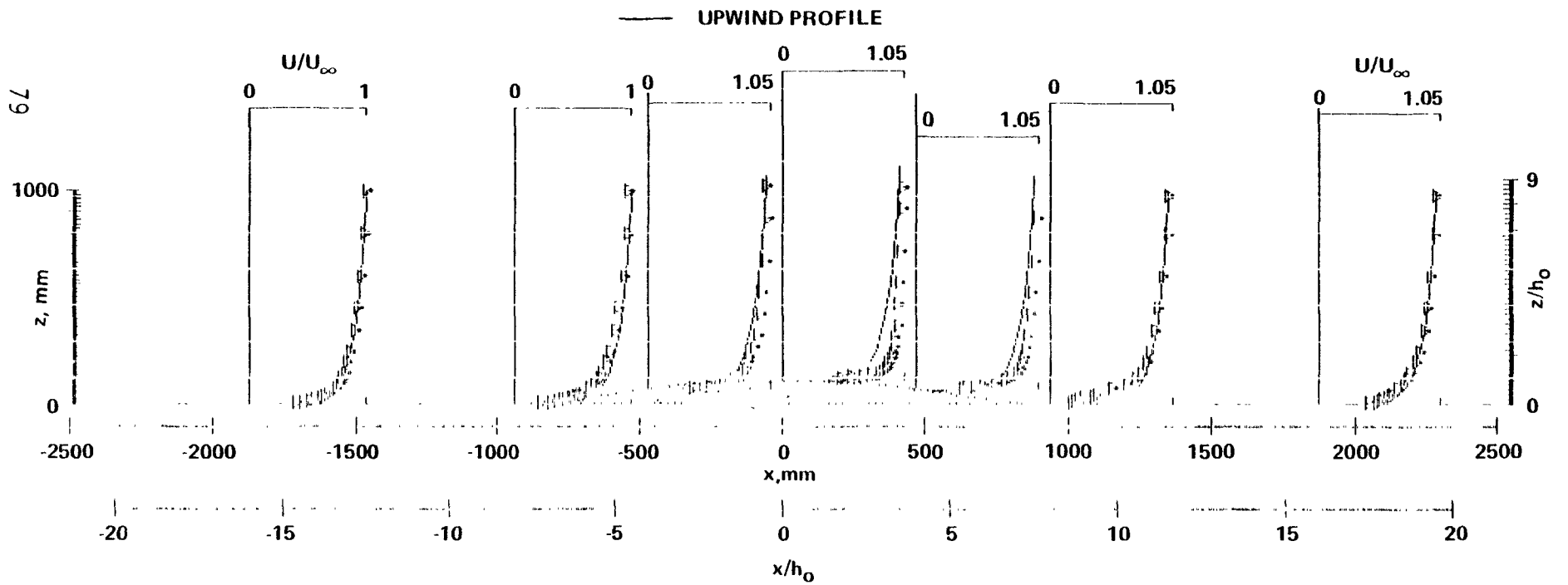

Figure 43. Vertical profiles of mean velocity over hill 8.

velocity (compared with those at the same distance above the surface far upstream) were observed at the upwind and downwind bases, whereas increases were observed elsewhere. A maximum speed-up occurred at the hill top. The decrease over the downwind base was significantly greater than that over the upwind base, contrary to predictions of potential flow theory. The ratio of the velocity at a height $h_o/3$ over the downwind base to the velocity at the same elevation far upwind was 0.58. The ratio of that above the upwind base to that far upstream was 0.82. The decrease in velocity at the downwind base was relatively sharp and occurred mainly below the elevation of the hill top. The speed-up over the top covered a much greater depth of the boundary layer. The maximum speed-up took place at an elevation of $h_o/6$ and had a value of $U(h_o/6)/U_\infty(h_o/6) = 1.5$. The mean velocity profile had almost completely recovered (within 10%) 100 hill heights downwind.

Separate flow visualization studies using smoke showed no separation, at least in the usual sense, of the flow on the lee side of hill 8; however, intermittent separation was observed, as occasional (but rare) puffs of smoke were observed traveling short distances, and for very short time durations, in the reverse direction, i.e., up the lee slope.

Mean flow angles are shown in Figure 44. The trends here are as expected, with maximum angles of about 9° compared with a maximum hill slope of 10.5°. Angles very close to the surface, however, appeared to decrease toward zero. This is obviously an incorrect indication and probably resulted from the decreased angular sensitivity of the hot-wire anemometry at the very low flow speeds and very large, local turbulence intensities.

Streamwise as contrasted with longitudinal turbulence intensity profiles are presented in Figure 45. Except near the downwind base, changes of turbulence were generally less than 10%, decreasing in the upslope region and increasing near the top and on the downslope. An excess of about 30%, however, was seen at an elevation of $h_o/2$ above the downwind base. Similar trends occurred with the normal, as contrasted with vertical, turbulence intensities, presented in Figure 46. Note, in reviewing this figure, that there was a measurable decrease in the vertical turbulence intensity in the boundary layer in the absence of the hill, which is not shown on the figures.

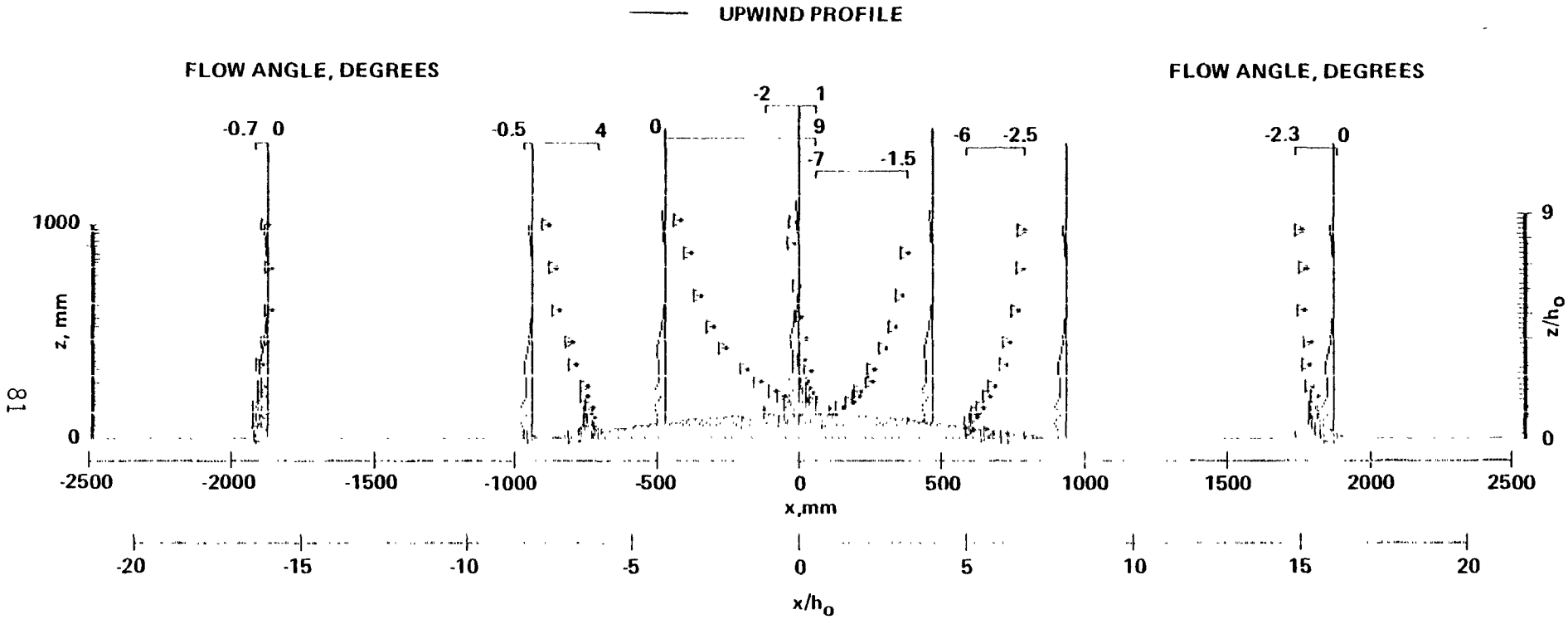

Figure 44. Flow-angle profiles over hill 8.

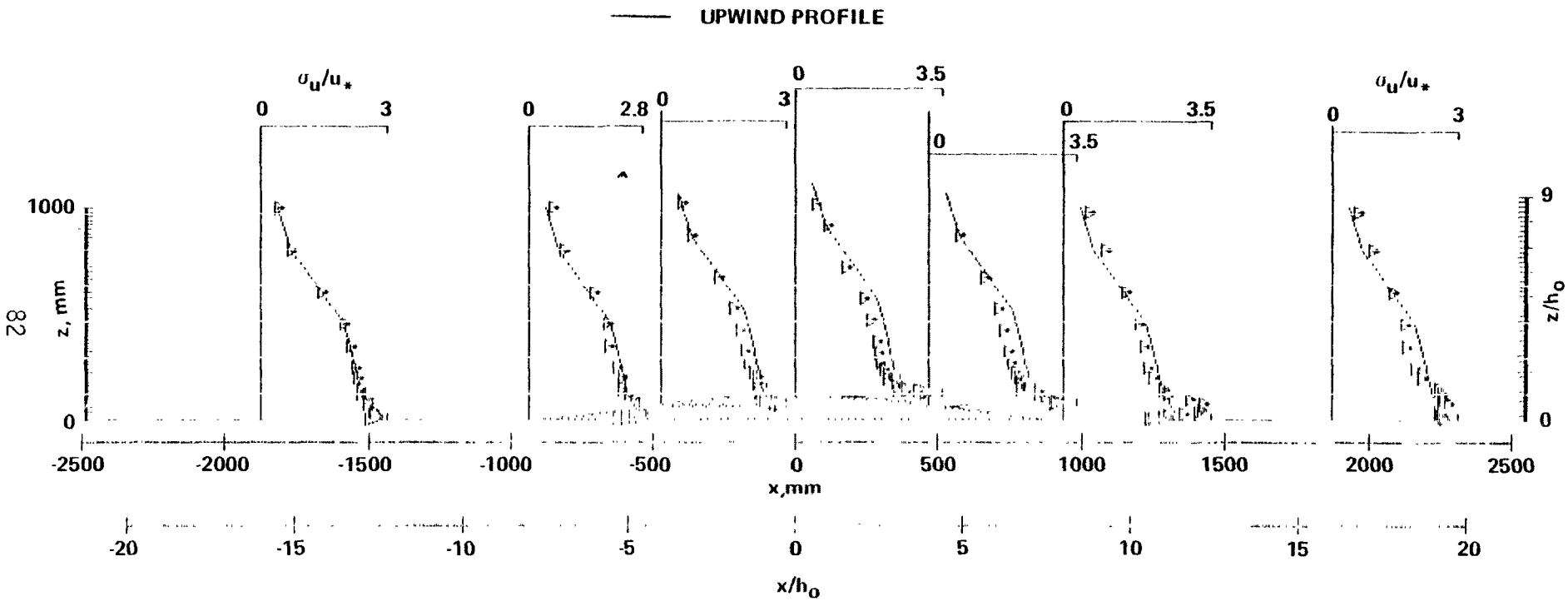

Figure 45. Steamwise turbulence intensity profiles over hill 8.

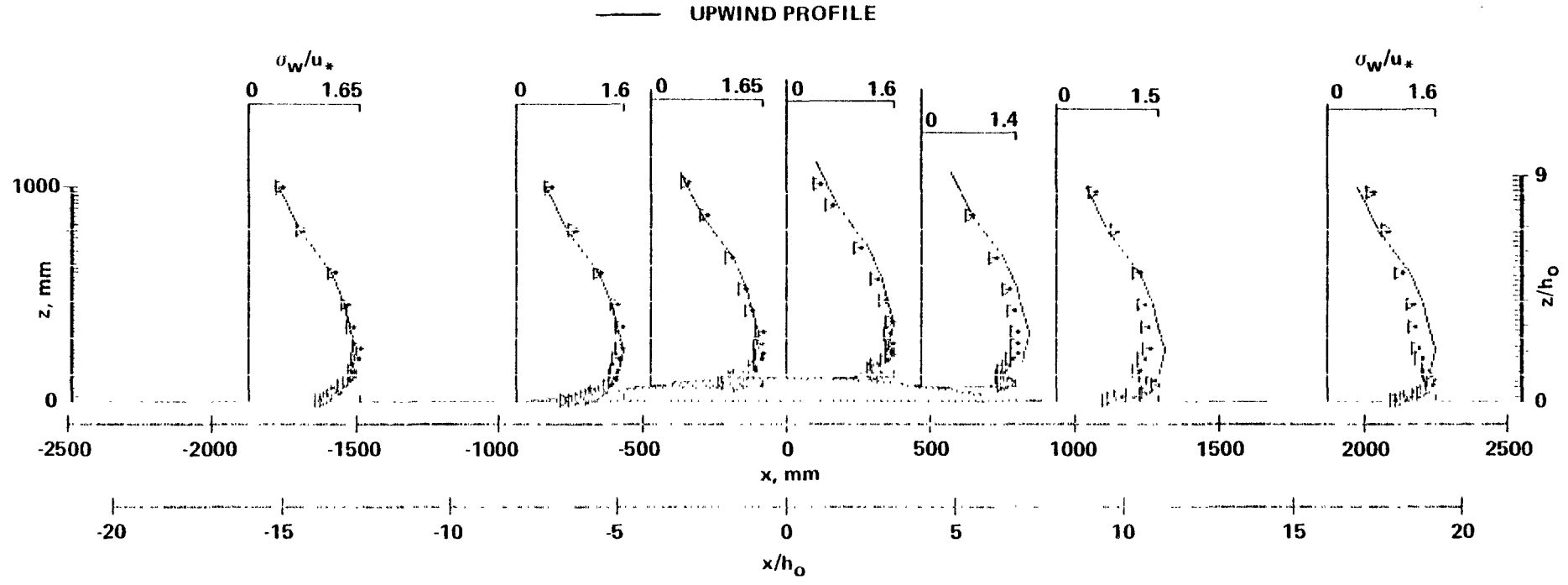

Figure 46. Normal turbulence intensity profiles over hill 8.

The Reynolds stresses are described in a "natural" coordinate system that is parallel and perpendicular to the streamlines (Figure 47). In the lower layers, the Reynolds stresses were considerably increased, reaching nearly a factor of 2 at the downwind base.

On the lee sides of hill 3, flow separation clearly occurred, as confirmed using flow visualization. Downwind of the separation point, there was a deep cavity region whose height was about equal to the hill height. The hot-wire anemometer was able, of course, to measure only the velocity magnitude, but not its direction. For velocity measurements on the lee side of hill 3, therefore, not only hot-wire anemometers, but also double-ended Pitot tubes were used. Comparisons of the two techniques are made in Figure 48, where mean velocity profiles over the downwind base of hill 3 are plotted. The data obtained with the Pitot tube show the existence of the reversed mean flow in the recirculation zone, whereas the hot-wire anemometer measurements indicate proper magnitudes of velocity, but obviously, the wrong direction. Note that the elevation of the zero-longitudinal mean velocity was about half the hill height. This figure contains additional information on special experiments with large hill 3 and variations with Reynolds number (see later discussion in Section 5.3).

Mean velocity profiles over the upwind base and top of hills 3 and 5 resembled those over hill 8, except that the deviations from the velocity profile in the incident flow were larger. Downwind of the hill centers, of course, the flow structure changed drastically because of the separation.

Velocity measurements within the suspected cavity region of hill 5 were also made with a pulsed-wire anemometer, which is sensitive to flow direction (Bradbury and Castro, 1971). Velocity profiles measured by both pulsed-wire and hot-wire anemometers at the downwind base of hill 5 are presented in Figure 49. It is evident that, at least above 10 mm height, there was no flow separation in terms of the mean velocity pattern. This was surprising because the smoke visualization showed transport up the lee slope, opposite in direction to the free-stream flow. The visualization seemed to indicate that a cavity region existed with height equal to at least half the hill height! This discrepancy, however, may be understood through careful study

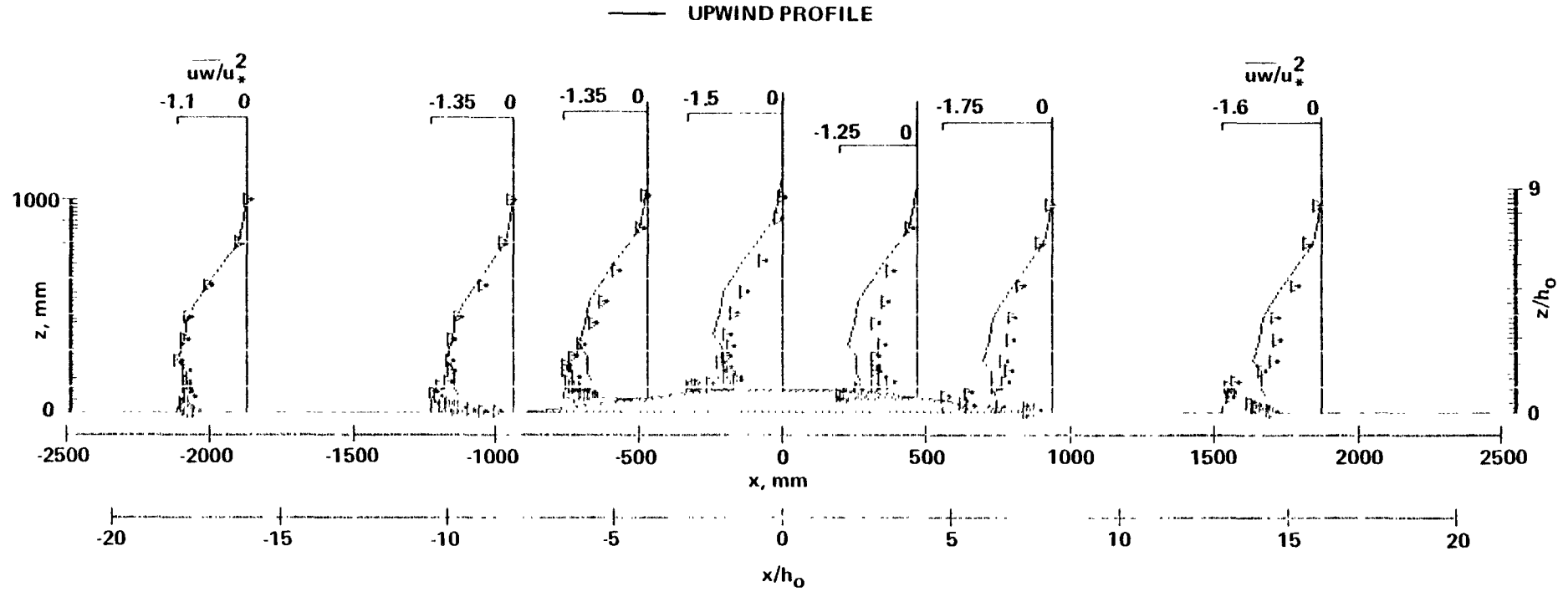

Figure 47. Reynolds stress profiles over hill 8.

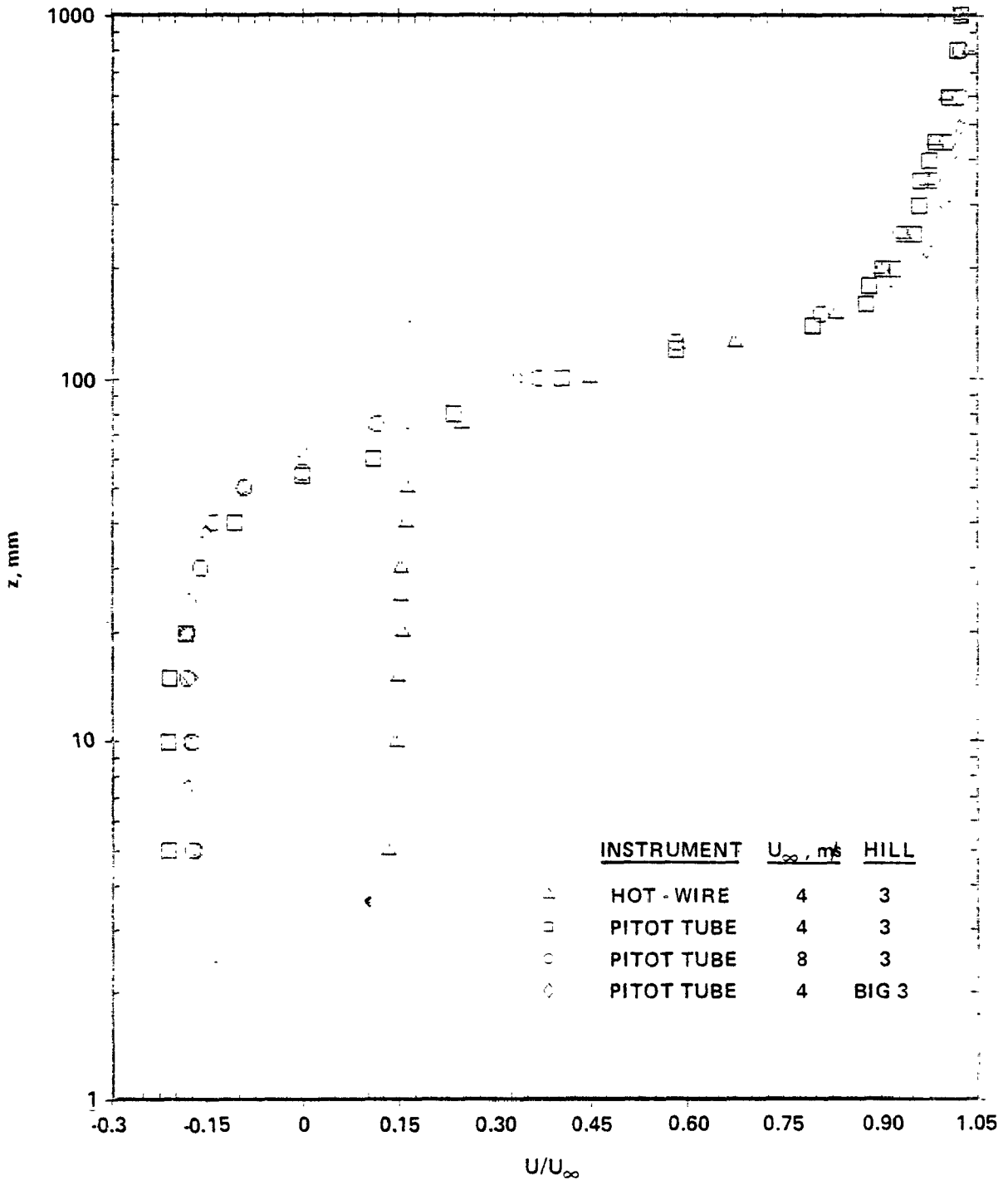

Figure 48. Mean velocity profiles inside cavity region of hill 3.

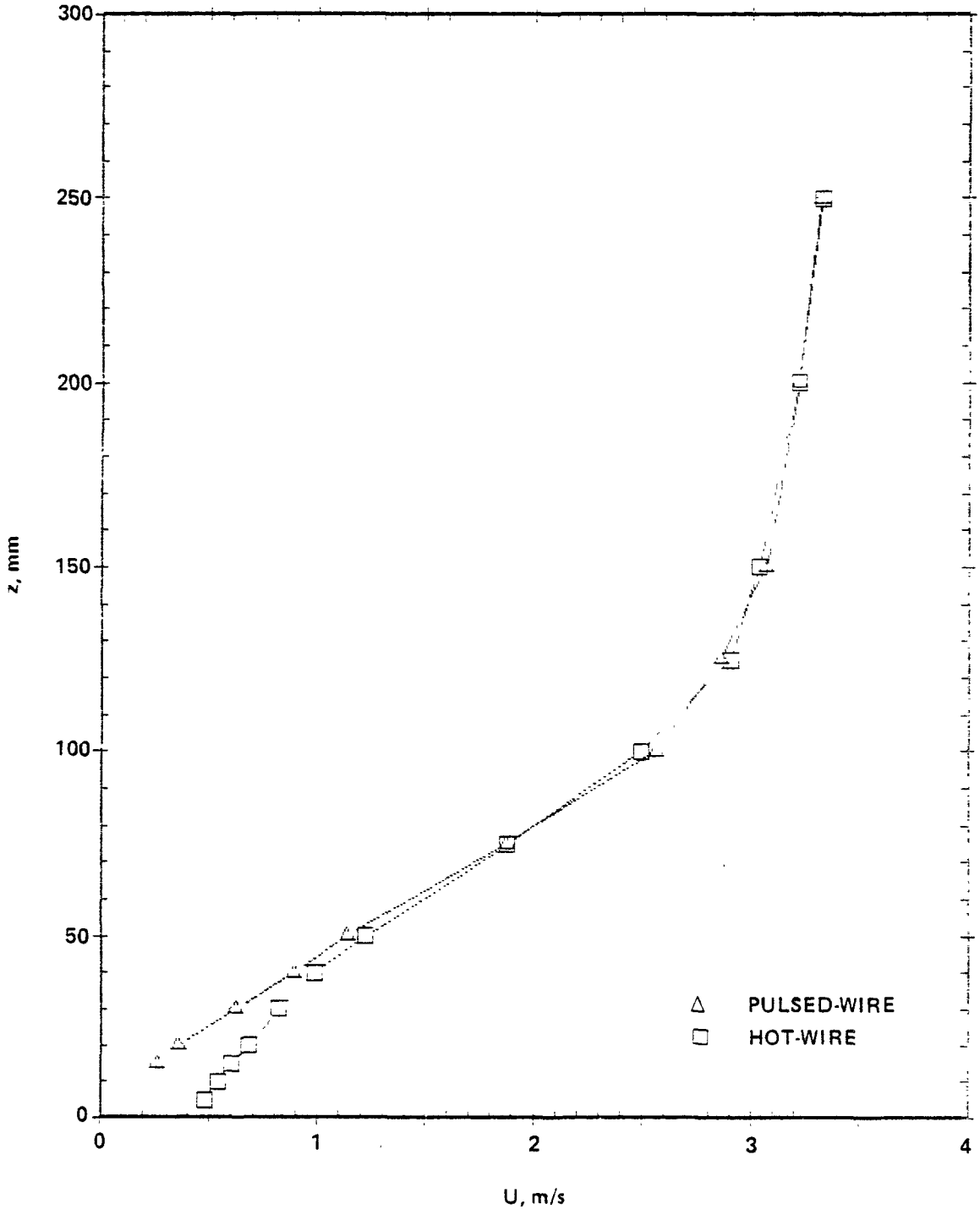

Figure 49. Mean velocity profiles measured at downwind base of hill 5.

of the probability density distribution of velocity fluctuations, shown in Figure 50. The average velocity U_A was small but positive. The turbulence intensity was extremely large compared with the mean velocity, and the instantaneous velocity was negative perhaps 40% of the time. Thus, the longitudinal turbulent transport exceeded the mean transport, giving the illusion of a separated recirculating cavity region. In this figure, at a height of 20 mm, the longitudinal turbulence intensity was twice as large as the mean velocity. (The large probability at zero velocity as well as the small probabilities near zero are due to the limited yaw response of the pulsed-wire as explained by Bradbury (1976); they should be ignored).

From Figure 49, it is evident that the hot-wire anemometer indicated larger velocities in the region below 50 mm; this is so because the hot-wire rectified the velocity signal, which was frequently negative. It is evident that the values measured by the hot-wire need to be corrected when the indicated longitudinal turbulence intensity exceeds $\sim$ 45%.

The double-ended Pitot tube can also rectify signals and over-estimate the value of mean velocity because of its nonlinear response. A comparison of this device with the pulsed-wire anemometer measurements inside the recirculation zone downwind of an obstacle is shown in Figure 51. It is important to note for later discussion that the point of zero-mean velocity was located with reasonable accuracy. Below the point of zero-mean velocity, the intensity of turbulence exceeded 60%, and the double-ended Pitot tube indicated larger absolute values of velocity (up to 40% larger).

5.5.2. Concentration measurements

Surface concentrations resulting from the stack of height 59 mm ($h_o/2$) placed at different positions relative to the three small hills are shown in Figures 52 through 54 (x_s = (1): upwind base; x_s = (2): top center; x_s = (3): downwind base of hills). When the stack was placed upwind of the hills, the maximum surface concentrations occurred at or upwind of the hill crests, and the values of these were significantly increased. For hill 3, x_{mx} was increased by a factor of 2.5 over that which would have occurred over flat terrain, albeit further downstream. The influence of the highly turbulent

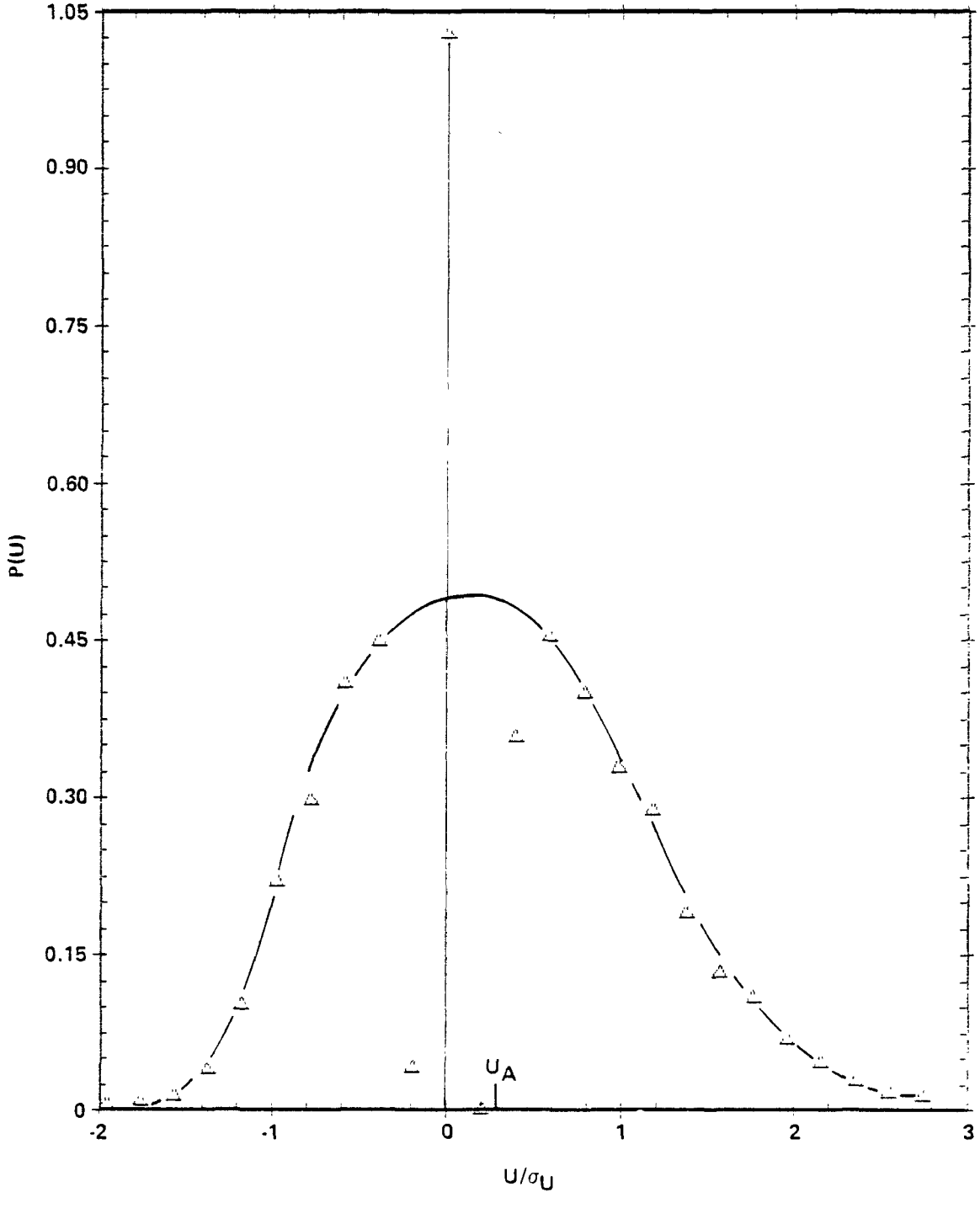

Figure 50. Probability density of velocity fluctuations at 20 mm above down wind base of hill 5.

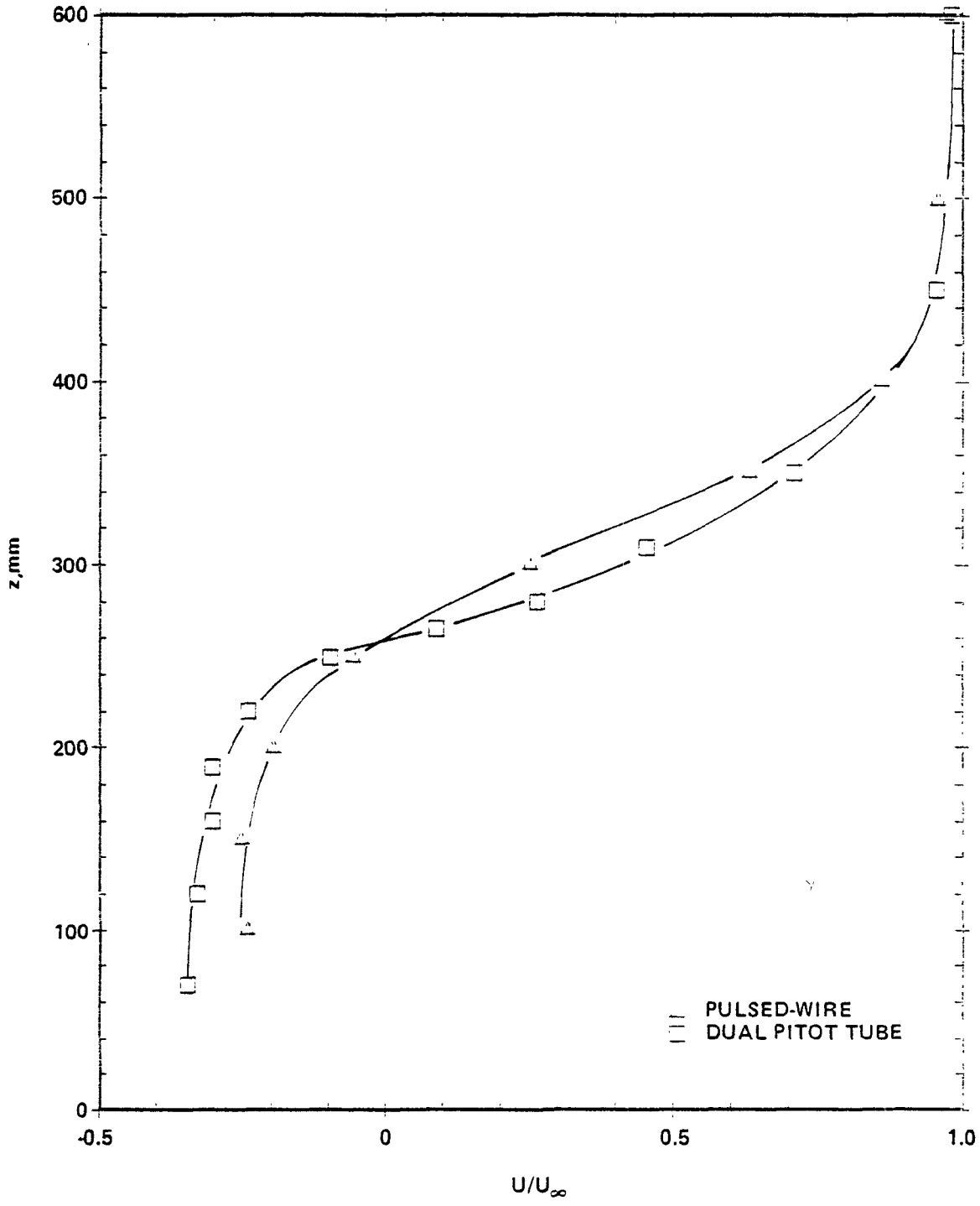

Figure 51. Mean velocity profiles measured in the recirculating wake of an obstacle.

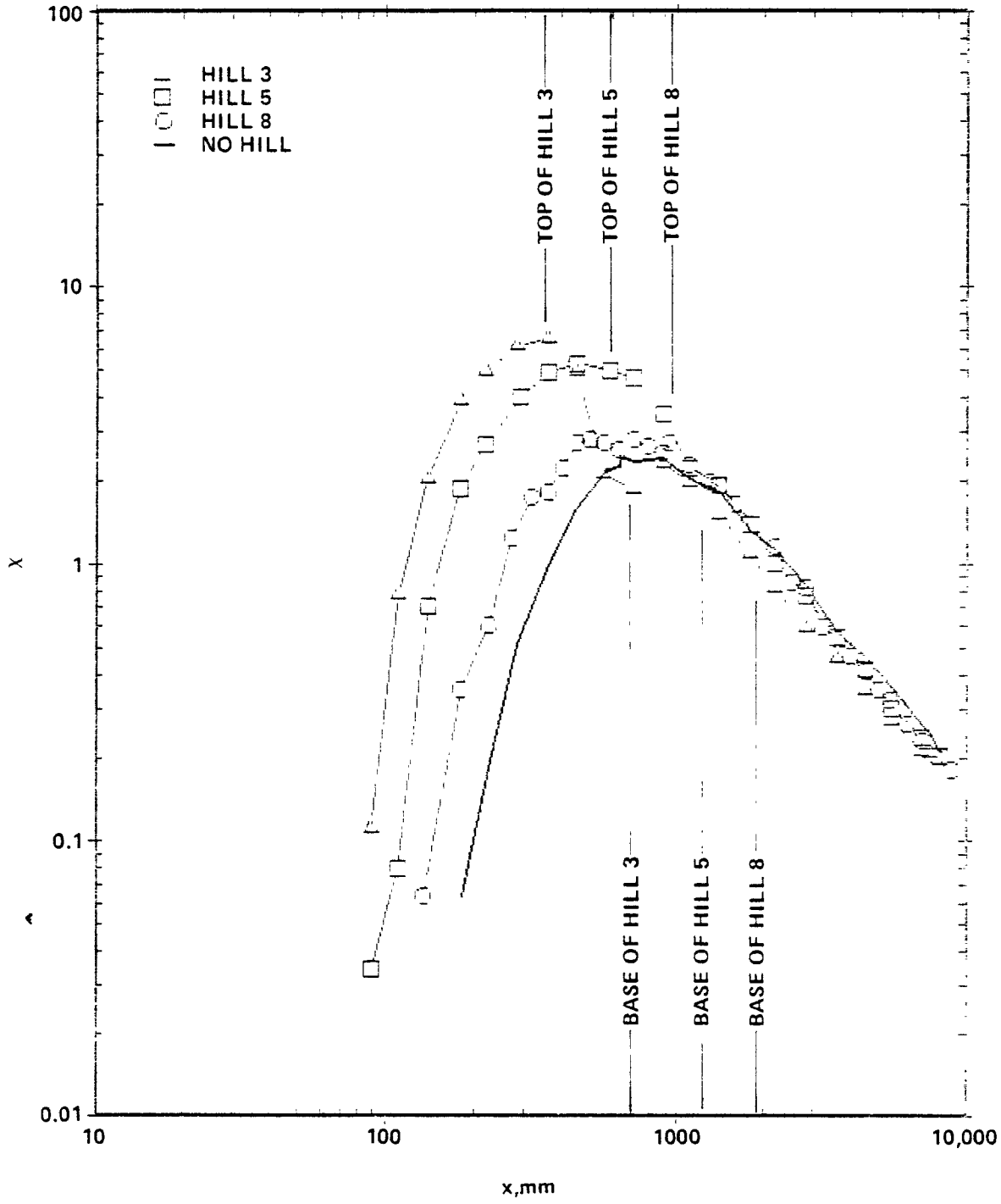

Figure 52. Surface concentration profiles over hills; upwind base stack location; H_s = 59 mm.

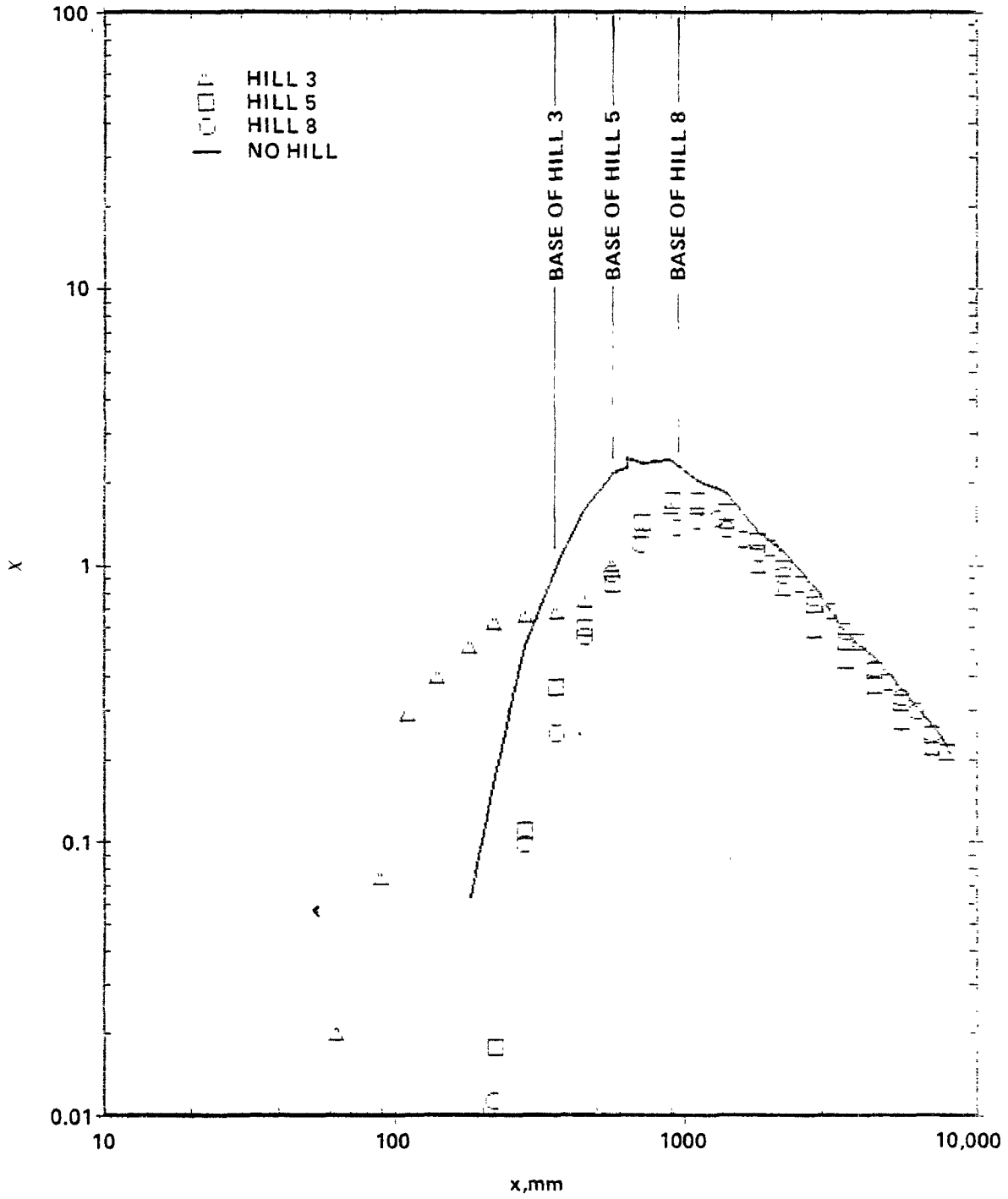

Figure 53. Surface concentration profiles over hills; hill top stack location; H_s = 59 mm.

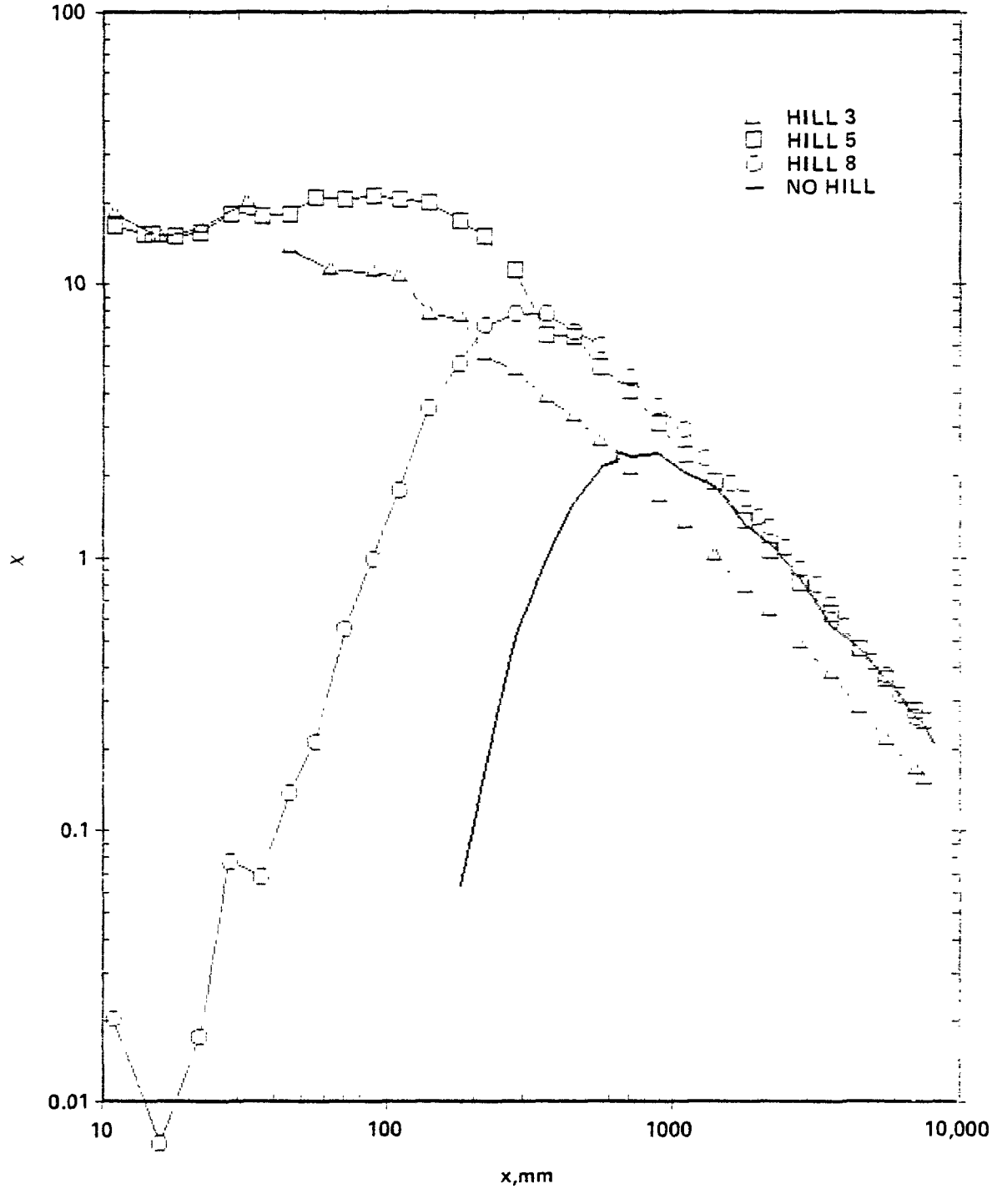

Figure 54. Surface concentration profiles over hills; downwind base stack location; H_s = 59 mm.

zone is noticeable for hill 5; the influence of the separate flow region is unmistakable for hill 3.

For this particular configuration, surface concentrations within the cavity region were sharply reduced from the upstream value. The bulk of the plume evidently remained outside the cavity. This cavity region appeared to have a permanent influence on concentrations farther downwind in that they followed the same dilution rate but the magnitude of the concentrations was reduced by about 20%. This phenomenon was probably the result of greatly increased lateral diffusion (see later discussion) because of the flow separation in the lee of the hill.

Figure 53 shows results of placing the stack on the top of each of the hills. The significant reductions in surface concentrations and increases in the distances to the points of maximum concentration were probably caused by the divergence of streamlines from the top to the downwind bases of the hills. For hill 3, however, an abrupt change in the curvature of the surface profile occurred slightly beyond the downwind base. The location of the maximum concentration evidently marks the reattachment point of the separation streamline, which is the end of the cavity region.

When the stack was placed at the downwind base (Figure 54), maximum concentrations were increased and distances to the points of maximum concentration were decreased. For hills 3 and 5, maximum surface concentrations were increased by an order of magnitude. Maximum concentrations for hills 3 and 5 were located very close to the base of the stack--for hill 5, virtually beneath the stack, and for hill 3, slightly upwind (!) of the stack, as may be seen on Figure 55. The maxima were located at the same positions when the stack height was 29 mm. In both cases, significant concentrations were measured upwind of the stack. These phenomena reflect the presence of the highly turbulent zone, where the turbulent transport exceeded the mean transport. An additional cause for hill 3 was the reversed wind flow.

The largest terrain correction factor (TCF) from all the measurements made was with a stack of height $h_0/4$ located at the downwind base of hill 5, that is, the maximum surface concentration was found to be 15 times the maximum observed in the absence of the hill. For hill 3, the largest TCF ($\sim$ 11)

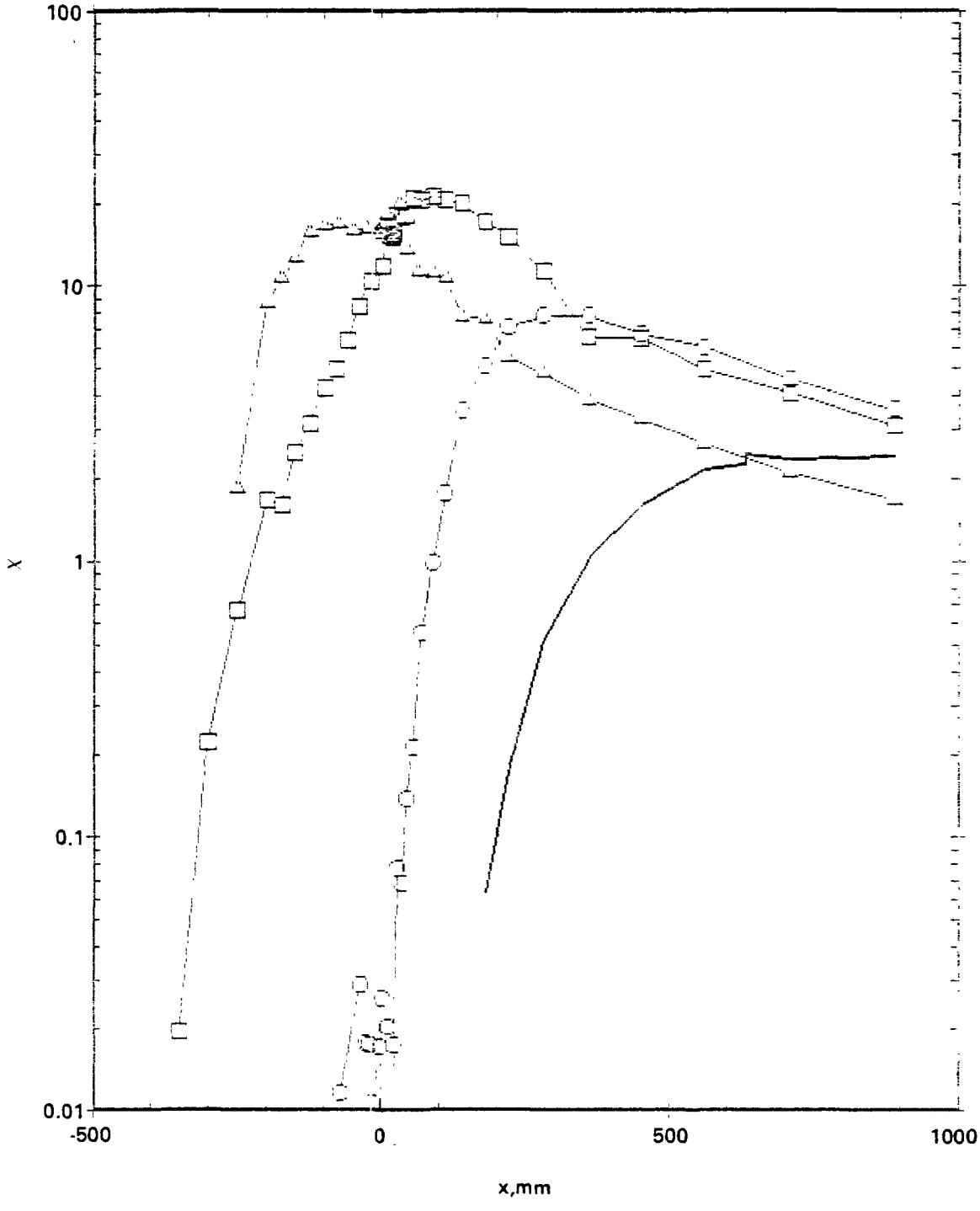

Figure 55. Surface concentration profiles over hills; downwind base stack location; H_s = 59 mm; semilogarithmic plot.

was observed when the stack height was equal to the hill height, so that the source location was very close to the reattachment streamline. In this case, the region of very low mean wind speed (hill 5) was evidently more dangerous than the reversed flow in the cavity region (hill 3).

Figure 56 shows the development of vertical concentration profiles downwind of a source 117 mm high (h_o) placed upwind of hill 8. Profiles obtained from the same source in flat terrain are shown for reference. At the crest of the hill, the profile shapes are similar, but the plume over the hill is obviously narrower and closer to the surface than is the reference plume. This resulted, of course, from the convergence of streamlines over the hill. Just the opposite occurred at the downwind base; the plume was wider and farther from the surface than the reference plume, due to the rather strong divergence of streamlines there. Sixteen hill heights downwind of the crest, the profiles were practically indistinguishable.

Similar but less noticeable changes were observed for the plume from the 29 mm source shown in Figure 57. These were rather surprising, since more marked changes would be expected with the smaller stack. However, the maximum concentration was located very close to the source, hence, very close to the upwind base of the hill, a fact that may help to explain the less noticeable changes.

Figure 58 shows that the effect of hill 3 on an upwind stack 117 mm high was to downwash the plume on the lee side. Resulting surface concentrations downwind of the hill were significantly higher than in the absence of the hill. Notice that in the cavity region, concentrations were essentially uniform with height, indicating very rapid mixing.

Lateral plume widths were generally enhanced by the presence of the hills. As shown in Figure 59, the amount of enhancement depended upon the source height, the position of the stack relative to the hill, and to the hill shape; enhancement was greater for shorter stacks, downwind base locations and steeper hills. When the stack was placed on the top of hill 8, however, the lateral plume widths were very slightly decreased.

Interestingly, the data for all hills, all stack heights and all stack positions can be collapsed reasonably well onto a single curve when plotted

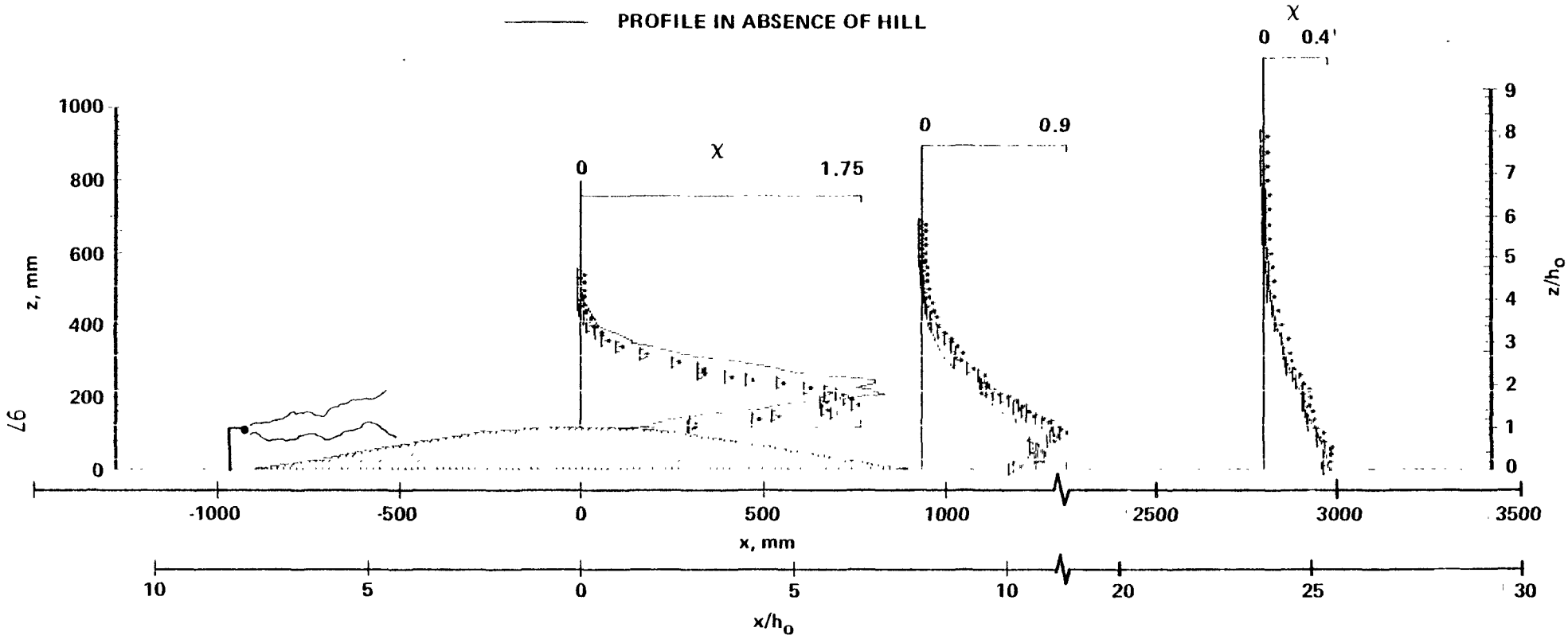

Figure 56. Vertical concentration profiles over hill 8; $H_s = h_o$.

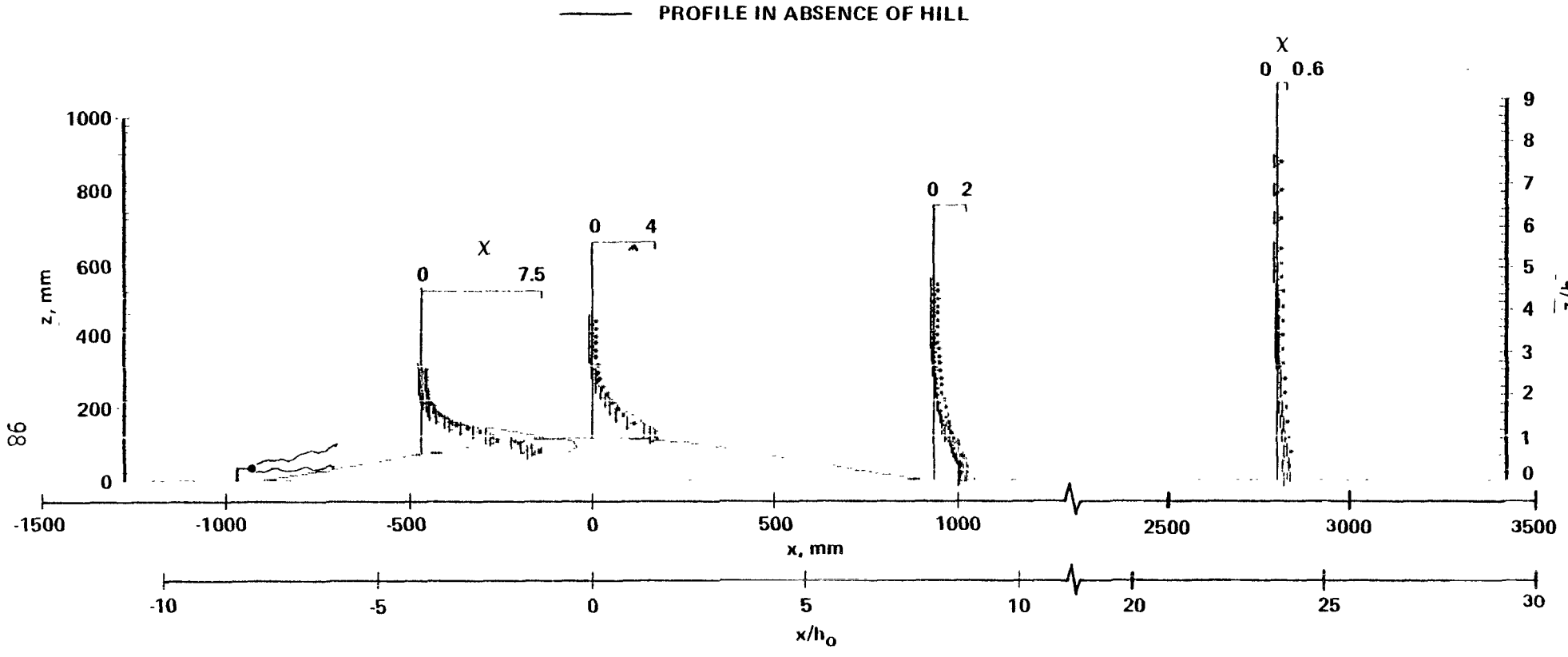

Figure 57. Vertical concentration profiles over hill 8; $H_s = h_o/4$.

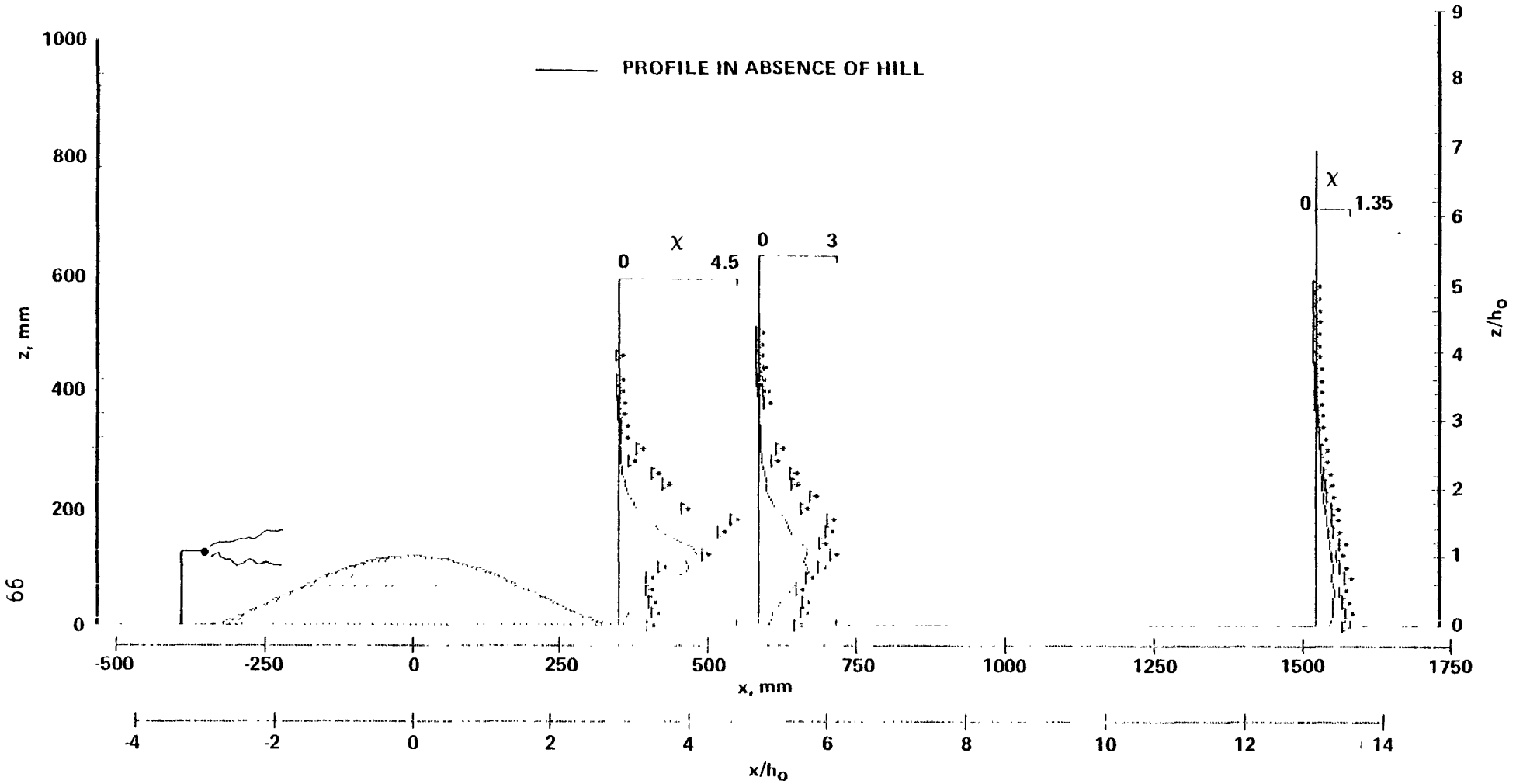

Figure 58. Vertical concentration profiles over hill 3 showing influence of recirculation zone; $H_s = h_o$.

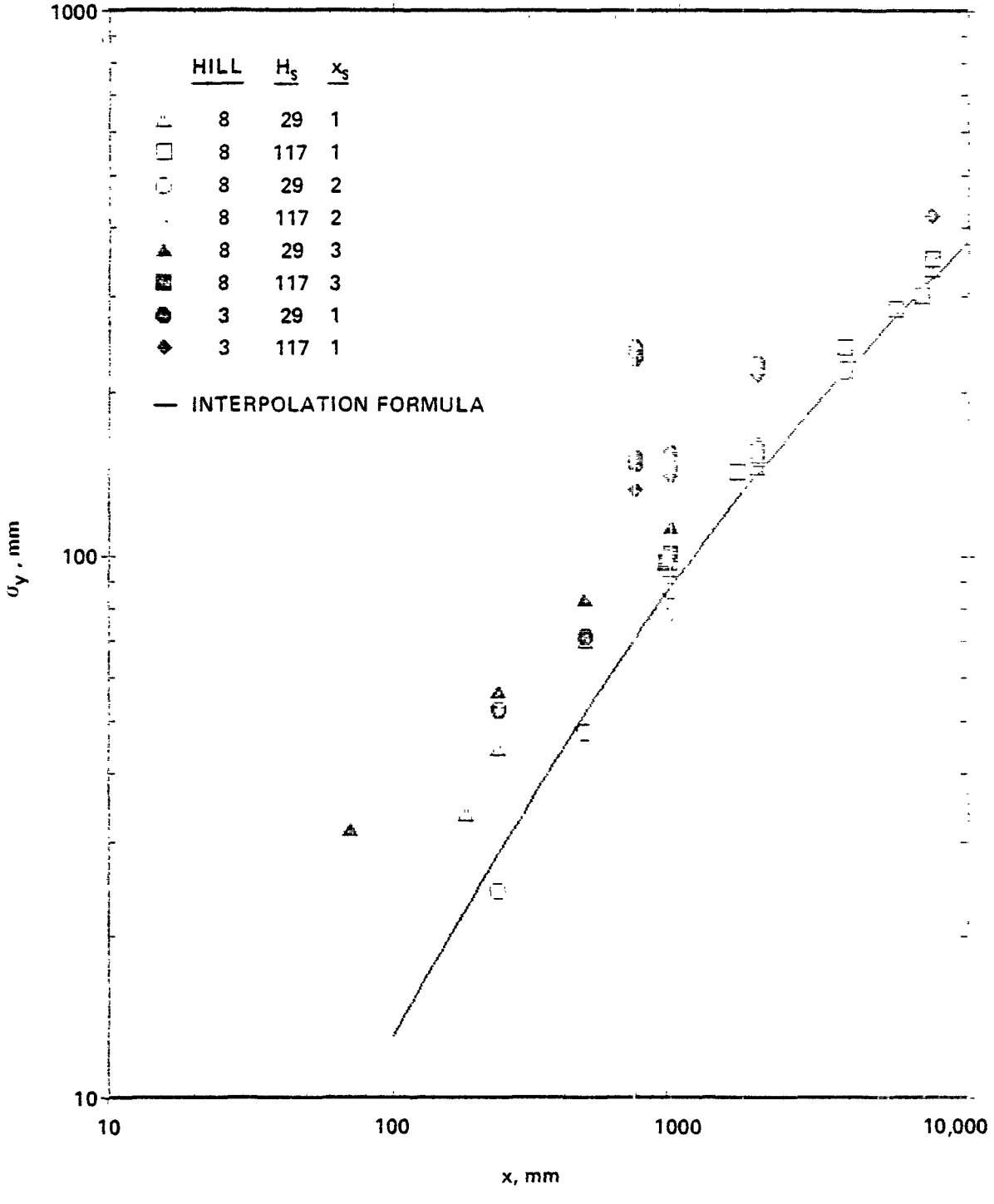

Figure 59. Growth of lateral plume width in presence of hills.

as χ_{mx} versus x_{mx}. This is shown in Figure 60, where a virtual origin of 50 mm has been assumed in order to straighten the curve at small distances. In a sense, this graph indicates that the maximum surface concentration depended only upon the travel distance of the plume in getting from the source to the point of maximum concentration, independent of the means of travel (whether through diffusion or through distortion of the mean streamline pattern).

5.2.3. Comparison with theory

The QPM model was used to calculate terrain correction factors for predicting the values and positions of maximum surface concentrations and also surface concentrations as functions of downwind distance from the source. The results of these calculations were compared with the experimental data.

Calculations were made with typical field input parameters, since QPM was developed for predicting terrain correction factors (TCF's) in the real atmosphere. The assumed height of the full-scale hill was chosen as 50 m. In this case, the model scale ratio was about 400 and the corresponding field roughness length was approximately 5 cm. The value of the field roughness length was obtained using the roughness length in the wind tunnel as 0.127 mm. (The differences between that value and the corrected value of z_o = 0.157 is not significant here). Given z_o, it was possible to determine the ratio of the wind speed in the incident flow u_1 (at 1 m height) to the corresponding eddy diffusivity k_1. Since the TCF does not depend on u_1 or k_1 separately, but only upon their ratio, the friction velocity u_* for the atmospheric flow was chosen as 0.27 m/s (not 0.2 m/s as in the wind tunnel) in order to have more realistic field values of wind speed and eddy diffusivity (e.g., u_1 = 2 m/s and k_1 = 0.114 m^2/s).

TCF's are listed in Tables 1 and 2 for the values and locations, respectively, of maximum surface concentrations calculated with QPM and obtained from measurements. The TCF's for the value of the maximum surface concentrations are the same for stack positions 1 and 3 (upwind and downwind base) because of the symmetry of the QPM. Comparison of the TCF's with the measured data was rather difficult, because of the unavoidable scatter in the measured data.

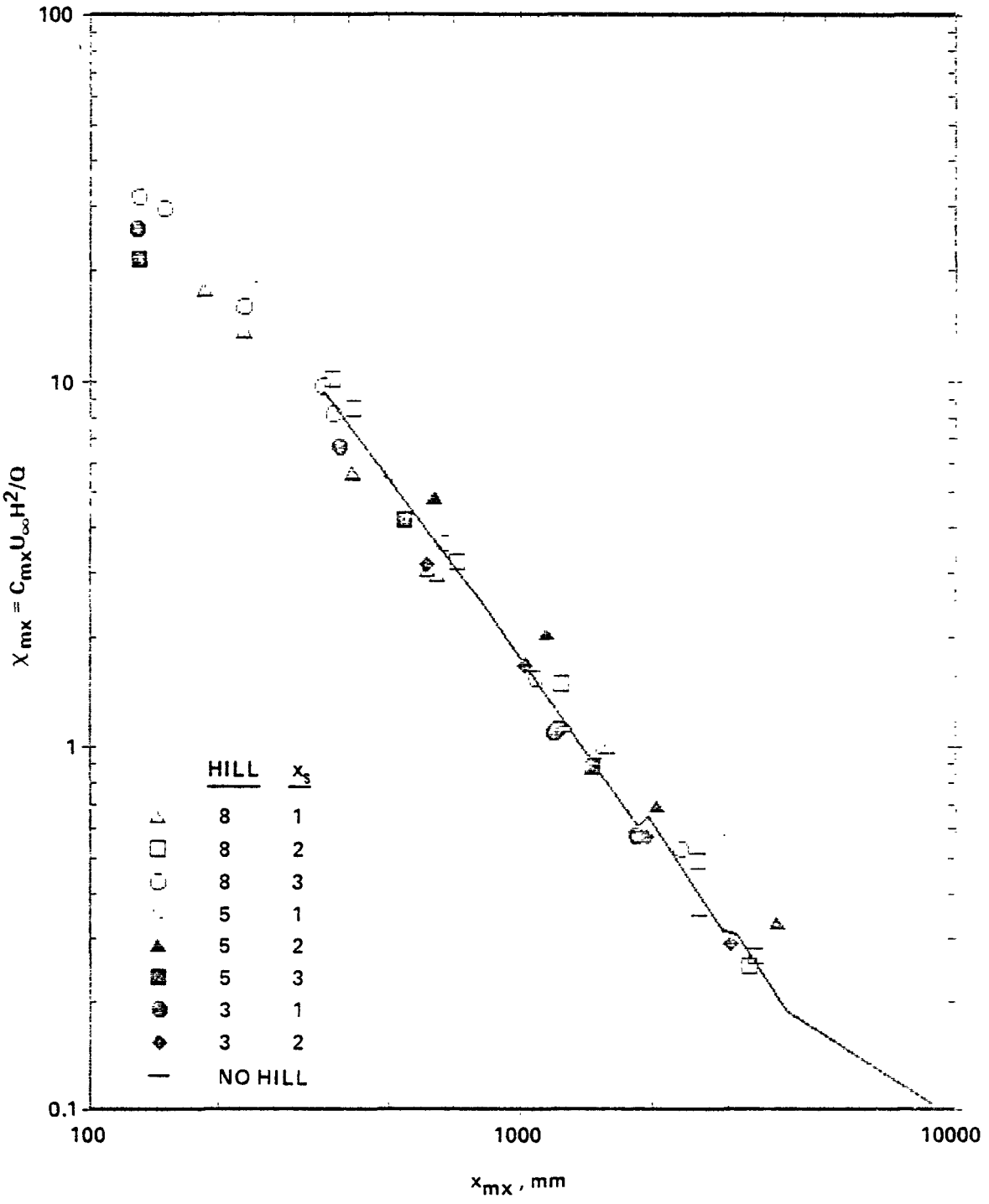

Figure 60. Relation between maximum surface concentration and distance to its location in presence of hills.

TABLE 1. TERRAIN CORRECTION FACTORS FOR MAXIMUM SURFACE CONCENTRATION

	HILL, N=8					
	xs = (1)		xs = (2)		xs = (3)	
$\frac{H_s}{h_o}$	From Measur.	Calcul.	From Measur.	Calcul.	From Measur.	Calcul.
0.25	1.45	1.42	0.91	0.66	3.43	1.42
0.50	1.12	1.37	0.56	0.67	2.99	1.37
1.00	1.47	1.24(1.31)*	0.78	0.74(0.68)	2.39	1.24(1.34)
1.50	1.16	1.20	0.82	0.75	1.68	1.20
		HILL, N=5				
0.25	1.96	1.70	0.54	0.53	15.00	1.70
0.50	2.04	1.59	0.63	0.54	8.12	1.59
1.00	1.74	1.35(1.46)	0.86	0.65(0.58)	5.63	1.35(1.46)
1.50	1.20	1.28	1.04	0.67	2.90	1.28
		HILL, N=3				
0.25	2.81	2.29	0.34	0.38	7.50	2.29
0.50	2.47	2.02	0.69	0.41	6.42	2.02
1.00	1.78	1.52(1.70)	0.91	0.55(0.47)	10.80	1.52(1.70)
1.50	1.87	1.39	0.94	0.59	7.77	1.39

* Values obtained using Equation 41a.

TABLE 2. TERRAIN CORRECTION FACTORS FOR LOCATION OF MAXIMUM SURFACE CONCENTRATION

	HILL, N=8					
	xs = (1)		xs = (2)		xs = (3)	
$\frac{H_s}{h_o}$	From Measur.	Calcul.	From Measur.	Calcul.	From Measur.	Calcul.
0.25	0.6	0.90	1.14	1.05	0.30	0.90
0.50	0.81	0.84	1.63	1.14	0.44	0.89
1.00	0.81	0.82(0.80)*	1.31	1.20(1.20)	0.55	0.89(0.90)
1.50	0.82	0.87	1.11	1.19	0.75	0.90
			HILL, N=5			
0.25	0.66	0.82	1.00	1.12	--	0.84
0.50	0.61	0.72	1.26	1.32	0.11	0.84
1.00	0.64	0.79(0.77)	1.05	1.31(1.31)	0.26	0.85(0.85)
1.50	0.76	0.84	1.25	1.28	0.49	0.87
			HILL, N=3			
0.25	0.26	0.66	1.87	1.51	--	0.75
0.50	0.45	0.56	1.33	1.54	--	0.76
1.00	0.62	0.74(0.72)	1.00	1.46(1.46)	0.084	0.79(0.79)
1.50	0.58	0.80	0.97	1.39	0.24	0.82

* Values obtained using Equation 41a.

Their calculation involved quotients of measured values, and the scatter in the quotients was naturally greater than the scatter of the individual values. Hence, the true situation may appear significantly distorted, especially when the TCF's are close to unity. It is noteworthy that, in some cases, the changes in the TCF's for maximum surface concentration were nonmonotonic with stack height (fixed stack position). This feature is especially puzzling in the cases of hills 8 and 5, where the flow did not separate from the lee side of the hill. For hill 3, such nonmonotonic behavior may be explained as due to the influence of the recirculation zone, especially when the stack was positioned at $x_s = (3)$. To elucidate this question, further theoretical and experimental efforts are needed.

Although QPM usually assumes a linear growth of lateral diffusivity with downwind distance (characteristic of field conditions for distances up to a few tens of kilometers), in this study different dependences of the lateral diffusivity were used to make the calculation model closer to the wind tunnel conditions. For stack heights lower than the hill height, a formula analogous to Eq. 41a was used; for higher stacks, Eq. 41b was used. Table 1 shows that, for hill 8, the TCF for the maximum surface concentration was significantly greater for stack position $x_s = (3)$ than for $x_s = (1)$. This was the most important difference (for hill 8) between the data and QPM predictions. When the stack position was $x_s = (1)$ or $x_s = (2)$, the measured data and QPM both showed similar magnitudes for the changes in TCF's.

The comparison of the TCF's calculated using QPM with those obtained from the wind tunnel data is rather poor for hills 3 and 5 because of the existence in these cases of the recirculation zone or zone of very high turbulence intensity. Nevertheless, there is reasonable agreement between both sets of values when the stack is located at position $x_s = (1)$ or $x_s = (2)$.

Surface concentration profiles were obtained using a formula similar to Eq. 44. In all cases, the variable ζ was substituted for x in Equations 41a, 41b and 44.

Figures 61 to 63 show normalized surface concentrations plotted as functions of normalized distance from the source x/x_m for hill 8. The triangles on these figures mark the curve calculated using Eq. 44. It may be seen

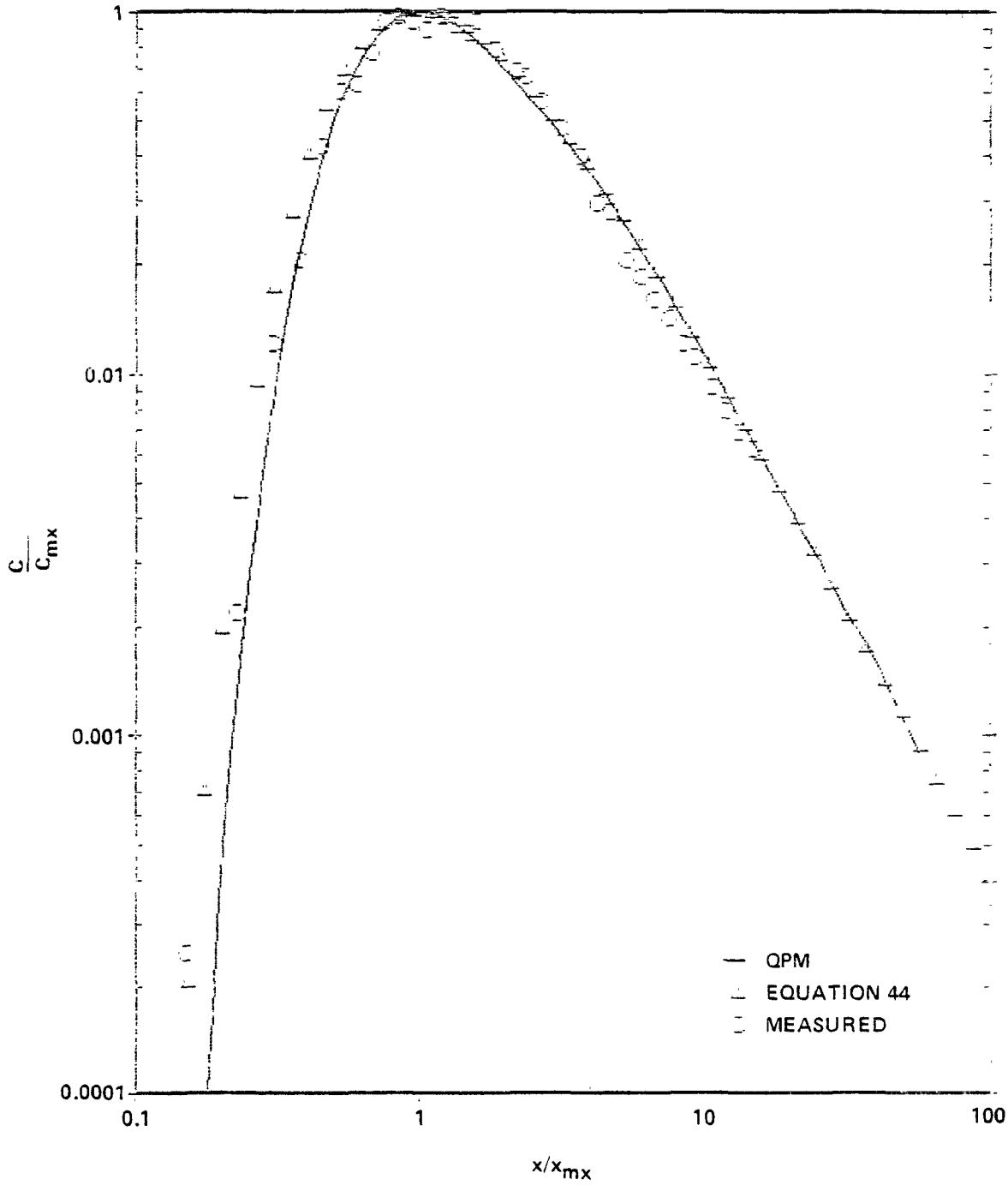

Figure 61. Comparison of surface concentrations predicted by QPM and experimental data; hill 8; $H_s = h_o/2$; $x_s = (1)$.

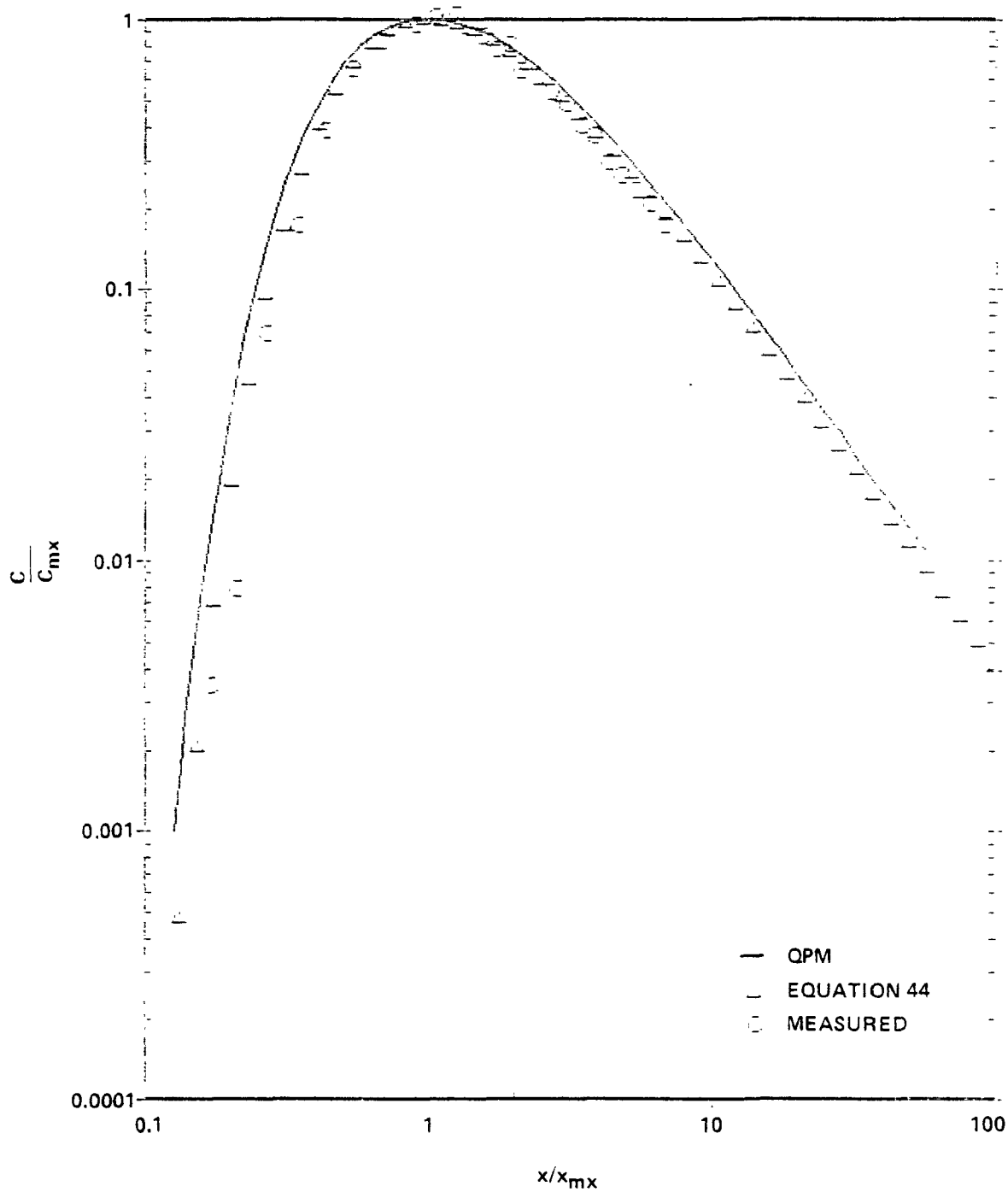

Figure 62. Comparison of surface concentrations predicted by QPM and experimental data; hill 8; $H_s = h_o/2$; x_s =(2).

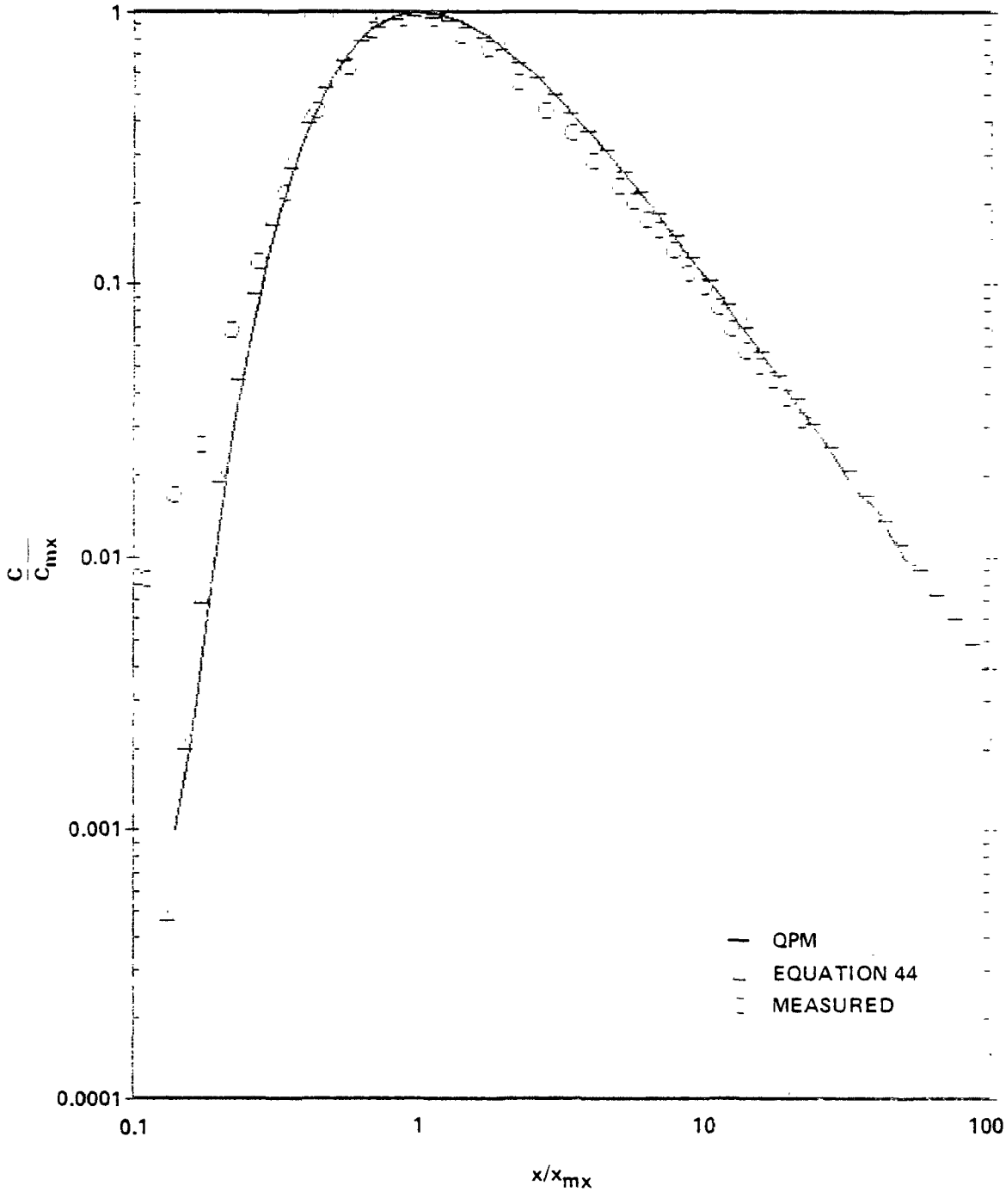

Figure 63. Comparison of surface concentrations predicted by QPM and experimental data; hill 8; $H_s = h_o/2$; $x_s = (3)$.

that the hill had very little influence on the shape of the profile. The difference between the calculated curve and that obtained from measurements is also small. For the steeper hills, 3 and 5, a comparison between calculated and measured profiles is not appropriate, since QPM admits neither flow separation nor great increase of turbulence, which change the profile shape (see Figure 52).

For hill 8, numerical calculations of maximum surface concentrations were made using WMDM. The parameters used in the calculations were adjusted to match the wind tunnel flow, not the corresponding atmospheric flow. The incident flow structure was modeled in accordance with Eq. 5, the parameter values being taken from the measured data. The results are shown in Figures 64 to 69. Figure 68 shows that, when the stack is located at the downwind base of the hill, WMDM predicts maximum surface concentrations significantly better than QPM, which gives the same maximum surface concentrations independent of whether the stack is located at the upwind or downwind base of the hill. Nevertheless, the discrepancy between the measured data and those calculated is notable. The agreement between the measurements and the calculations improves when the stack is located at the upwind base or at the top of the hill. (See Figures 64 and 66). The model was a poor predictor of maximum surface concentrations (see Figures 65, 67, and 69), especially for low stacks located at the downwind base of the hill. TCF's for all these data are listed in Tables 3 and 4.

In summary, the calculations, for both hilly and flat terrain, usually underpredicted values of maximum surface concentrations and overpredicted distances to their position, but the discrepancy was larger over the hills. Comparisons of the results of WMDM with the experimental data bear further study, particularly regarding (1) the mean flow patterns produced by WMDM; (2) the measurements for short stacks--why they give such small distances to maximum surface concentration; and (3) further calculations for different source locations. WMDM could not be used to make calculations for hills 3 or 5, since the wind velocity measurements were not completely reliable at the time the calculations were conducted. When regions of reversed mean flow and/or very small mean velocity exist in conjunction with very high turbulence intensities, longitudinal diffusion must be included in the model,

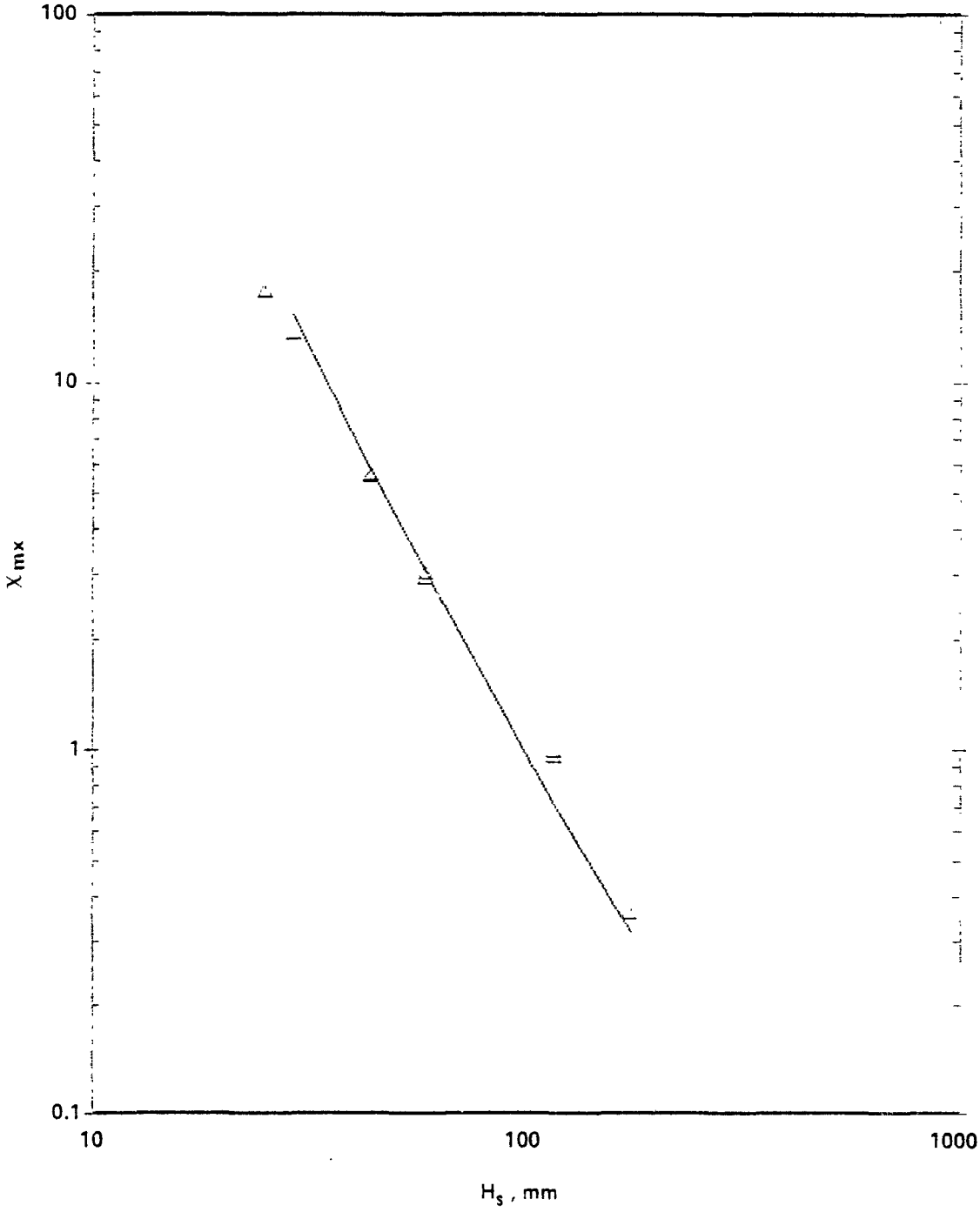

Figure 64. Comparison of maximum surface concentrations predicted by WMDM and experimental data; hill 8; x_s = (1).

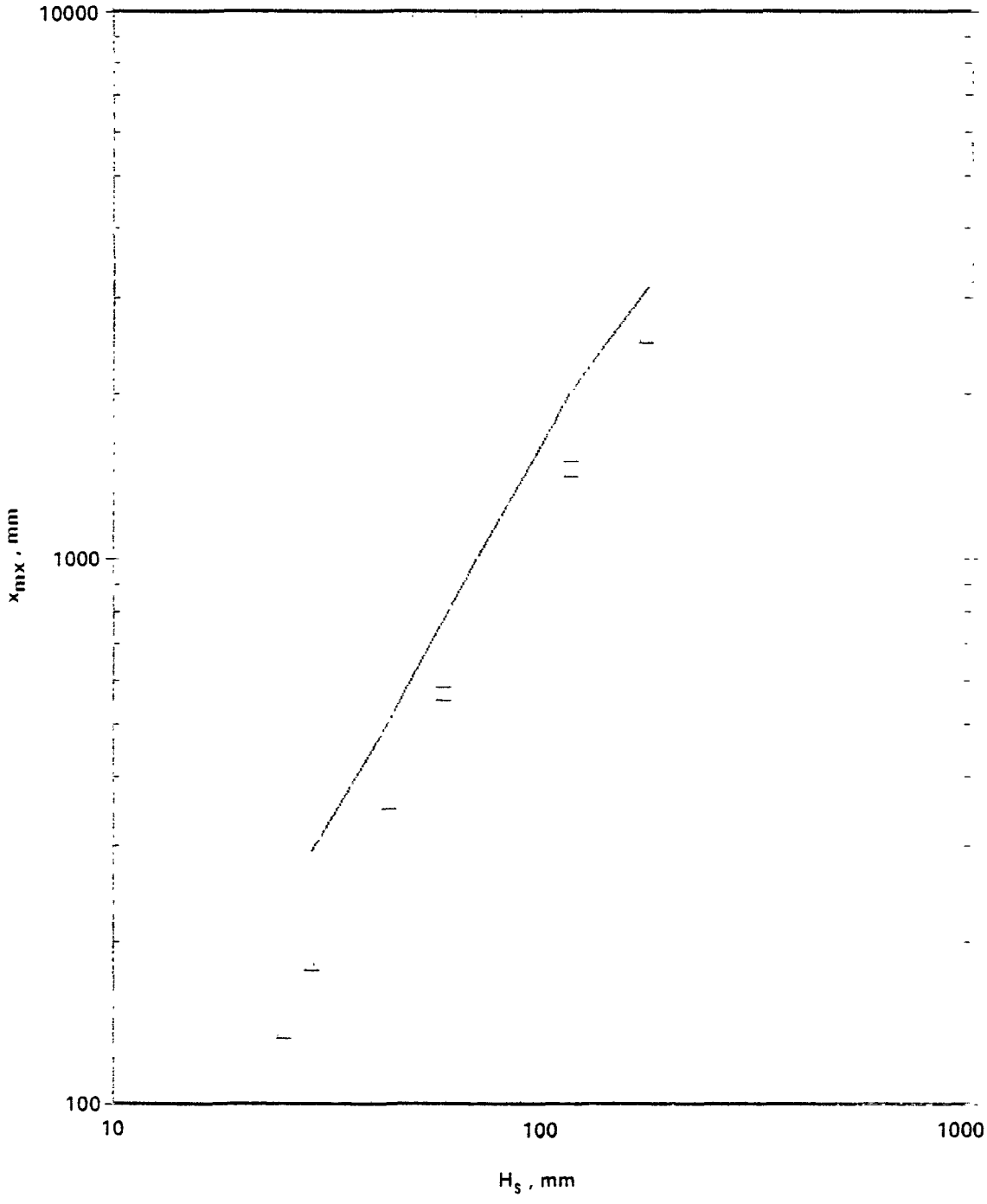

Figure 65. Comparison of distances to location of maximum surface concentration predicted by WMDM and experimental data; hill 8; x_s = (1).

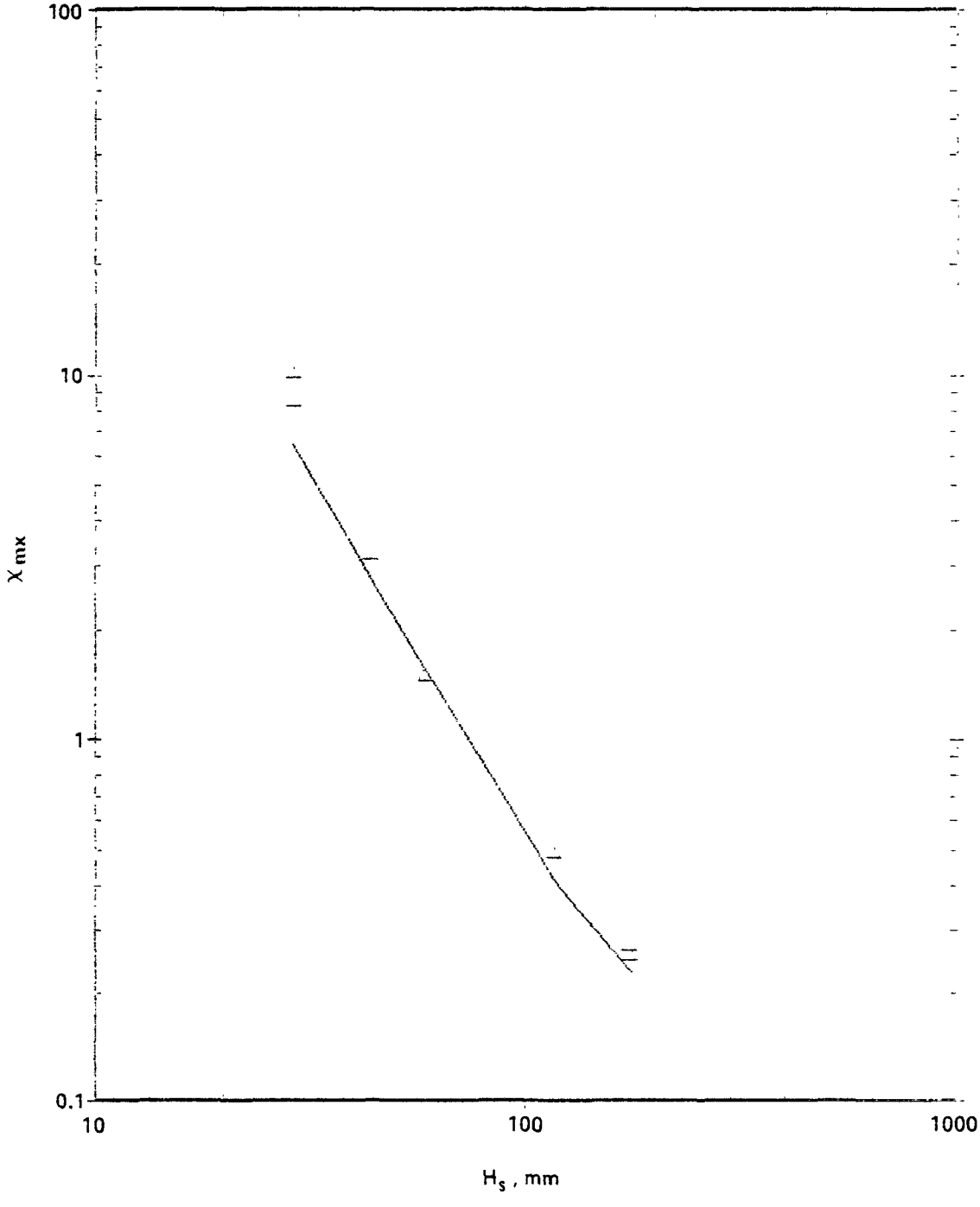

Figure 66. Comparison of maximum surface concentrations predicted by WMDM and experimental data; hill 8; x_s = (2).

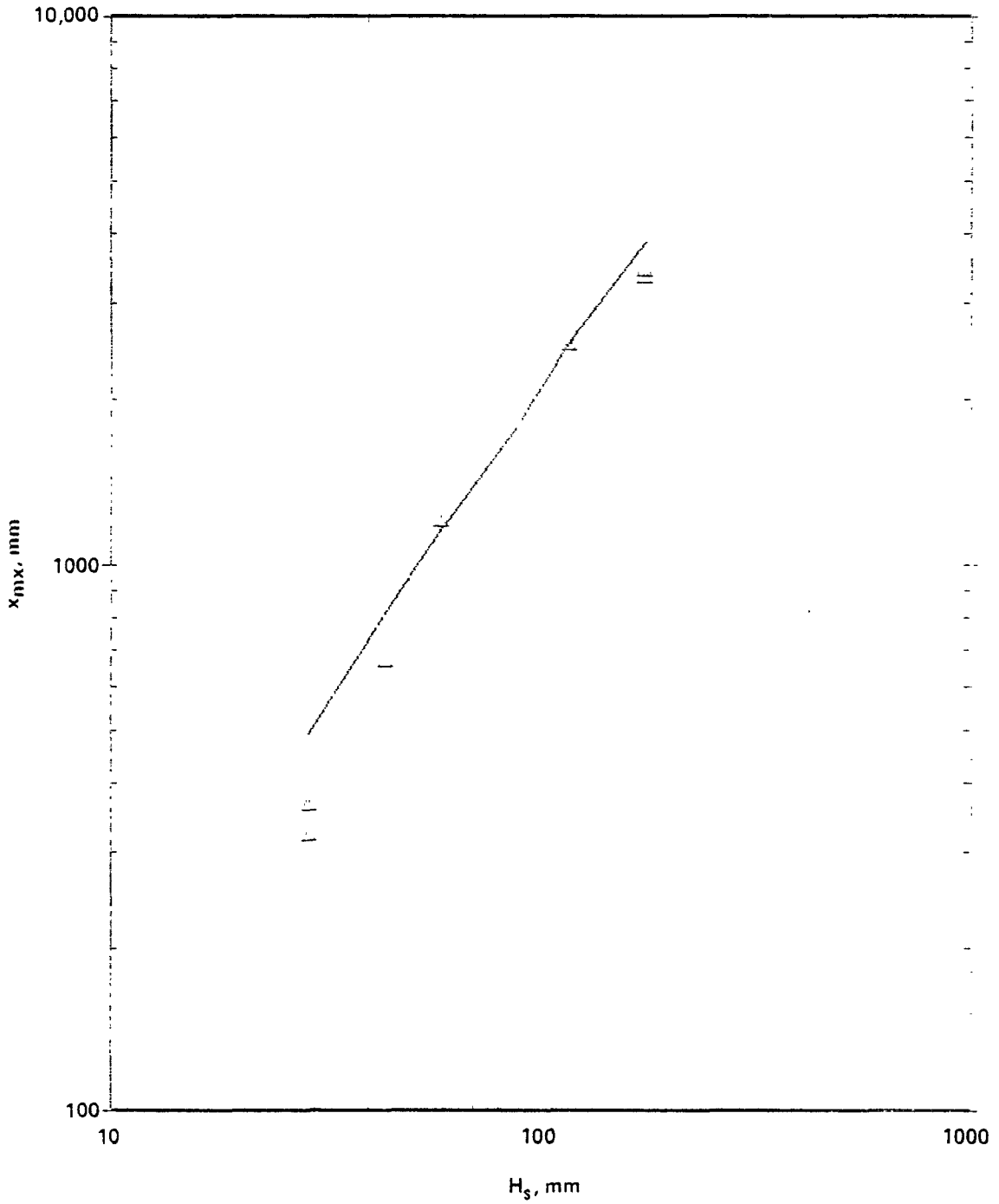

Figure 67. Comparison of distances to location of maximum surface concentration predicted by WMDM and experimental data; hill 8; x_s = (2).

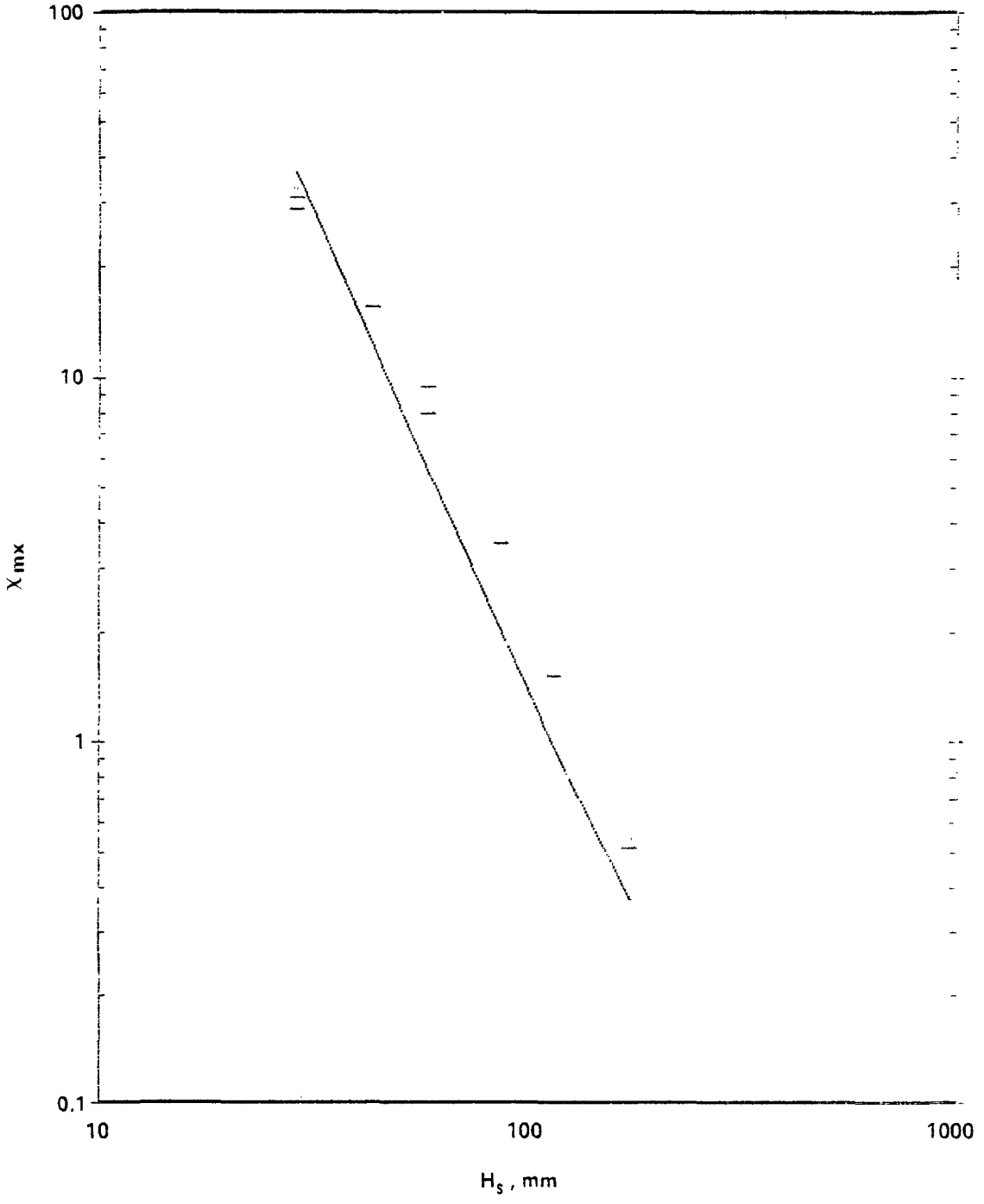

Figure 68. Comparison of maximum surface concentrations predicted by WMDM and experimental data; hill 8; x_s = (3).

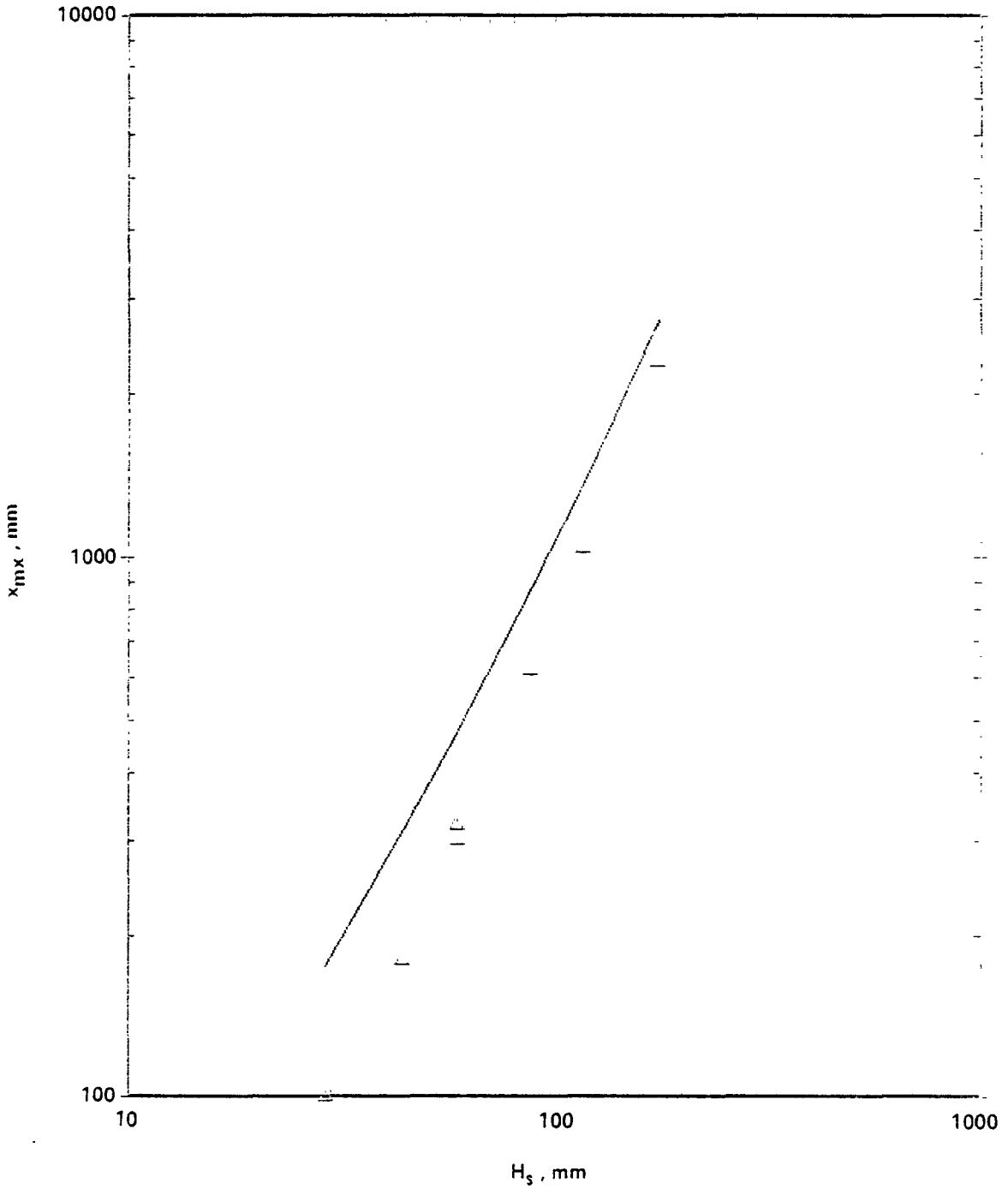

Figure 69. Comparisons of distances to location of maximum surface concentration predicted by WMDM and experimental data; hill 8; x_s = (3).

TABLE 3. COMPARISON OF MEASURED MAXIMUM CONCENTRATIONS AND THOSE CALCULATED WITH WMDM FOR HILL 8

	xs = (1)		xs = (2)		xs = (3)	
$\frac{H_s}{h_o}$	Measur.	Calcul.	Measur.	Calcul.	Measur.	Calcul.
0.25	13.44	15.25	9.28	6.74	30.79	36.52
0.5	2.96	3.11	1.49	1.58	8.93	5.76
1.0	0.97	0.71	0.49	0.42	1.55	0.97
1.5	0.36	0.32	0.26	0.23	0.53	0.37

TABLE 4. COMPARISON OF MEASURED DISTANCES TO MAXIMUM CONCENTRATION AND THOSE CALCULATED WITH WMDM FOR HILL 8

	xs = (1)		xs = (2)		xs = (3)	
$\frac{H_s}{h_o}$	Measur.	Calcul.	Measur.	Calcul.	Measur.	Calcul.
			all dimensions in mm			
0.25	180	293	342	491	91	176
0.5	578	772	1196	1147	310	468
1.0	1488	2012	2500	2527	1040	1357
1.5	2520	3118	3364	3879	2300	2738

a task that WMDM cannot perform without further development.

Attempts were made to evaluate the accuracy of WMDM. For this purpose, the wind field over hill 8 assumed in OPM was used. The values of the wind velocity components at the points where the measurements were conducted in the wind tunnel were input to WMDM. The eddy diffusivity in this case was also assumed to be the same as in QPM. The values of the TCF's for maximum surface concentration were calculated. The source location was changed in the same way as in the wind tunnel experiments. The discrepancy between the predictions of QPM and WMDM was on average about 7%. Of course, these calculations can be considered only as a rather approximate example of the validation of WMDM. Further work should be done along these lines. As was mentioned in Section 3.2, WMDM could be improved by the use of a more accurate interpolation of wind field measurements (rather than bilinear interpolation as was used in this study). Further improvements may be expected with the emergence of models for predicting structural changes in turbulence over irregular terrain.

5.3. Special Experiments

A few additional experiments were conducted to examine, at least in limited fashion, the effects of otherwise unvaried parameters. These special tests included (1) variation of mean flow speed to determine whether the flow structure was Reynolds-number independent, (2) maintenance of a flat wind-tunnel ceiling (non-zero longitudinal pressure gradient) to determine whether the ceiling height adjustment was critical, and (3) use of a larger but similar-shaped hill 3 (big hill 3) to determine whether the ratio of hill height to boundary-layer height had a significant influence on the flow structure over the hill. These experiments as well as some streamline patterns derived from the measured velocity profiles are presented in this section.

5.3.1. Reynolds number and hill-height effects

As mentioned in Section 5.2.1, a double-ended Pitot tube was used to probe the velocity profiles in the separated flow region or cavity on the lee side of hill 3 (see Figure 48). Additional measurements were made to determine the locus of zero-mean longitudinal velocity within the cavity region,

since this was felt to be a sensitive measure of the mean flow structure. This locus of zero-mean velocity is shown in Figure 70 to be slightly greater than half the zero-streamline height. The cavity, defined as the region enclosed by the lee side of the hill and the separation-reattachment streamline (or zero-streamline), is seen to extend to approximately 6.5 hill heights downwind, but to be limited in vertical extent to less than the hill height. The freestream wind speed, hence, the Reynolds number, was then doubled, and the locus of zero-mean velocity was measured again. The difference in the loci is indistinguishable, indicating Reynolds number independence, at least within this limited range. (Note that the boundary layer structure was previously shown to be Reynolds number independent in the range of 4 to 8 m/s).

Big hill 3 was next installed in the tunnel and similar measurements were conducted at free-stream wind speeds of 2, 4 and 8 m/s. These results are also shown in Figure 70 (see also Figure 48). Whereas the big hill 3 results at 4 and 8 m/s are indistinguishable from the small hill 3 results, those at 2 m/s are noticeably different. Because the big hill 3 results at 4 and 8 m/s matched the small hill 3 results at 4 and 8 m/s, one may conclude that the ratios of hill height to boundary layer height and roughness length to hill height are relatively unimportant parameters. The deviations at 2 m/s could result from any of 3 effects: (1) direct variations with Reynolds number, (2) indirect variations with Reynolds number (possibly the approach flow structure varied with Reynolds number), or (3) insensitivity of the measuring device.

Effect (1), direct variations with Reynolds number, is ruled out because the Reynolds number for big hill 3 at 2 m/s is the same as that for small hill 3 at 4 m/s, which was previously shown to be Reynolds number independent. Effect (2), indirect variations with Reynolds number, is a possible cause, as independent measurements of the approach boundary layer structure at 2 m/s were not made. Effect (3), insensitivity of the measurement device, however, is the most likely cause for the discrepancy in the results. Study of Figure 48, for example, shows that, in order to determine the location of the zero-mean velocity point to within 10 mm, the double-ended Pitot tube/manometer combination must be able to sense mean wind speeds (and within a highly turbulent flow) of less than 10 cm/s, a dubious possibility at best. We thus conclude that, within the limitations of the instrumentation and over the

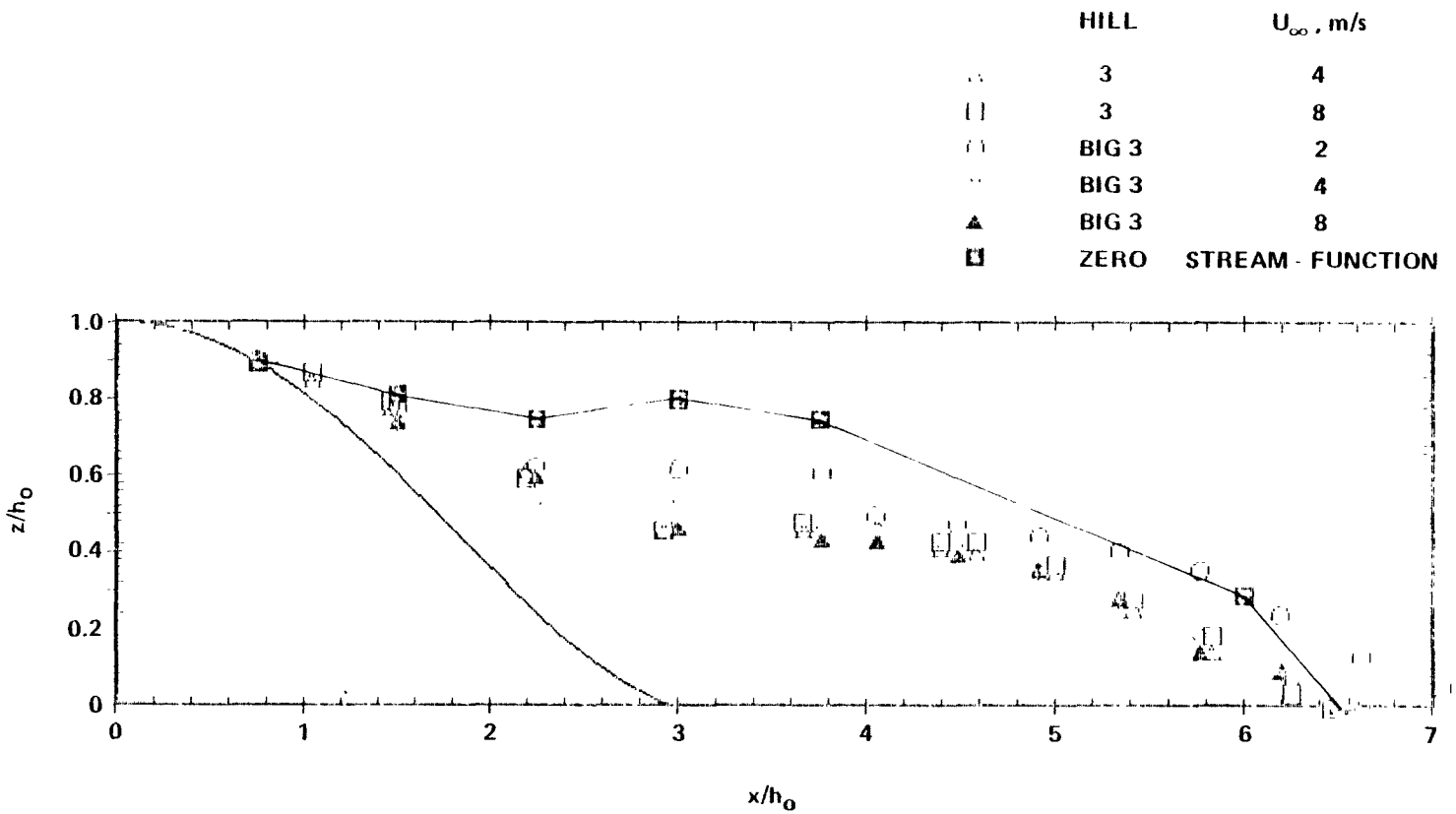

Figure 70. Locus of zero-mean velocity in cavity as function of Reynolds number and hill size.

limited ranges measured, the flow structure is relatively insensitive to Reynolds number, h_o/δ, or z_o/δ.

It may be hypothesized that the flow structure is independent of Reynolds number up to very large values such as found in the field. In fact, measurements by Wilson et al (1979) suggest that separation may disappear at a large enough Reynolds number, but his results have not yet been substantiated. Proof will be available only after adequate field measurements have been conducted.

5.3.2. Effects of ceiling adjustment

Measurements made to examine the effects of the ceiling adjustment were surface concentration profiles for hill 8 with a stack height of half the hill height and the stack located at the downwind base of the hill. Measurements were made with adjusted (zero-longitudinal pressure gradient) and non-adjusted (flat) ceilings. This configuration was expected to be one of the most sensitive ones with respect to ceiling adjustment. Surface concentration profiles thus measured are compared in Figure 71. It is apparent that the ceiling adjustment had some effect on the concentrations field near the stack, presumably because, with the flat ceiling, the streamlines converged more strongly on the lee side. Time limitations prevented a detailed examination of this effect. It is widely believed that the proper ceiling-height adjustment is that which produces a zero-pressure gradient flow, i.e., a non-accelerating free-stream.

5.3.3. Streamline patterns over hills

Figure 72 shows streamline patterns over hill 8, derived from the velocity profiles measured over the hill. As suggested in Section 5.2.1, the streamlines diverged upstream of the upwind base, converged over the upwind slope, diverged over the downwind slope, and converged beyond the downwind base. The separation between the streamlines above the downwind base is significantly larger than between those above the upwind base. The "kinks" in the streamline above the upwind base, especially noticeable at the higher elevations, probably resulting from an error of only 2% in the measurement of the reference velocity. With this in mind, it may be surmised that the mean

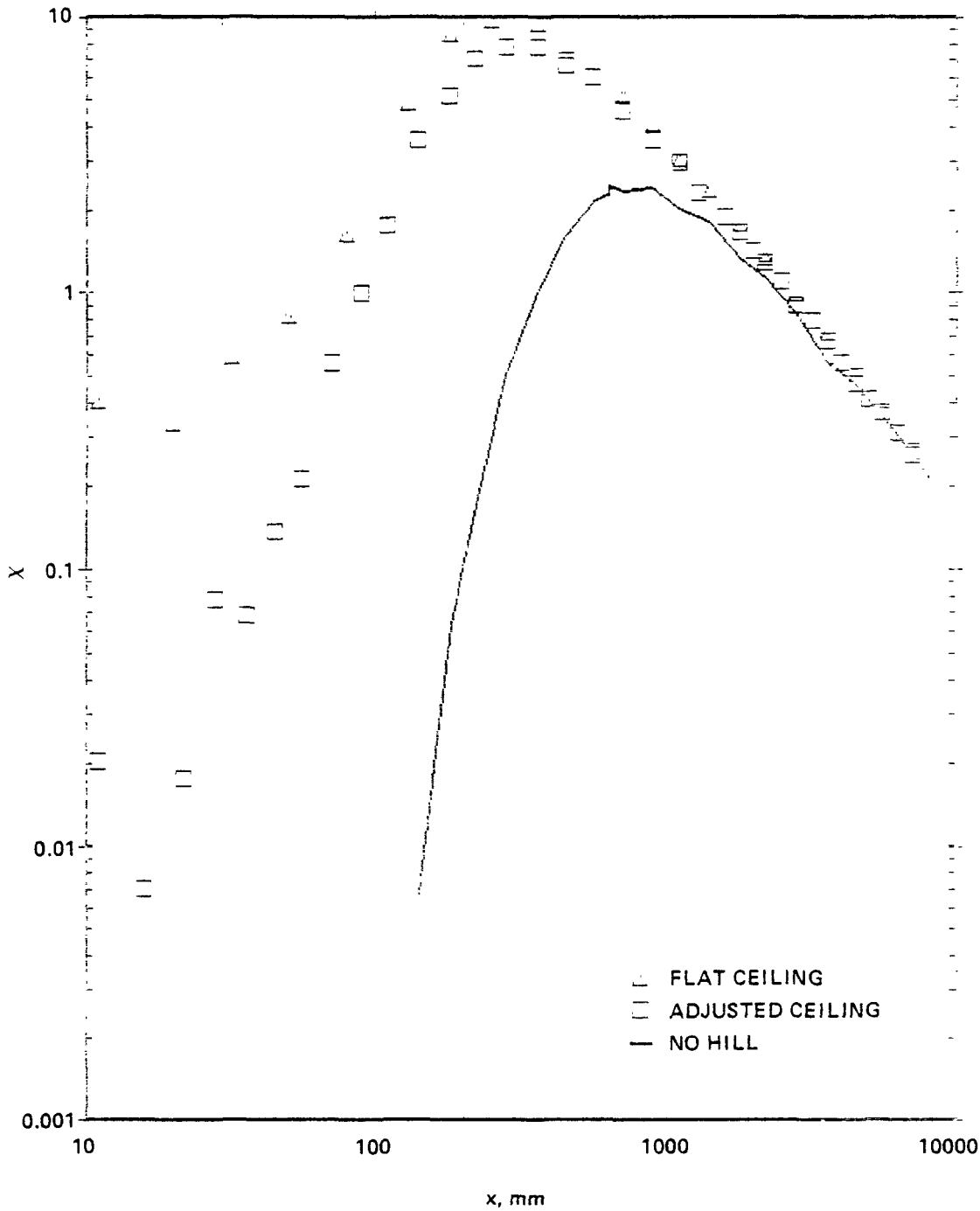

Figure 71. Dependence of surface concentrations on wind tunnel ceiling adjustment; hill 8; $H_s = h_o/2$; x_s = (3).

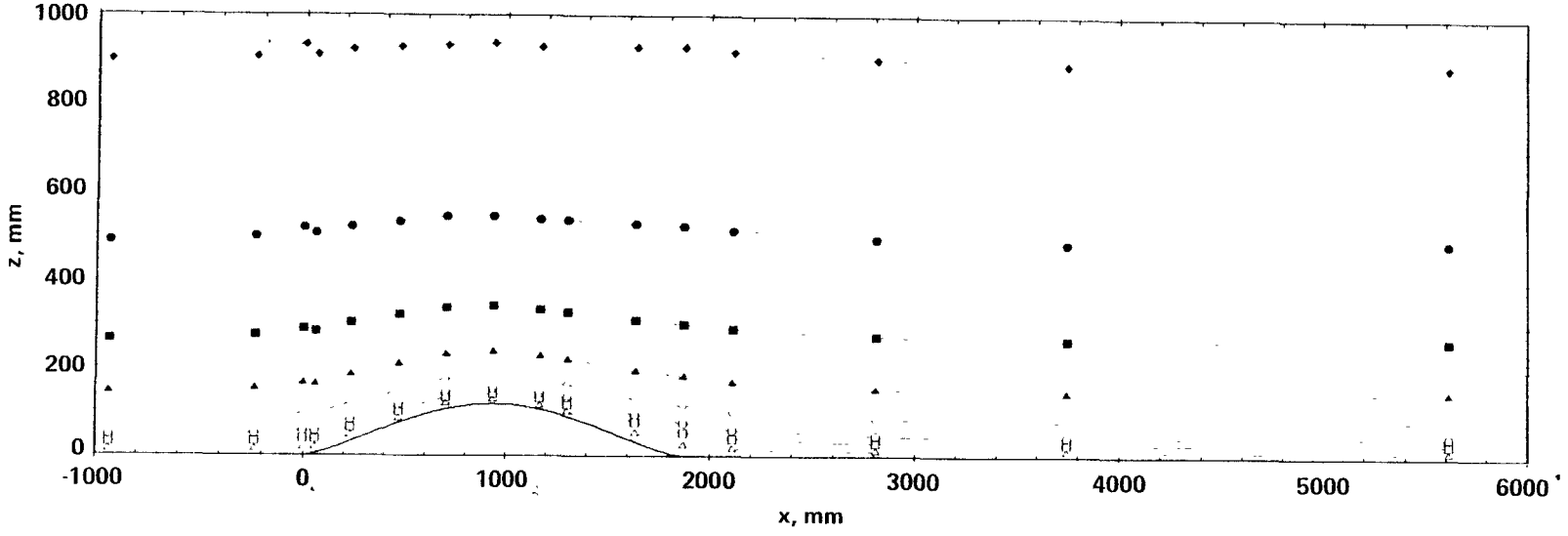

Figure 72. Streamline pattern over hill 8 from experimental data.

velocity profiles are extremely accurate, or at least, extremely consistent with one another.

Streamlines patterns over hill 3 are shown in Figure 73. The cavity region is clearly evident. In some respects, it would be useful to treat the hill/cavity combination as a solid body for the purpose of calculating streamline trajectories. After the streamline trajectories were obtained, concentrations outside the cavity could possibly be calculated with QPM or WMDM, whereas concentrations within the cavity could be calculated using the kind of model constructed by Puttock and Hunt (1979).

The streamline patterns over hill 5 are shown in Figure 74. The small kinks in the streamlines over the downwind slope probably result from the usage of data obtained with the pulsed-wire anemometer. In contrast to the hot-wire, the pulsed-wire does not rectify the signal, but the data probably have slightly different normalization factors. (Likewise, the kinks over the cavity region on Figure 73 are probably due to the usage of the double-ended Pitot tube).

As discussed earlier, a recirculating cavity region does not exist on the lee slope of hill 5 (at least not in the mean), but the divergence of streamlines over the lee slope is very significant. The ratio of a streamline height over the downwind base to that of the same streamline in the approach flow may be taken as a quantitative measure of this phenomenon. For example, this ratio for the streamline at a height of 29 mm ($h_o/4$) far upwind is 4 for hill 5 and 2 for hill 8. These ratios allow a rough explanation of the TCF's for maximum surface concentration. The measured TCF's were 15 and 3.43, respectively. If it is assumed that $\chi_{mx} \propto h_{sl}^{-2}$, where h_{sl} is the height at the stack position of the streamline going through the source, then the TCF's are 16, and 4, respectively, quite close to the measured values.

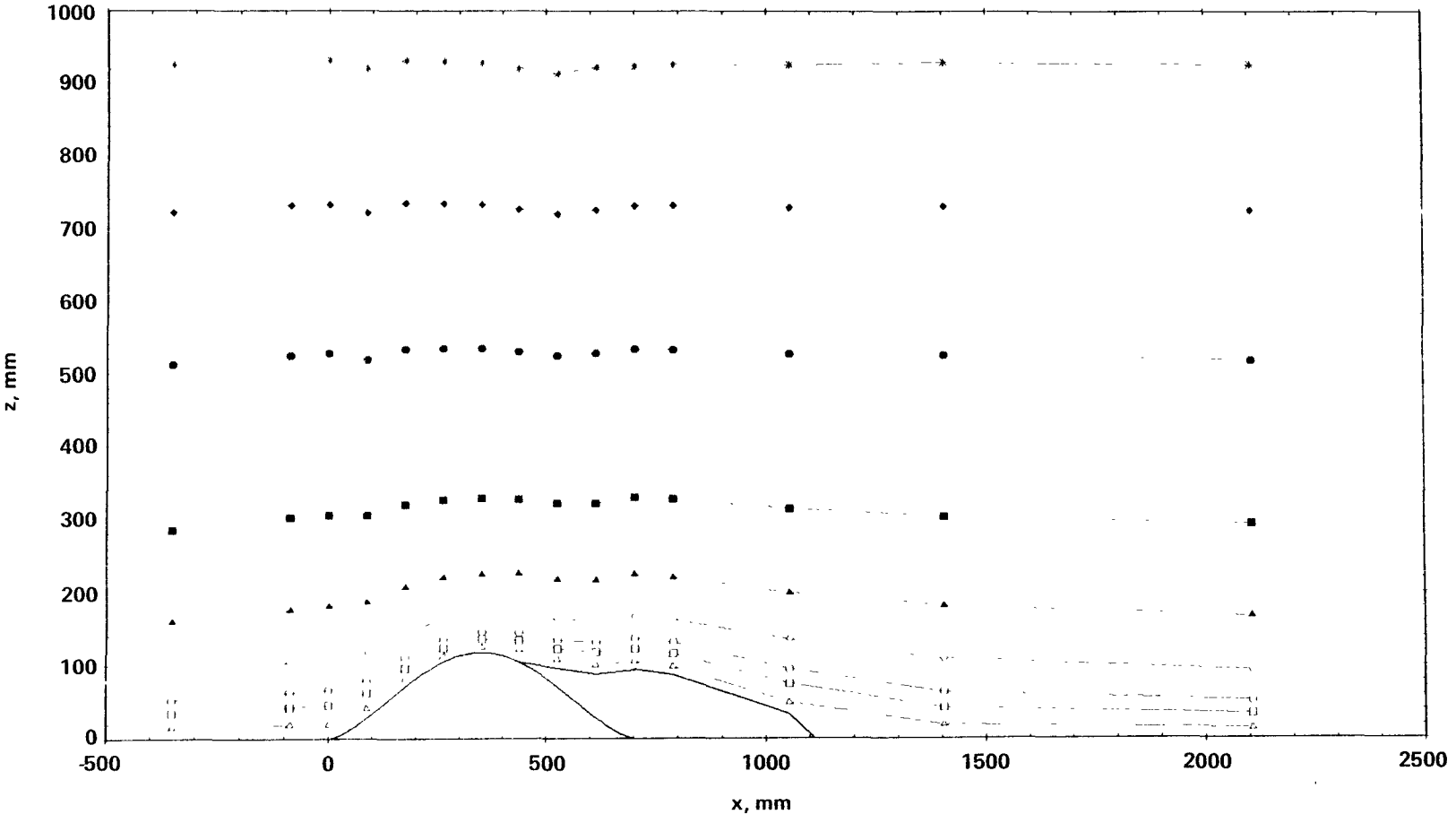

Figure 73. Streamline pattern over hill 3 from experimental data.

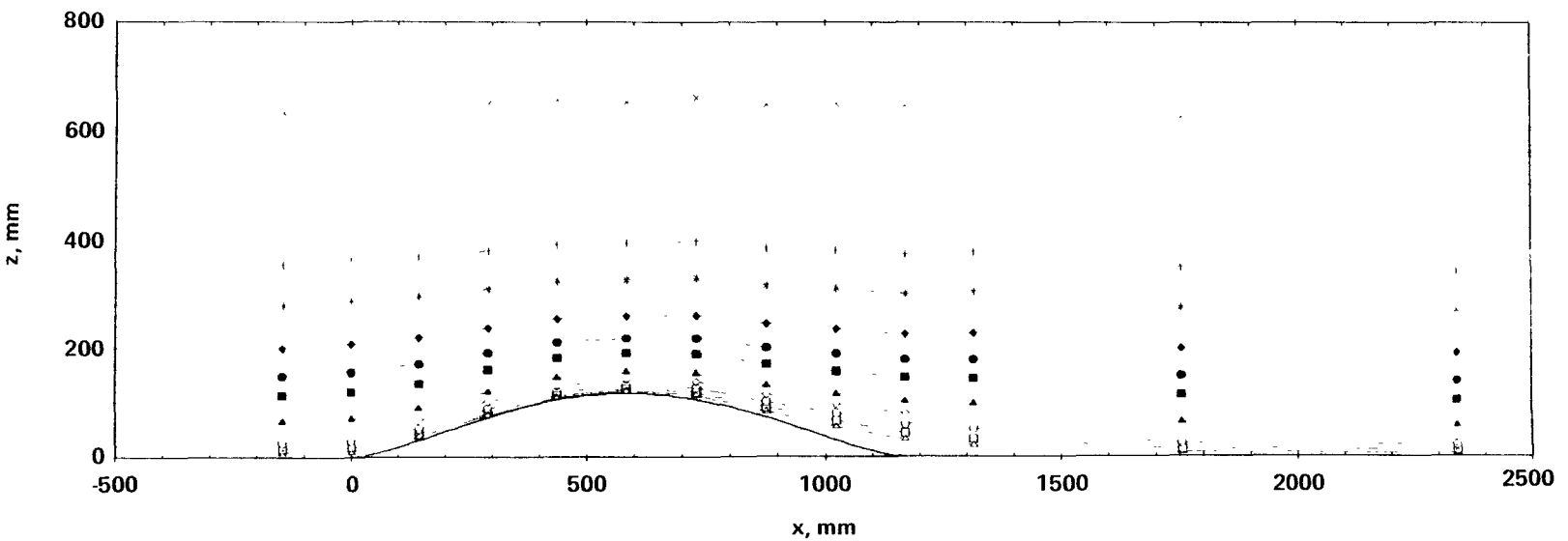

Figure 74. Streamline pattern over hill 5 from experimental data.

6. REFERENCES

Arya, S.P.S. and Shipman, M.S., 1979: A Model Study of Boundary Layer Flow and Diffusion Over a Ridge, Proc. AMS Fourth Symp. on Turbulence, Diffusion and Air Pollution, Jan. 15-18, Reno, NV, Am. Meteorol. Soc., Boston, MA, p. 584-91.

Arya, S.P.S. and Shipman, M.S., 1981: An Experimental Investigation of Flow and Diffusion in the Disturbed Boundary Layer over a Ridge; Part I: Mean Flow and Turbulence Structure, Atmos. Envir. (In Press).

Barr, S., Luna, R.E., Clements, W.E. and Church, H.W., 1977: Workshop on Research Needs for Atmospheric Transport and Diffusion in Complex Terrain, Available from Nat. Tech. Info. Serv., Springfield, VA, 17p.

Berlyand, M.E., 1975: Contemporary Problems of Atmospheric Diffusion and Air Pollution, Hydromet. Press, Leningrad, USSR, 448p.

Berlyand, M.E. and Genikhovich, E.L., 1971: Atmospheric Diffusion and the Structure of the Air Flow above an Inhomogeneous Surface, Proc. Int. Symp. on Meteorol. Aspects of Air Poll., 1968, Leningrad, p. 49-69, Hydromet. Press, Leningrad, USSR.

Berlyand, M.E., Genikhovich, E.L., Gracheva, I.G. and Onikul, R.I., 1979: Peculiarities of Pollutant Diffusion over Crossed Terrain, Atmos. Diff. and Air Poll., Trudy GGO, no. 417, p. 19-35, Hydromet Press, Leningrad, USSR.

Berlyand, M.E., Genikhovich, E.L. and Khurshudyan, L.H., 1975: Use of the Results of Modeling of an Air Stream in Wind Tunnels for the Calculation of Air Pollution, Atmos. Diff. and Air Poll., Trudy GGO, no. 352, p. 3-15, Hydromet. Press, Leningrad, USSR (EPA Transl. TR-79-0431).

Berlyand, M.E., Genikhovich, E.L. and Kurenbin, O.I., 1968: The Influence of Relief on the Diffusion of Pollutants from a Source, Atmos. Diff. and Air Poll., Trudy GGO, no. 234, p. 28-44, Hydromet. Press, Leningrad, USSR.

Berlyand, M.E. and Kisselev, V.B., 1973: On Influence of Relief on Dispersion of Pollutants Taking Plume Rise into Account, Meteorology and Hydrology, no.3, p. 3-10, Hydromet. Press, Leningrad, USSR.

Bradbury, L.J.S., 1976: Measurements with a Pulsed-Wire and a Hot-Wire Anemometer in the Highly Turbulent Wake of a Normal Flat Plate, J. Fluid Mech., v. 77, pt. 3, p. 473-97.

Bradbury, L.J.S. and Castro, I.P., 1971: A Pulsed-wire Technique for Velocity Measurements in Highly Turbulent Flows, J. Fluid Mech., v. 49, pt. 4, p. 657-91.

Britter, R.E., Hunt, J.C.R. and Richards, K.J., 1981: Air Flow over a Two-dimensional Hill: Studies of Velocity Speed-up, Roughness Effects and Turbulence, Quart. J. Roy. Meteorol. Soc., v. 107, p. 91-110.

Bruun, H.H., 1975: On the Temperature Dependence of Constant Temperature Hot-wire Probes with Small Wire Aspect Ratio, J. Physics E: Rev. Sci. Insts., v. 8, p. 942-51.

Burt, E.W. and Slater, H.H., 1977: Evaluation of the Valley Model, Paper pres at the AMS-APCA Joint Conf. on Appl. of Air Pol. Meteorol., Salt Lake City, Utah.

Cermak, J.E., Sandborn, V.A., Plate, E.J., Binder, G.H., Chuang, H., Meroney, R.N. and Ito, S., 1966: Simulation of Atmospheric Motion by Wind Tunnel Flows, Fluid Dyn. and Diff. Lab. Rpt. No. CER66JEC-VAS-EJP-GJB-HC-RNM-SI17, Colo. State Univ., Ft. Collins, CO, 102p.

Clarke, R.H. and Hess, G.D., 1974: Geostrophic Departure and the Functions A and B of Rossby-Number Similarity Theory, Bound.-Layer Meteorol., v. 7, no. 3, p. 267-87.

Counihan, J., 1975: Adiabatic Atmospheric Boundary Layers: A Review and Analysis of Data from the Period 1880-1972, Atmos. Envir., v. 9, p. 871-905.

Courtney, L.Y., 1979: A Wind Tunnel Study of Flow and Diffusion over a Two-Dimensional Low Hill, M.S. Thesis, Dept. of Meteorol., NC State Univ., Raleigh, NC, 134p.

Dickerson, M.H., 1978: MASCON - A Mass Consistent Atmospheric Flux Model for Regions with Complex Terrain, J. Appl. Meteorol., v. 17, p. 241-53.

Dickerson, M.H., and Gudiksen, P.H., 1980: The Department of Energy's Complex Terrain (ASCOT) Program, Proc. AMS/APCA 2nd Jt. Cof. on Appl. of Air Poll. Met., Mar. 24-27, New Orleans, LA, Amer. Meteorol. Soc., Boston, MA.

Egan, B.A., 1975: Turbulent Diffusion in Complex Terrain, Workshop on Air Poll. Meteorol. and Envir. Assess., Amer. Meteorol. Soc., Sept. 30-Oct. 3, Boston, MA.

Gorlin, S.M. and Zrazhevsky, I.M., 1968: Study of Flow around Model Relief and Urban Construction in a Wind Tunnel, Atmos. Diff. and Air Poll., Trudy GGO, no. 234, p. 45-59, Hydromet. Press, Leningrad, USSR.

Hilst, G.R., 1978: Plume Model Validation, EPRI EA-917-SY, Electric Power Research Institute, Palo Alto, CA.

Holzworth, G.C., 1980: The EPA Program for Dispersion Model Development for Sources in Complex Terrain, Pres. at 2nd Jt. Conf. on Appl. of Air Poll. Meteorol., March 24-27, New Orleans, LA, 4p.

Hovind, E.L., Edelstein, M.W. and Sutherland, V.C., 1979: Workshop on Atmospheric Dispersion Models in Complex Terrain, Envir. Prot. Agcy. Rpt. No. EPA-600/9-79-041, Res. Tri. Pk., NC, 213p.

Huber, A.H., Snyder, W.H., Thompson, R.S., and Lawson, R.E. Jr., 1976: Stack Placement in the Lee of a Mountain Ridge: A Wind Tunnel Study, Envir. Prot. Agcy. Rept. No. EPA-600/4-76-047, Res. Tri. Pk., NC., 45p.

Hunt, J.C.R. and Fernholz, H., 1975: Wind-Tunnel Simulation of the Atmospheric Boundary Layer: A Report on Euromech 50, J. Fluid Mech., v. 70, pt. 3, p. 543-59.

Hunt, J.C.R. and Mulhearn, P.J., 1973: Turbulent Dispersion from Sources Near Two-Dimensional Obstacles, J. Fluid Mech., v. 61, pt. 2, p. 245-74.

Hunt, J.C.R., Puttock, J.S. and Snyder, W.H., 1979: Turbulent Diffusion from a Point Source in Stratified and Neutral Flows around a Three-Dimensional Hill: Part I: Diffusion Equation Analysis, Atmos. Envir., v.13, p.1227-39.

Hunt, J.C.R. and Snyder, W.H., 1980: Experiments on Stably and Neutrally Stratified Flow over a Model Three-Dimensional Hill, J. Fluid Mech., v. 96, pt. 4, p. 671-704.

Hunt, J.C.R., Snyder, W.H., and Lawson, R.E. Jr., 1978: Flow Structure and Turbulent Diffusion around a Three-Dimensional Hill: Fluid Modeling Study on Effects of Stratification; Part I: Flow Structure, Envir. Prot. Agcy. Rpt. No. EPA 600/4-78-041, Res. Tri. Pk., NC.

Isaacs, R.G., Bass, A. and Egan, B.A., 1979: Application of Potential Flow Theory to a Gaussian Point Source Diffusion Model in Complex Terrain, Fourth Symp. on Turb., Diff. and Air Poll., Jan. 15-18, Reno, NV, Am. Meteorol. Soc., Boston, MA, p. 189-96.

Jackson, P.S. and Hunt, J.C.R., 1975: Turbulent Wind Flow Over a Low Hill, Quart. J. Roy. Meteorol. Soc., v. 101, p. 929-55.

Lawson, R.E. Jr. and Britter,R.E., 1981: A Note on the Yaw Sensitivity of Heated Cylindrical Sensors, J. Phys. E., Rev. Sci. Insts. (In Press).

Mage, D.T. and Noghrey, J., 1972: True Atmospheric Pollutant Levels by Use of Transfer Function for an Analyzer System, J. Air Poll. Contr. Assoc., v. 22, no. 2, p. 115-8.

Mason, P.J. and Sykes, R.I., 1979: Flow over an Isolated Hill of Moderate Slope, Quart. J. Roy. Meteor. Soc., v. 105, p. 383-95.

Ogura, M., 1969: A Direct Solution of Poisson Equation by Dimension Reduction Method, J. Meteorol. Soc. Japan, v. 47, no. 4.

Pasquill, F., 1974: Atmospheric Diffusion, 2nd Ed., Chichester, Ellis Horwood Ltd., John Wiley and Sons, NY, NY, 429p.

Pepper, D.W. and Baker, A.J., 1979: Modeling Pollutant Dispersion over Irregular Terrain with Second Moments and Cubic Splines, Proc. Fourth Symp. on Turb., Diff. and Air Poll., Reno. NV, Am. Meteorol. Soc., Boston, MA.

Puttock, J.S. and Hunt, J.C.R., 1979: Turbulent Diffusion from Sources Near Obstacles with Separated Wakes; Part I: An Eddy Diffusivity Model, Atmos. Envir., v. 13, p. 1-13.

Samarskii, A.A., 1977: Theory of Finite Difference Schemes, Nauka Press, Moscow, USSR, 656p.

Sasaki, Y., 1958: An Objective Analysis Based on the Variational Method, J. Meteorol. Soc. Japan, v. 36, p. 77-88.

Sasaki, Y., 1970: Numerical Variational Analysis Formulated under the Constraints Determined by Long Wave Equations and Low-Pass Filter, Mon. Wea. Rev. v. 98, p. 884-98.

Sasaki, Y., 1970: Some Basic Formalisms in Numerical Variational Analysis, Mon. Wea. Rev., v. 98, p. 875-83.

Sherman, C.A., 1978: A Mass-Consistent Model for Wind Fields over Complex Terrain, J. Appl. Meteorol., v. 17, p. 312-9.

Snyder, W.H., 1972: Similarity Criteria for the Application of Fluid Models to the Study of Air Pollution Meteorology, Bound. Layer Meteorol., v. 3, no. 2, p. 113-34.

Snyder, W.H., 1979: The EPA Meteorological Wind Tunnel: Its Design, Construction, and Operating Characteristics, Envir. Prot. Agcy. Rpt. No. EPA-600/4-79-051, Res. Tri. Pk., NC, 78p.

Snyder, W.H., 1981: Guideline for Fluid Modeling of Atmospheric Diffusion, Envir. Prot. Agcy. Rpt. No. EPA-600/8-81-009, Res. Tri. Pk., NC, 200p.

Snyder, W.H., Britter, R.E. and Hunt, J.C.R., 1979: A Fluid Modeling Study of the Flow Structure and Plume Impingement on a Three-Dimensional Hill in Stably Stratified Flow, Proc. Fifth Int. Conf. on Wind Engr. (J.E. Cermak, ed.), v. 1, p. 319-29, Pergamon Press, NY, NY.

Taylor, P.J. and Gent, P.R., 1974: A Model of Atmospheric Boundary Layer Flow above an Isolated Two-dimensional Hill: An Example of Flow above Gentle Topography, Bound.-Layer Meteorol., v. 7, p. 349-62.

Turner, D.B., 1970: Workbook of Atmospheric Dispersion Estimates, Office of Air Programs, Pub. No. AP-26, U.S. Envir. Prot. Agcy., Res. Tri. Pk., NC.

Wilson, D.J., Winkel, G. and Neiman, O., 1979: Reynolds Number Effects on Flow Recirculation behind Two-dimensional Obstacles in a Turbulent Boundary Layer, Proc. Fifth Int. Conf. on Wind Engr. (J.E. Cermak, ed.), v. 2, p. 965-74, Pergamon Press, NY, NY.

Zoric, D.L. and Sandborn, V.A., 1972: Similarity of Large Reynolds Number Boundary Layers, Boundary-Layer Meteorol., v. 2, p. 326-33.

Zrazhevsky, I.M., Doroshenko, V.N. and Chepik, N.G., 1968: Investigation of the Effect of Various Types of Relief on the Characteristics of an Air Stream in a Wind Tunnel, Atmos. Diff. and Air Poll., Trudy GGO, no. 207, Hydromet. Press, Leningrad, USSR.

Zrazhevsky, I.M. and Klingo, V.V., 1971: Modeling of Atmospheric Turbulent Movements over an Inhomogeneous Surface, Atmos. Diff. and Air Poll., Trudy GGO, no. 254, p. 39-56, Hydromet. Press, Leningrad, USSR.

TECHNICAL REPORT DATA
(Please read Instructions on the reverse before completing)

1. REPORT NO	2	3. RECIPIENT'S ACCESSION NO.
EPA-600/4-81-067		

4. TITLE AND SUBTITLE
FLOW AND DISPERSION OF POLLUTANTS OVER TWO-DIMENSIONAL HILLS
Summary Report on Joint Soviet-American Study

5. REPORT DATE
August 1981

6. PERFORMING ORGANIZATION CODE

7. AUTHOR(S)
Leon H. Khurshudyan[1], William H. Snyder[2], and Igor V. Nekrasov[3]

8. PERFORMING ORGANIZATION REPORT NO
Fluid Modeling Report No. 11

9. PERFORMING ORGANIZATION NAME AND ADDRESS
Environmental Sciences Research Laboratory
Office of Research and Development
U.S. Environmental Protection Agency
Research Triangle Park, NC 27711

10. PROGRAM ELEMENT NO
ADTA1D/03-1313 (FY-81)

11. CONTRACT/GRANT NO

12. SPONSORING AGENCY NAME AND ADDRESS
Environmental Sciences Research Laboratory - RTP, NC
Office of Research and Development
U.S. Environmental Protection Agency
Research Triangle Park, NC 27711

13. TYPE OF REPORT AND PERIOD COVERED
In-house

14. SPONSORING AGENCY CODE
EPA/600/09

15. SUPPLEMENTARY NOTES
[1]Main Geophysical Observatory, Leningrad, U.S.S.R. [2]On assignment from National Oceanic and Atmospheric Admin., U.S.Dept. of Commerce. [3]Moscow State Univ.,Moscow,U.S.S.R.

16. ABSTRACT

Wind tunnel experiments and theoretical models concerning the flow structure and pollutant diffusion over two-dimensional hills of varying aspect ratio are described and compared. Three hills were used, having small, medium and steep slopes. Measurements were made of mean and turbulent velocity fields upwind, over and downwind each of the hills. Concentration distributions were measured downwind of tracer sources placed at the upwind base, at the crest, and at the downwind base of each hill. These data were compared with the results of two mathematical models developed in the U.S.S.R. for treating flow and dispersion over two-dimensional hills. Measured concentration fields were reasonably well predicted by the models for a hill of small slope. The models were less successful for hills of steeper slope, because of flow separation from the lee side of the steepest hill and high turbulence and much-reduced mean velocity downwind of the hill of medium slope.

17. KEY WORDS AND DOCUMENT ANALYSIS

a. DESCRIPTORS	b. IDENTIFIERS/OPEN ENDED TERMS	c. COSATI Field/Group

18. DISTRIBUTION STATEMENT	19. SECURITY CLASS *(This Report)*	21. NO. OF PAGES
RELEASE TO PUBLIC	UNCLASSIFIED	143
	20. SECURITY CLASS *(This page)*	22. PRICE
	UNCLASSIFIED	

EPA Form 2220-1 (9-73)